STUDY OF SPIN, PARITY AND COUPLINGS OF A BOSONIC RESONANCE AT COLLIDERS

By

Tanmoy Modak

(PHYS10201004001)

The Institute of Mathematical Sciences, Chennai

A thesis submitted to the

Board of Studies in Physical Sciences

In partial fulfillment of requirements

For the Degree of

DOCTOR OF PHILOSOPHY

of

HOMI BHABHA NATIONAL INSTITUTE

March, 2016

Homi Bhabha National Institute

Recommendations of the Viva Voce Committee

As members of the Viva Voce Committee, we certify that we have read the dissertation prepared by Mr. Tanmoy Modak entitled "Study of spin, parity and couplings of a bosonic resonance at colliders" and recommend that it maybe accepted as fulfilling the thesis requirement for the award of Degree of Doctor of Philosophy.

____________________________________ Date: ____________
Chairman - Prof. Rahul Sinha

____________________________________ Date: ____________
Guide/Convener - Prof. Rahul Sinha

____________________________________ Date: ____________
Examiner - Prof. B. Ananthanarayan

____________________________________ Date: ____________
Member 1 - Prof. V. Ravindran

____________________________________ Date: ____________
Member 2 - Prof. Balachandran Sathiapalan
(for Prof. D. Indumathi)

____________________________________ Date: ____________
Member 3 - Prof. Ronojoy Adhikari

Final approval and acceptance of this thesis is contingent upon the candidate's submission of the final copies of the thesis to HBNI.

I hereby certify that I have read this thesis prepared under my direction and recommend that it maybe accepted as fulfilling the thesis requirement.

Date:____________ ______________________________
Place: IMSc, Chennai Guide: Prof. Rahul Sinha

STATEMENT BY AUTHOR

This dissertation has been submitted in partial fulfilment of requirements for an advanced degree at Homi Bhabha National Institute (HBNI) and is deposited in the Library to be made available to borrowers under rules of the HBNI.

Brief quotations from this dissertation are allowable without special permission, provided that accurate acknowledgement of source is made. Requests for permission for extended quotation from or reproduction of this manuscript in whole or in part may be granted by the Competent Authority of HBNI when in his or her judgement the proposed use of the material is in the interests of scholarship. In all other instances, however, permission must be obtained from the author.

Tanmoy Modak

DECLARATION

I, Tanmoy Modak, hereby declare that the investigation presented in the thesis has been carried out by me. The work is original and has not been submitted earlier as a whole or in part for a degree / diploma at this or any other Institution / University.

Tanmoy Modak

List of Publications arising from the thesis

Journal

1. Arjun Menon, Tanmoy Modak, Dibyakrupa Sahoo, Rahul Sinha and Hai-Yang Cheng,
   "Inferring the nature of the boson at 125–126 GeV",
   Physical Review D **89**, 095021 (2014)
   arXiv:1301.5404[hep-ph]

2. Tanmoy Modak, Dibyakrupa Sahoo, Rahul Sinha, Hai-Yang Cheng and T.C. Yuan,
   "Disentangling the Spin-Parity of a Resonance via the Gold-Plated Decay Mode",
   arXiv:1408.5665[hep-ph],
   Chinese Physics C Vol. 40, No. 3 (2016) 033002

Conferences

Study of the Spin-Parity of a Resonance via the Gold-Plated Decay Mode

Conference Proceedings, *Springer Proc.Phys. 174 (2016) 571-576*

Others

- Biplob Bhattacherjee , Tanmoy Modak, Sunando Kumar Patra and Rahul Sinha.
  " Probing Higgs couplings at LHC and beyond ",
  arXiv:1503.08924 ,
  .

Tanmoy Modak

Dedicated to my parents and supervisor

ACKNOWLEDGEMENTS

First and foremost I wish to thank my advisor Prof. Rahul Sinha for chaperoning the most significant part of my life. After completion of my course works I have this unique opportunity to work under him as a Ph. D. student. Throughout this years I have learned how to unravel the never ending mysteries of physics. I remember, he used to say “Physics is not just bunch of equations... It’s how you use them”. After spending these wonderful years with him today I am beginning to understand what he meant. He made me realize how physics is done. This thesis is result of his sustained effort and how he enlightened me by his vast knowledge in the last six years. His never ending patience and kindness reassured me, even when I used to make the most trivial mistakes. It would not be overstatement to say that he made me what I am today. My doctoral committee members, Prof. M.V.N. Murthy, Prof. D. Indumathi, Prof. V. Ravindran, Prof. Ronojoy Adhikari guided and helped me thoroughly throughout all these years.

I would like to thank my collaborators Prof. Hai-Yang Cheng, Prof. T.C. Yuan, Prof. Arjun Menon, Prof. Biplob Bhattacherjee, Dr. Rahul Srivastava, Dr. Sunando Patra and Dibyakrupa Sahoo for all the knowledge shared, discussed and assimilated thereof. I am forever grateful to Prof. Arjun Menon, Prof. Biplob Bhattacherjee and Dr. Sunando Patra for helping me learn several packages which are essential for research in High Energy Physics Phenomenology.

I am extremely thankful to Prof. Nita Sinha for letting me be her Teaching Assistant for particle physics course. I have learned so many things form her during that time which were crucial for my research. I would also like to convey my gratitude to Prof. Rajesh Ravindran, Prof. Partha Mukhopadhyay, Lt. Prof. Rahul Basu , Prof. T. R. Govindarajan Prof. Ghanashyam Date, Prof. D. Indumathi , Prof. Sujay Ashok and Prof. Ronojoy Adhikari for offering courses and making me learn many interesting physics.

I would also like to thank my friends Tuhin, Soumya, Rusa, Ria, Arya, Archana, Ashraf, Vaibhav, Saurabh, Krishanu, Dhritiranjan, Nirmalya, Aritra, Jahanur, Anup Basil, Subhadeep, Joydeep, Abhrajit, Raja, Arijit for making my stay at IMSc pleasant and enjoyable. This list will not be complete without mentioning two of the seniors Diganta and Tanumoy, for helping me out in the early days of my career. I wish to thank everyone at IMSc specially the administration for their overall assistance throughout my journey at IMSc.

I offer my respect and gratitude to my parents and relatives for their support and blessings. I, finally want to dedicate my thesis to my parents and supervisor for their heartening and warmth presence in my life.

Contents

Synopsis

Abstract: Discovery of a new bosonic resonance (Higgs) around 125 GeV at Large Hadron Collider (LHC) has been the most significant event in particle physics research of the current epoch. The task currently at hand is to establish that it has no anomalous interactions. The Higgs discovery epitomizes the potential of modern machines such as LHC. The LHC and future colliders such as ILC may discover new particles in near future. It is essential to study the spin, parity and the couplings to understand the true nature of these particles. These resonances are the fundamental ingredients of different New Physics (NP) models. Therefore, determination of the spin, parity and couplings of these resonances will lay the foundation stone for phenomenological study of different NP models.

Introduction: After the discovery of a new resonance, a sustained effort is required to infer its true characteristics. The first step is to determine the spin and parity of the resonance and finally to measure the couplings of the resonance to existing particles. Study of the angular distributions in terms of the partial decay rate of a resonance are found to be critical in this regard. In this thesis we show how to disentangle the spin, parity and the couplings of a bosonic resonance in a step by step methodology. We take two benchmark resonances for our analysis : the 125 GeV Higgs (H) and a heavy Z' boson (mass $\sim$ 2 TeV); and study the spin, parity and couplings via so called the "*golden channel*" i.e. $H \to ZZ^* \to 4\ell$ and $Z' \to ZZ \to 4\ell$ for both H and Z'. The subsequent decay of the two Z bosons into four oppositely charged leptons makes the *golden channel* an experimentally clean mode to probe. Furthermore, the four lepton final state allows us to fully reconstruct the phase space of both H and Z'. In our work, we derive three uniangular distributions (i.e. angular distributions involving one angle) in terms experimentally measurable angular asymmetries (observables), starting from Lorentz invariant and gauge invariant vertices. These angular asymmetries have definite parity properties and are orthogonal to each other and can hence be measured independently. We finally use these observables to ascertain the spin, parity and couplings of a resonance.

The 125 GeV Higgs: After the discovery of 125 GeV Higgs by the ATLAS and CMS collaboration at the LHC [1-5], a lot of effort has been directed towards determining its spin, parity and couplings to confirm whether it is indeed the Standard Model (SM) Higgs or a Higgs predicted in several Beyond Standard Model (BSM) scenarios. The H is observed primarily in $H \to \gamma\gamma$, $H \to W^+W^-$ and $H \to ZZ$ channels, where one or both the Z's and W's are off-shell. Since it is observed in $H \to \gamma\gamma$ channel, Landau-Yang's theorem [6,7] forbids the Spin-1 assignment of H. Hence we consider H to be either a Spin-0 (scalar) or a Spin-2 (tensor) particle. Significance of the angular distributions to understand the spin, parity and couplings of H to a pair of Z bosons has been realized both before and after the discovery of the H boson [8-11]. Refs. [12-15] extended the idea and included higher spin possibilities of H into their analysis. In Ref. [16] we start by considering the most general Lorentz and gauge invariant vertices of H for both Spin-0 and Spin-2 possibilities and evaluate the partial decay rate of H in terms of the invariant mass squares of the dilepton produced from the non-resonant Z and the three uniangular distributions of the four lepton final state. We show how studying the uniangular distributions and angular asymmetries derived from the uniangular distributions, one can step by step determine the spin, parity and couplings of H to the Z bosons. A numerical analysis have also been performed to establish our approach for experimental implementation including detector effects. Finally we show [17] how to probe Charge-conjugation and Parity (CP) structure of HZZ couplings and determine the precision reach of LHC in measuring CP properties of HZZ vertex.

Z' **boson:** If a bosonic resonance is not observed to be decaying into two photons, the resonance could have all three spin (J) possibilities i.e. $J = 0, 1, 2$. However, the Spin-1 resonance could decay into two Z bosons, allowed by generalized Landau-Yang's theorem [18]. In Ref. [19] we include the Spin-1 possibility of a bosonic resonance and extend our formalism to any arbitrary mass. We again right down the most general Lorentz and gauge invariant vertex and extract out the angular asymmetries from three uniangular distributions for a Spin-1 resonance and perform benchmark analysis for a Spin-1 resonance (e.g. a heavy Z' boson). We first construct a effective model and estimate the discovery potential of such Z' in the golden channel at LHC. We finally extract the observables from uniangular distributions and show how to establish the spin and parity of the Z' boson to validate our formalism.

Conclusion: In Refs. [16,17,19] we have discussed how one can determine the spin, parity and couplings of a bosonic resonance using observables extracted from the three uniangular distributions via golden channel. These observables are orthogonal to each other and each of them can be measured independently. We perform numerical analysis to validate our approach including detector effects. We finally conclude that the uniangular distributions and angular asymmetries will play a key role in determining the spin, parity and couplings of a resonance.

References:

[1] G. Aad *et al.* [ATLAS Collaboration],Phys. Lett. B **716**, 1 (2012),[arXiv:1207.7214 [hep-ex]].

[2] G. Aad *et al.* [ATLAS Collaboration], Science 21 December 2012: Vol. 338 no. 6114 pp. 1576-1582.

[3] S. Chatrchyan *et al.* [CMS Collaboration], Phys. Lett. B **716**, 30 (2012) [arXiv:1207.7235 [hep-ex]].

[4] S. Chatrchyan *et al.* [CMS Collaboration], Science 21 December 2012: Vol. 338 no. 6114 pp. 1569-1575.

[5] S. Chatrchyan *et al.* [CMS Collaboration], arXiv:1212.6639 [hep-ex].

[6] L. D. Landau, Dokl. Akad. Nauk Ser. Fiz. **60**, 207 (1948).

[7] C. -N. Yang, Phys. Rev. **77**, 242 (1950).

[8] C. A. Nelson, Phys. Rev. D **30**, 1937 (1984).

[9] J. R. Dell'Aquila and C. A. Nelson, Phys. Rev. D **33**, 80 (1986).

[10] C. A. Nelson, Phys. Rev. D **37**, 1220 (1988).

[11] G. Buchalla, O. Cata and G. D'Ambrosio, Eur. Phys. J. C **74**, 2798 (2014) [arXiv:1310.2574 [hep-ph]].

[12] D. J. Miller, S. Y. Choi, B. Eberle, M. M. Muhlleitner and P. M. Zerwas, Phys. Lett. B **505**, 149 (2001) [hep-ph/0102023].

[13] S. Y. Choi, "Measuring the spin of the Higgs bosons," in 10th International Conference on Supersymmetry, Edited by P. Nath, P. M. Zerwas, C. Grosche. Hamburg, DESY, 2002.

[14] S. Y. Choi, D. J. Miller, M. M. Muhlleitner and P. M. Zerwas, Phys. Lett. B **553**, 61 (2003) [hep-ph/0210077].

[15] R. M. Godbole, S. Kraml, M. Krawczyk, D. J. Miller, P. Niezurawski and A. F. Zarnecki, hep-ph/0404024.

[16] A. Menon, T. Modak, D. Sahoo, R. Sinha and H. Y. Cheng, Phys. Rev. D **89**, no. 9, 095021 (2014) [arXiv:1301.5404 [hep-ph]].

[17] B. Bhattacherjee, T. Modak, S. K. Patra and R. Sinha, arXiv:1503.08924 [hep-ph].

[18] W. -Y. Keung, I. Low and J. Shu, Phys. Rev. Lett. **101**, 091802 (2008) [arXiv:0806.2864 [hep-ph]].

[19] T. Modak, D. Sahoo, R. Sinha, H. Y. Cheng and T. C. Yuan, arXiv:1408.5665

[hep-ph].

Publications in Refereed Journal:

Published and Accepted:

(1) Arjun Menon, Tanmoy Modak, Dibyakrupa Sahoo, Rahul Sinha and Hai-Yang Cheng,

"Inferring the nature of the boson at 125–126 GeV",

Physical Review D **89**, 095021 (2014)

arXiv:1301.5404[hep-ph]

(2) Tanmoy Modak, Dibyakrupa Sahoo, Rahul Sinha, Hai-Yang Cheng and T.C. Yuan,

"Disentangling the Spin-Parity of a Resonance via the Gold-Plated Decay Mode",

arXiv:1408.5665[hep-ph],

Chinese Physics C Vol. 40, No. 3 (2016) 033002

(3) Tanmoy Modak, Soumya Sadhukhan and Rahul Srivastava

" 750 GeV Diphoton excess from Gauged $B - L$ Symmetry",

arXiv:1601.00836 ,

Accepted for publication in Physics Letters B.

Communicated:

(4) Tanmoy Modak and Rahul Srivastava.

" On probing Higgs couplings in $H \to ZV$ decays",

arXiv:1411.2210 ,

(5) Biplob Bhattacherjee , Tanmoy Modak, Sunando Kumar Patra and Rahul Sinha.

" Probing Higgs couplings at LHC and beyond ",

arXiv:1503.08924 ,

.

<u>Other Publications:</u>

- Study of the Spin-Parity of a Resonance via the Gold-Plated Decay Mode

  Conference Proceedings, *Springer Proc.Phys. 174 (2016) 571-576*

List of Figures

List of Tables

PART I

Introduction

0.1 Preamble

The physics of fundamental particles and interactions between them are well described by the Standard Model (SM). It explains various experimental observations consistently and very efficiently. The SM is based on gauge sector, fermionic sector and scalar sector. The Gauge sector of the SM is based on the gauge theory $SU(3)_C \times SU(2)_L \times U(1)_Y$. The symmetry group $SU(2)_L \times U(1)_Y$ and $SU(3)_C$ describe the electroweak and strong interactions respectively. The gauge group for electromagnetic interaction $U(1)_{EM}$, is a subgroup of $SU(2)_L \times U(1)_Y$. The gauge bosons in the SM are: the photon (γ), $W^{\pm}$, Z coming from $SU(2)_L \times U(1)_Y$ group and eight gluons (g) which are the gauge mediator of $SU(3)_C$. The gluons are massless, electrically neutral particles but have color quantum number. The weak mediators $W^{\pm}$ are massive and have electric charge ± 1 respectively. The weak gauge boson Z is massive and has zero electric charge and self interacting. The γ is chargeless, massless and not self interacting.

The fermionic sector of the SM is comprised of three generations leptons and quarks. These three families of fermions are identical in their properties except mass. The three families are:

$$\text{1st generation:} \begin{pmatrix} \nu_{eL} \\ \\ e^-_L \end{pmatrix}, e^-_R, \begin{pmatrix} u_L \\ \\ d_L \end{pmatrix}, u_R, d_R$$

$$\text{2nd generation:} \begin{pmatrix} \nu_{\mu L} \\ \\ \mu^-_L \end{pmatrix}, \mu^-_R, \begin{pmatrix} c_L \\ \\ s_L \end{pmatrix}, c_R, s_R$$

$$\text{3rd generation:} \begin{pmatrix} \nu_{\tau L} \\ \\ \tau_L^- \end{pmatrix}, \tau_R^-, \begin{pmatrix} t_L \\ \\ b_L \end{pmatrix}, t_R, b_R$$

with subscript L and R stands for left and right chiral fields defined by the chirality operators $P_{L,R} = \dfrac{1 \mp \gamma_5}{2}$ respectively.

The scalar sector is the most intriguing sector amongst all. The massiveness of the gauge bosons $W^\pm$ and Z indicates that $SU(2)_L \times U(1)_Y$ is not a symmetry of the vacuum. In the SM, the symmetry

$$SU(3)_C \times SU(2)_L \times U(1)_Y$$

is spontaneously broken by one of the most celebrated mechanism namely "Higgs Mechanism". Higgs mechanism generates the masses for $W^\pm$, Z and the fermions in a gauge invariant way and predicts a new particle called the "Higgs" boson. This particle has to be a scalar, massive and electrically neutral.

Combining all three sector the $SU(2)_L \times U(1)_Y$ Lagrangian for SM is written [1] in Table. 2.3.2:

$-\frac{1}{4}B^{\mu\nu}B_{\mu\nu} - \frac{1}{4}\mathbf{W}^{\mu\nu}.\mathbf{W}_{\mu\nu}$	$W^\pm, Z, \gamma$ kinetic and self interactions
$\bar{L}\gamma^\mu\left(i\partial_\mu - g\frac{1}{2}\tau.\mathbf{W}_\mu - g'\frac{Y}{2}B_\mu\right)L$	kinetic terms and interactions leptons of left handed quarks and with $W^\pm$, Z and γ
$\left\|\left(i\partial_\mu - g\frac{1}{2}\tau.\mathbf{W}_\mu - g'\frac{Y}{2}B_\mu\right)\phi\right\|^2 - V(\phi)$	$W^\pm$, Z and γ and Higgs masses and couplings
$-G_\ell\bar{\ell}_L\phi\ell_R - G_\ell\bar{\ell}_R\phi_c\ell_L + \text{h.c}$ $-G_d\,\bar{d}_L\phi d_R - G_u\,\bar{u}_L\phi_c u_R + \text{h.c}$	mass terms fermions and quarks and couplings to Higgs

Table 1: Different terms of $SU(2)_L \times U(1)_Y$ Lagrangian. L and R denotes the left handed fermion doublet and R denotes the right handed fermion singlet. τ is the generator of $SU(2)_L$, g is the $SU(2)_L$ coupling constant and g' is the coupling constant for $U(1)_Y$ group.

The scalar field ϕ is an isospin doublet with weak hypercharge $Y = 1$:

$$\phi = \begin{pmatrix} \phi^+ \\ \phi^0 \end{pmatrix} \tag{1}$$

with $\phi^+ = (\phi_1 + i\phi_2)/\sqrt{2}$ and $\phi^0 = (\phi_3 + i\phi_4)/\sqrt{2}$. The fields ϕ_i belong to $SU(2)_L \times U(1)_Y$ multiplet.

To generate masses for gauge bosons the “Higgs potential”

$$V(\phi) = \lambda(\phi^\dagger\phi)^2 + \mu^2(\phi^\dagger\phi) \tag{2}$$

can be spontaneously broken by $\mu^2 < 0$ and $\lambda > 0$ and substitute

$$\phi(x) = \begin{pmatrix} 0 \\ v + H(x) \end{pmatrix}. \tag{3}$$

where v is vacuum expectation value and $H(x)$ is the Higgs field. After spontaneous breaking of the $SU(2)_L \times U(1)_Y$ symmetry, $W^\pm$ acquire mass $M_{W^\pm} = \frac{1}{2}gv$ and Z acquires the mass $M_Z = \frac{1}{2}v\sqrt{g^2 + g'^2}$. The Higgs boson itself gets a mass $\sqrt{2\lambda\ v^2}$ and the photon becomes massless($M_\gamma = 0$). Finally the ratio between the coupling constants g' and g related as :

$$\frac{g'}{g} = \tan\theta_W, \tag{4}$$

where θ_W is known as Weinberg angle. One can also find a relationship between M_W, M_Z and θ_W as

$$\frac{M_W}{M_Z} = \cos\theta_W \tag{5}$$

with $\rho = \frac{M_W^2}{M_Z^2\ \cos^2\theta_W}$. In the SM ρ has a unique prediction which gives the quantitative measure of the relative strength of Neutral Current (NC) and charged current interactions of the EW theory.

Let us look back the construction of the SM chronologically. The group structure of electroweak theory i.e. $SU(2)_L \times U(1)_Y$ was first proposed by Glashow [2] in 1961 to unify weak and electromagnetic interactions into a symmetry group. The Goldstone theorem was proved and analyzed by Goldstone in 1961 and Salam, Weinberg and Goldstone in 1962 [3]. This was generalization of the work of Nambu proposed in 1960 [4]. This theorem suggests existence of massless spinless unphysical excitation due to spontaneous breaking of global symmetry.

P. Higgs, F. Englert and R. Brout, Guralnik, Hagen and Kibble in 1964 and later [5] proposed that the spontaneous breaking of local symmetry is required to break $SU(2)_L \times U(1)_Y$ symmetry. This procedure of spontaneous breaking of gauge symmetry is known as the Higgs mechanism. The electroweak (EW) theory was developed by Weinberg, Salam and Glashow [6] in 1967-68. This is called the Glashow-Weinberg-Salam Model. The renormalizablity of EW theory with and without symmetry breaking was first proved by 't Hooft[7] in 1971.

The only way of testing a theory is to verify its predictions in experiments. In 1973, $\sin^2\theta_W$ was measured experimentally[8] along with the discovery of Neutral Current. Glashow, Iliopoulos and Maiani showed in 1970 Flavor Changing Neutral Currents (FCNC) is suppressed in SM, which is known as GIM mechanism [10]. In the year 1974, existence of the charm quark (c) was confirmed[11] after the discovery of J/ψ particle which is a bound state of c quark. The discovery of bottom quark (b) [13] and τ , ν_τ [12] strongly indicated the existence of three generations of fermions. It took several years but finally in 1994 top (t) quark was discovered [14–17] and three generations of quark families are complete. The CP violation in the SM was explained by CKM quark mixing matrix named after Cabibbo, Kobayashi and Maskawa[18]. This matrix shows how three generations of quarks mix to give the CP violation in the SM. The discovery of $W^{\pm}$ and Z [19] was confirmed at the Super Proton Synchrotron(SPS) collider at CERN in 1983. This is one of the most significant discovery of particle physics and established SM as “The“ theory of particle physics. *So far the most important particle of all, the Higgs boson was not discovered.*

0.2 Why spin, parity and couplings?

The primary objective of the LHC was to discover the Higgs boson and study of its properties. The discovery of a new boson in 2012 by ATLAS and CMS Collaborations [20–24] with mass around 125 GeV and decaying into ZZ^*, $\gamma\gamma$, and WW^* channel was a milestone for research in High Energy Physics. If this resonance is Higgs, study of its properties would unravel some of the most tantalizing mysteries of particle physics such as electroweak symmetry breaking, how elementary particles get mass etc. Higgs is the fundamental building block of the most celebrated theory in particle physics: the Standard Model (SM).

Several BSM (Beyond Standard Model) theories also have multiple bosonic particles in their particle spectrum. The first and foremost question would be: Is the 125 GeV resonance indeed the Higgs predicted by SM (spin $J = 0$) or a scalar predicted by several BSM theories? The bosonic nature of the 125 GeV resonance incorporates other possibilities i.e. it could be a Spin-1 (such as Z') or even a Spin-2 (such as KK graviton). Since the resonance was seen to be decaying into two photons, Landau-Yang theorem [25, 26] excludes Spin-1 ($J = 1$) possibility, leaving only Spin-0 and Spin-2 possibilities. In this thesis we denote 125 GeV resonance as H for both Spin-0 and Spin-2 possibilities.

To understand whether 125 GeV resonance is indeed the Higgs boson predicted by the SM, one has to study the spin, parity and couplings of H. Angular distributions and angular asymmetries derived from them are of the most efficient tools to study the spin, parity and couplings of a resonance. Amongst all the decay modes of H, the *gold-plated* mode (also called as " *golden channel* ") $H \to ZZ^* \to \ell_1^- \ell_1^+ \ell_2^- \ell_2^+$ took the leading role in disentangling the spin, parity of 125 GeV H. Having four charged leptons in the final state, this channel is experimentally clean and four momenta of H can be easily reconstructed and hence is called *gold-plated* mode. In this thesis we first write down the most general Lorentz and gauge invariant vertex factor for H for both $J = 0$ and $J = 2$. We then obtain three uniangular [27, 28] distributions (*angular distributions involving one angle*) in terms of several experimentally measurable asymmetries (observables). These observables are functions of helicity amplitudes[1] written in transversity basis and thus have definite parity properties. Moreover these angular asymmetries are orthogonal to each other and hence each of them can be measured independently. We finally layout a step by step methodology to uniquely determine the spin, parity and the couplings of H to two Z bosons.

The Spin-1 Z' bosons arise in different BSM models such as E_6 models [29–33], sequential Z' [34], super string Z' [35] model etc. In this regard, Ref. [36] discusses the decay of a Z' boson ($J = 1$) into four charged leptons via two Z bosons and generalized Landau-Yang theorem. In this thesis we also show [37], how using observables extracted from three uniangular distributions, one can confirm the spin, parity and the couplings of a Z' boson decaying to two Z bosons. Furthermore, we will construct a effective model for a Z' decaying via gold-plated mode and find out the discovery potential of such resonance in future LHC runs. We finally discuss how precisely one can extract these angular asymmetries for 14 TeV and 33 TeV LHC runs.

We finally combine these result to show how uniangular asymmetries derived from three uniangular distributions can be used to determine the spin, parity and couplings to two Z bosons of a bosonic resonance.

[1] For more on Helicity amplitudes see Sec. 0.3

0.3 A Primer to Helicity Amplitude Technique

The decay of a particle into daughter particles is characterised by the number of independent helicity amplitudes. In this section we will discuss about the number of helicity amplitudes of a resonance $\mathcal{X}$ decaying into two Z bosons for all three spin possibilities $J = 0, 1, 2$. If we specify the polarizations of the initial and final particles, then the Feynman amplitude or transition amplitude can always be written in terms of helicity amplitudes. We shall represent the polarisation state of a particle by a ket $\left|\text{spin, spin projection to } z \text{ axis}\right\rangle$. Then the Feynman amplitude for the process

$$\underbrace{|\mathbf{J}, J_z\rangle}_{\mathcal{X}} \to \underbrace{|\mathbf{1}, \lambda_1\rangle}_{Z_1}\ \underbrace{|\mathbf{1}, \lambda_2\rangle}_{Z_2}$$

is given by the well known expression [38,39] involving the Wigner-D function $\mathscr{D}^{J*}_{J_z\lambda}(\phi, \theta, -\phi)$:

$$\mathscr{M}(J_z, \lambda_1, \lambda_2) = \left(\frac{2J+1}{4\pi}\right)^{\frac{1}{2}} \mathscr{D}^{J*}_{J_z\lambda}(\phi, \theta, -\phi)\ A_{\lambda_1\lambda_2}, \tag{6}$$

where $\lambda = |\lambda_1 - \lambda_2|$ with $\lambda_{1,2} \in \{\pm 1, 0\}$, $J = |\mathbf{J}|$, and $A_{\lambda_1\lambda_2}$ is called the *helicity amplitude*. Conservation of angular momentum implies that

$$|\lambda| = |\lambda_1 - \lambda_2| \leqslant J. \tag{7}$$

Since there are no interferences amongst the amplitudes with different helicity configurations, we will have to sum over all the allowed values of λ_1 and λ_2 that are not constrained by the value of J_z after squaring each individual amplitude:

$$|\mathscr{M}|^2 = \sum_{\substack{\lambda_1, \lambda_2 \\ |\lambda_1 - \lambda_2| \leqslant J}} |\mathscr{M}(J_z, \lambda_1, \lambda_2)|^2$$

Spin of $\mathcal{X}$	Allowed Helicity Amplitudes	N
0	$A_{++}, A_{00}, A_{--}.$	3
1	$A_{+0} = -A_{0+}, A_{0-} = -A_{-0}.$	2
2	$A_{++}, A_{00}, A_{--}, A_{+-} = A_{-+},$ $A_{+0} = A_{0+}, A_{0-} = A_{-0}.$	6

Table 2: Allowed helicity amplitudes considering only the different spin possibilities.

$$= \left(\frac{2J+1}{4\pi}\right) \sum_{\substack{\lambda_1,\lambda_2 \\ |\lambda_1-\lambda_2|\leqslant J}} \left|\mathscr{D}^{J*}_{J_z\lambda}(\phi,\theta,-\phi)\right|^2 \left|A_{\lambda_1\lambda_2}\right|^2. \tag{8}$$

Thus the probability of contribution of the helicity amplitude $A_{\lambda_1\lambda_2}$ to the transition amplitude ca be found as $\mathscr{M}(J_z,\lambda_1,\lambda_2)$ is $\left(\frac{2J+1}{4\pi}\right)\left|\mathscr{D}^{J*}_{J_z\lambda}(\phi,\theta,-\phi)\right|^2$. We can therefore write down the following important fact of the helicity amplitude formalism: *All the allowed helicity amplitudes for a given decay process contribute, but with different definite probability, to the Feynman amplitude, irrespective of the polarization of the parent (decaying) particle. The probability, however, depends on the polarization of the parent particle and for all allowed helicity amplitudes is non-zero.* Since the two Z bosons are Bose symmetric, the helicity amplitudes satisfy the relation

$$A_{\lambda_2\lambda_1} = (-1)^J A_{\lambda_1\lambda_2} = \begin{cases} +A_{\lambda_1\lambda_2} & \text{for Spin-0, 2} \\ -A_{\lambda_1\lambda_2} & \text{for Spin-1} \end{cases}. \tag{9}$$

This relationship is useful in getting the correct number of independent helicity amplitudes. All the allowed helicity amplitudes in the decay $\mathcal{X} \to ZZ$ are given in Table 2 where N denotes the total number independent helicity amplitudes possible for the particular spin case.

It is also known that, if the particle $\mathcal{X}$ were a parity eigenstate with eigenvalue $\eta_{\mathcal{X}} =$

J^P of X	Allowed Helicity Amplitudes	N
0^+	$A_{++} = A_{--}$, A_{00}.	2
0^-	$A_{++} = -A_{--}$.	1
1^+	$A_{+0} = -A_{-0} = A_{0-} = -A_{0+}$.	1
1^-	$A_{+0} = A_{-0} = -A_{0-} = -A_{0+}$.	1
2^+	$A_{++} = A_{--}$, A_{00}, $A_{+-} = A_{-+}$, $A_{+0} = A_{-0} = A_{0-} = A_{0+}$.	4
2^-	$A_{++} = -A_{--}$, $A_{+0} = -A_{-0} = -A_{0-} = A_{0+}$.	2

Table 3: Relationships amongst the allowed helicity amplitudes for the different Spin-parity cases.

$+1$ (parity-even) or -1 (parity-odd), then the helicity amplitudes are related by:

$$A_{\lambda_1 \lambda_2} = \eta_X \ (-1)^J \ A_{-\lambda_1 \, -\lambda_2}. \tag{10}$$

The allowed helicity amplitudes for the different Spin-parity possibilities can thus be related and are given in Table 3. It is clearly evident from above that for the Spin-0 case out of the three helicity amplitudes two describe the parity-even scenario and only one describes the parity-odd scenario. Similarly, for Spin-1 both parity-even and parity-odd cases are described by one helicity amplitude each. For the Spin-2 case, we have four helicity amplitudes describing the parity-even scenario and two helicity amplitudes for the parity-odd scenario.

Let us now analyse the decay process from the point-of-view of partial wave decompositions. If we describe the two Z boson system by a ket specifying the total spin ($\mathbf{L}_{\text{spin}}$), the relative orbital angular momentum ($\mathbf{L}_{\text{orbital}}$), the spin of the parent particle (its $\mathbf{J}$ here) and its projection along the direction of flight of one of the Z bosons (J_z):

$\mathbf{L}_{\text{spin}}$	$\mathbf{L}_{\text{orbital}}$	$\mathbf{J}$	Partial wave
0	**0**	**0**	S-wave
0	**2**	**2**	D-wave
1	**1**	$\mathbf{2, 1, 0}$	P-wave
1	**3**	**2**	F-wave
2	**0**	**2**	S-wave
2	**2**	$\mathbf{2, 1, 0}$	D-wave
2	**4**	**2**	G-wave

Table 4: Allowed partial waves for all the spin considerations.

$\left|\mathbf{J}, J_z; \mathbf{L}_{\text{orbital}}, \mathbf{L}_{\text{spin}}\right\rangle$, then

$$\hat{P}_{12}\left|\mathbf{J}, J_z; \mathbf{L}_{\text{orbital}}, \mathbf{L}_{\text{spin}}\right\rangle = (-1)^{L_{\text{orbital}}+L_{\text{spin}}}\left|\mathbf{J}, J_z; \mathbf{L}_{\text{orbital}}, \mathbf{L}_{\text{spin}}\right\rangle, \tag{11}$$

where $\hat{P}_{12}$ is the operator that exchanges the two Z bosons (it exchanges both their momenta and spins or polarisations), L_{orbital} and L_{spin} are the modulus of $\mathbf{L}_{\text{orbital}}$ and $\mathbf{L}_{\text{spin}}$ respectively. It is obvious that for Bose symmetry to be satisfied $L_{\text{orbital}} + L_{\text{spin}}$ must be even. The allowed partial waves for the decay $\mathcal{X} \to ZZ$ are listed in Table 4.

It is easy to observe that when $\mathcal{X}$ has Spin-0, then there are three helicity amplitudes and three partial wave contributions (one S-wave, one P-wave and one D-wave). When $\mathcal{X}$ has Spin-1, then there are only two independent helicity amplitudes and two partial wave contributions (one P-wave and one D-wave). Finally when $\mathcal{X}$ has Spin-2, then there are six independent helicity amplitudes and six partial wave contributions (one S-wave, one P-wave, two D-waves, one F-wave and one G-wave). It is interesting to note that for the Spin-0 case the vertex factor has three form factors, for Spin-1 case there are two form factors. However, for the Spin-2 case we have eight form factors in the vertex factor instead of six. So one needs to consider only six form factors out of which four should be of parity-even nature and two should be of parity-odd nature.

0.4 Outline of the Thesis

This thesis is organized as follows:

Part II: In this Part we discuss how the uniangular distributions can be used to determine the spin, parity and couplings of 125 GeV resonance.

Chapter 1 is dedicated to study the spin parity of 125 GeV resonance. A short review on resonance Discovery is made in Sec. 1.1 In Sec. 1.2 we layout the details of our analysis, with Subsec. 1.2.1 and 1.2.2 devoted exclusively to Spin-0 and Spin-2 boson respectively. A step by step comparison with detailed procedure to distinguish the spin and parity states of the new boson is discussed in Subsec. 1.2.3. In Subsec.1.2.4 we present a numerical study to demonstrate the discriminating power of the uniangular distribution analysis compared to the current approach by ATLAS. We find that uniangular distribution is more powerful in discriminating between the scalar (0^+) and pseudoscalar (0^-) hypothesis. We conclude emphasizing the advantage of our approach in Sec. 1.3.

Chapter 2 outlines how to probe CP-odd admixture in HZZ couplings. This Chapter is divided into four Sections. We start with a general overview in Sec. 2.1 and derive the required technique to study the CP-odd admixture in HZZ couplings in Sec. 2.2. In Sec. 2.3 we perform the numerical analysis and examine how precisely one can CP-odd admixture HZZ. We draw inference in Sec.2.4.

Part III: The Chapter 3 we analyze the how to measure the spin, parity and couplings of a heavy Spin-1 particle via three uniangular distributions. This Chapter is divided into four Sections. We give a brief overview in Sec. 3.1. In Sec. 3.2 we write down the most general vertex factors and three uniangular distributions for a Spin-1 resonance. We then

study the possibility of discovering such resonance in Sec. 3.3. We summarize in Sec. 3.4
.

Part IV: Finally in Part IV we conclude our results.

Part V: This Part contains all the appendices and lists all the references.

PART II

Spin-0 and Spin-2

1

Spin, Parity and Couplings of the 125 GeV Resonance

1.1 Introduction

A new bosonic resonance with a mass of about 125 GeV has recently been observed at the Large Hadron Collider by both ATLAS Collaboration [20, 21] and CMS Collaboration [22–24]. Significant effort is now directed at determining the properties and couplings of this new resonance to confirm that it is indeed the Higgs boson of the Standard Model. In this work we specify this new boson by the symbol H and we call it the Higgs, even though it has not been proved to be the Higgs of the Standard Model. This resonance is observed primarily in three decay channels $H \to \gamma\gamma$, $H \to ZZ$ and $H \to WW$, where one (or both) of the Z's and W's are off-shell. It is well known that the spin and parity of the resonance and its couplings can be determined by studying the momentum and angular distributions of the decay products. Indeed there is little doubt that a detailed numerical fit to the invariant masses of decay products and their angular distributions will reveal the true nature of this resonance. However, a detailed study of the angular distributions requires large statistics and may not be feasible currently. Several studies existed in the literature before the discovery of this new resonance [40–70] and yet several papers have appeared recently on strategies to determine the spin and parity of the resonance [71–84]. Yet, there is no clear conclusion on the step by step methodology to determine these properties and convincingly establish that the new resonance is indeed the Standard Model Higgs boson. The recent result [24] from CMS Collaboration on the determination of spin and parity of the new boson is not conclusive.

In this thesis [27] we are exclusively concerned with Higgs decaying to four charged leptons, which proceeds via a pair of Z bosons: $H \to ZZ \to (\ell_1^- \ell_1^+)(\ell_2^- \ell_2^+)$, where ℓ_1, ℓ_2 are leptons e or μ. Since the Higgs is not heavy enough to produce two real Z bosons, we can have one real and another off-shell Z, or both the Z's can be off-shell. While we deal with the former case in detail our analysis applies equally well to the later case. We find that only in a very special case dealing with $J^P = 2^+$ boson it is more likely that both the Z bosons are off-shell. We emphasize that the final state $(e^+e^-)(\mu^+\mu^-)$ is not equivalent to $(e^+e^-)(e^+e^-)$ or $(\mu^+\mu^-)(\mu^+\mu^-)$ as sometimes mentioned in the literature, since the latter final states have to be anti-symmetrized with respect to each of the two sets of identical fermions in the final state. The anti-symmetrization of the amplitudes is not done in our analysis and hence our analysis applies only to $(e^+e^-)(\mu^+\mu^-)$. We examine the angular distributions and present a strategy to determine the spin and parity of H, as well as its couplings to the Z-bosons with the least possible measurements. Assuming charge conjugation invariance, the observation of $H \to \gamma\gamma$ also implies [44] that H is a charge conjugation $C = +$ state. In making this assignment of charge conjugation it is assumed that H is an eigenstate of charge conjugation. With the charge conjugation of H thus established we will only deal with the parity of H henceforth. We consider only Spin-0 and Spin-2 possibilities for the H boson. Higher spin possibilities need not be considered for a comparative study as the number of independent helicity amplitudes does not increase any more [49, 85]. The process under consideration requires that Bose symmetry be obeyed with respect to exchange of the pair of Z bosons. This constraints the number of independent helicity amplitudes to be less than or equal to six. Even if the Spin-J of H is higher (i.e. $J \geqslant 3$), the number of independent helicity amplitudes still remains six. However, the helicity amplitudes corresponding to higher spin states involve higher powers of momentum of Z, independent of the momentum dependence of the form factors describing the process. We will show that even for $J^P = 2^+$ under a special case only two independent helicity amplitudes may survive just as in the case of $J^P = 0^+$. The two cases are in principle indistinguishable unless one makes an assumption on the momentum dependence of the form factors involved.

We start by considering the most general decay vertex for both scalar and tensor resonances H decaying to two Z bosons. We evaluate the partial decay rate of H in terms of the invariant mass squared of the dilepton produced from the non-resonant Z and the angular distributions of the four lepton final state. We demonstrate that by studying three uniangular distributions one can almost completely determine the spin and parity of H and also explore any anomalous couplings in the most general fashion. We find that $J^P = 0^-$ and 2^- can easily be excluded. The $J^P = 0^+$ and 2^+ possibilities can also be easily distinguished, but may require some lepton invariant mass measurements if the most general tensor vertex is considered. Only if H is found to be of Spin-2, a complete three angle fit to the distribution is required to distinguish between $J^P = 2^+$ and 2^-.

The determination of couplings and spin, parity of the boson is important as there are other Spin-0 and Spin-2 particles predicted, such as the $J = 0$ radion [87–93] and $J = 2$ Kaluza-Klein graviton [79, 94–96], which can easily mimic the initial signatures observed so far. Such cases have already been considered in the literature even in the context of this resonance. Our analysis is most general and such extensions are limiting cases in our analysis as the couplings are defined by the model.

1.2 Decay of H to four charged leptons via two Z bosons

Let us consider the decay of H to four charged leptons via a pair of Z bosons:

$$H \to Z_1 + Z_2 \to (\ell_1^- + \ell_1^+) + (\ell_2^- + \ell_2^+),$$

where ℓ_1, ℓ_2 are leptons e or μ. As mentioned in the introduction we assume ℓ_1 and ℓ_2 are not identical. The kinematics for the decay is as shown in Fig. 1.1. The Higgs at

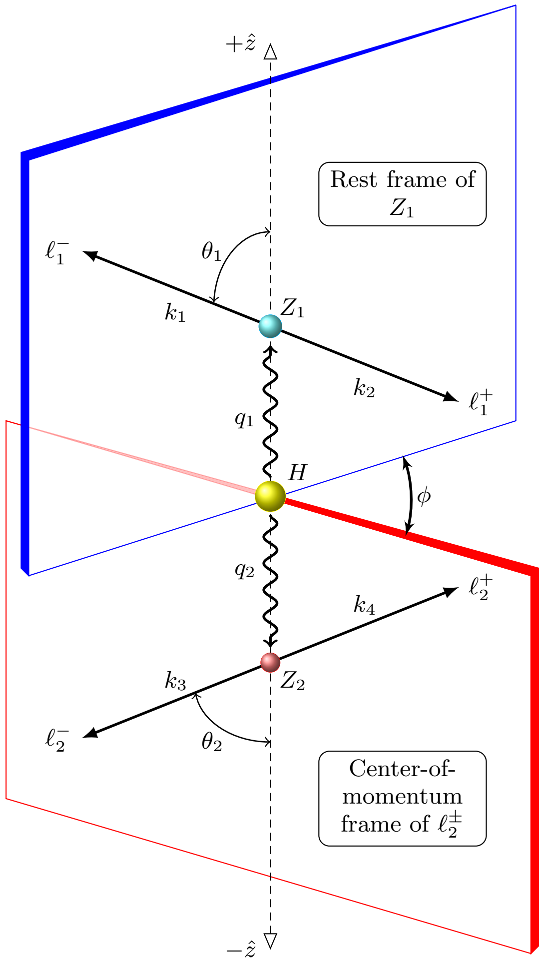

Figure 1.1: Definition of the polar angles (θ_1 and θ_2) and the azimuthal angle (ϕ) in the decay of Higgs (H) to a pair of Z's, and then to four charged leptons: $H \to Z_1 + Z_2 \to (\ell_1^- + \ell_1^+) + (\ell_2^- + \ell_2^+)$, where $\ell_1, \ell_2 \in \{e, \mu\}$. It should be clear from the figure that $\vec{k}_1 = -\vec{k}_2$ and $\vec{k}_3 = -\vec{k}_4$. Since Z_2 is off-shell, we cannot go to its rest frame. However, given the momenta of ℓ_2^+ and ℓ_2^- we can always go to their center-of-momentum frame.

rest is considered to decay with the on-shell Z_1 moving along the $+\hat{z}$ axis and off-shell Z_2 along the $-\hat{z}$ axis. The decays of Z_1 and Z_2 are considered in their rest frame. The angles and momenta involved are as described in Fig. 1.1. The 4-momenta of H, Z_1 and Z_2 are defined as P, q_1 and q_2 respectively. We choose Z_1 to decay to lepton pair $\ell_1^\pm$ with momentum k_1 and k_2 respectively and Z_2 to decay to $\ell_2^\pm$ with momentum k_3 and k_4 respectively. The phase space is shown in Appendix .A.1.

Nelson [40–42] and Dell'Aquilla [41] realized the significance of studying angular correlations in this process with Higgs boson decaying to a pair of Z bosons for inferring the nature of the Higgs boson. Refs. [46, 48, 49] were the first to extend the analysis to include higher spin possibilities so that any higher spin particle can effectively be distinguished from SM Higgs. We study similar angular correlations in this thesis. We begin the study by considering the most general HZZ vertices for a $J = 0$ and a $J = 2$ resonance H. We shall first discuss the two spin possibilities separately. Later we will layout the approach to distinguish them assuming the most general HZZ vertex.

1.2.1 If the 125 GeV resonance were Spin-0

The most general HZZ vertex factor $V^{\alpha\beta}_{HZZ}$ for Spin-0 Higgs is given by

$$V^{\alpha\beta}_{HZZ} = \frac{igM_Z}{\cos\theta_W}\Big(a\, g^{\alpha\beta} + b\, P^\alpha P^\beta + ic\, \epsilon^{\alpha\beta\mu\nu}\, q_{1\mu}\, q_{2\nu}\Big), \tag{1.1}$$

where θ_W is the *weak mixing angle*, g is the electroweak coupling, and a, b, c are some arbitrary form factors dependent on the 4-momentum squares specifying the vertex. The vertex $V^{\alpha\beta}_{HZZ}$ is derived from an effective Lagrangian (see for example Ref. [86]) where higher dimensional operators contribute to the momentum dependence of the form factors. Since the effective Lagrangian in the case of arbitrary new physics is not known, no momentum dependence of a, b and c can be assumed if the generality of the approach has to be retained. Approaches using constant values for the form factors therefore cannot provide unambiguous determination of Spin-parity of the new boson. We emphasize that even though the momentum dependence of a, b and c is not explicitly specified, they must be regarded as being momentum dependent in general. In SM, however, a, b, c are constants and take the value $a = 1$ and $b = c = 0$ at tree level.

In Eq. (1.1) the term proportional to c is odd under parity and the terms proportional to both a and b are even under parity. Partial-wave analysis tells that such a decay gets contributions from the first three partial waves, namely $\mathcal{S}$-wave, $\mathcal{P}$-wave and $\mathcal{D}$-wave. Since $\mathcal{S}$- and $\mathcal{D}$-waves are parity even while the $\mathcal{P}$-wave is parity odd, the term associated with c effectively describes the $\mathcal{P}$-wave contribution. The terms proportional to a and b are admixtures of $\mathcal{S}$- and $\mathcal{D}$-wave contributions. The decay of a Spin-0 particle to two Spin-1 massive particles is hence always described by three helicity amplitudes.

The decay under consideration is more conveniently described in terms of helicity amplitudes A_L, $A_{||}$ and $A_\perp$ defined in the transversity basis as

$$A_L = q_1 \cdot q_2\, a + M_H^2\, X^2\, b, \tag{1.2}$$

$$A_{||} = \sqrt{2q_1^2\, q_2^2}\, a, \tag{1.3}$$

$$A_\perp = \sqrt{2q_1^2\, q_2^2}\, X\, M_H\, c, \tag{1.4}$$

where $\sqrt{q_1^2}$ and $\sqrt{q_2^2}$ are the invariant masses of the $\ell_1^\pm$ and $\ell_2^\pm$ lepton pairs, i.e. $q_1^2 \equiv (k_1 + k_2)^2$, $q_2^2 \equiv (k_3 + k_4)^2$,

$$X = \frac{\sqrt{\lambda(M_H^2, q_1^2, q_2^2)}}{2M_H}, \tag{1.5}$$

a, b and c are the coefficients that enter the most general vertex we have written in Eq. (1.1) and

$$\lambda(x, y, z) = x^2 + y^2 + z^2 - 2\,x\,y - 2\,x\,z - 2\,y\,z\,. \tag{1.6}$$

It should be remembered that the helicities A_L, $A_{||}$ and $A_\perp$ are in general functions of q_1^2

and q_2^2, even though the functional dependence is not explicitly stated. The advantage of using the helicity amplitudes is that the helicity amplitudes are orthogonal. Our helicity amplitudes are defined in the transversity basis and thus differ from those given in Ref. [86]. Our amplitudes can be classified by their parity: A_L and $A_\parallel$ are parity even and $A_\perp$ is parity odd. This is unlike the amplitudes used in Ref. [86]. Throughout the thesis we use linear combinations of the helicity amplitudes such that they have well defined parity. This basis may be referred to as the transversity basis. Even though we work in terms of helicity amplitudes in the transversity basis, we will show below, it is in fact possible to uniquely extract out the coefficients a, b, c which characterize the most general HZZ vertex for $J = 0$ Higgs.

We will assume that Z_1 is on-shell while Z_2 is off-shell, unless it is explicitly stated that both the Z bosons are off-shell. The off-shell nature of the Z is denoted by a superscript '*'. One can easily integrate over q_1^2 using the narrow width approximation of the Z. The helicity amplitudes are then defined at $q_1^2 \equiv M_Z^2$ and q_2^2. In principle q_1^2 could also have been explicitly integrated out in both the cases when either Z_1 is off-shell or fully on-shell, resulting in some weighted averaged value of the helicities. The differential decay rate for the process $H \to Z_1 + Z_2^* \to (\ell_1^- + \ell_1^+) + (\ell_2^- + \ell_2^+)$, after integrating over q_1^2 (assuming Z_1 is on-shell or even otherwise) can now be written in terms of the angular distribution using the vertex given in Eq. (1.1) as:

$$
\begin{aligned}
\frac{8\pi}{\Gamma_f} \frac{d^4\Gamma}{dq_2^2\, d\cos\theta_1\, d\cos\theta_2\, d\phi} &= 1 + \frac{|F_\parallel|^2 - |F_\perp|^2}{4} \cos 2\phi (1 - P_2(\cos\theta_1))\,(1 - P_2(\cos\theta_2)) \\
&+ \frac{1}{2} \mathrm{Im}(F_\parallel F_\perp^*) \sin 2\phi (1 - P_2(\cos\theta_1))\,(1 - P_2(\cos\theta_2)) \\
&+ \frac{1}{2}(1 - 3\,|F_L|^2)\,(P_2(\cos\theta_1) + P_2(\cos\theta_2)) \\
&+ \frac{1}{4}(1 + 3\,|F_L|^2)\,P_2(\cos\theta_1) P_2(\cos\theta_2)
\end{aligned}
$$

$$
\begin{aligned}
&+ \frac{9}{8\sqrt{2}}\left(\mathrm{Re}(F_L F_\parallel^*)\cos\phi + \mathrm{Im}(F_L F_\perp^*)\sin\phi\right)\sin 2\theta_1 \sin 2\theta_2 \\
&+ \eta\Bigg(\frac{3}{2}\mathrm{Re}(F_\parallel F_\perp^*)\left(\cos\theta_2(2 + P_2(\cos\theta_1)) - \cos\theta_1(2 + P_2(\cos\theta_2))\right) \\
&\quad + \frac{9}{2\sqrt{2}}\mathrm{Re}(F_L F_\perp^*)(\cos\theta_1 - \cos\theta_2)\cos\phi\sin\theta_1\sin\theta_2 \\
&\quad - \frac{9}{2\sqrt{2}}\mathrm{Im}(F_L F_\parallel^*)(\cos\theta_1 - \cos\theta_2)\sin\phi\sin\theta_1\sin\theta_2\Bigg) \\
&- \frac{9}{4}\eta^2\left((1 - |F_L|^2)\cos\theta_1\cos\theta_2 + \sqrt{2}\left(\mathrm{Re}(F_L F_\parallel^*)\cos\phi + \mathrm{Im}(F_L F_\perp^*)\sin\phi\right)\sin\theta_1\sin\theta_2\right),
\end{aligned}
\tag{1.7}
$$

where the *helicity fractions* F_L, $F_\parallel$ and $F_\perp$ are defined as

$$
F_\lambda = \frac{A_\lambda}{\sqrt{|A_L|^2 + \left|A_\parallel\right|^2 + |A_\perp|^2}}, \tag{1.8}
$$

where $\lambda \in \{L, \parallel, \perp\}$ and

$$
\Gamma_f \equiv \frac{d\Gamma}{dq_2^2} = \mathcal{N}\left(|A_L|^2 + \left|A_\parallel\right|^2 + |A_\perp|^2\right), \tag{1.9}
$$

$$
\begin{aligned}
\text{with } \mathcal{N} &= \frac{1}{2^4}\,\frac{1}{\pi^2}\,\frac{g^2}{\cos^2\theta_W}\,\frac{\mathrm{Br}_{\ell\ell}^2}{M_H^2}\,\frac{\Gamma_Z}{M_Z} \\
&\times \frac{X}{\left(\left(q_2^2 - M_Z^2\right)^2 + M_Z^2\Gamma_Z^2\right)}.
\end{aligned}
\tag{1.10}
$$

where Γ_Z is the total decay width of the Z boson, $\mathrm{Br}_{\ell\ell}$ is the branching ratio for the decay of Z boson to two mass-less leptons: $Z \to \ell^+\ell^-$ and we have used the narrow width approximation for the on-shell Z. We emphasize that with q_1^2 integrated out the helicity amplitudes A_λ and helicity fractions F_λ are functions only of q_2^2. In Eq. (1.7) η is defined as

$$
\eta = \frac{2v_\ell a_\ell}{v_\ell^2 + a_\ell^2} \tag{1.11}
$$

with $v_\ell = 2I_{3\ell} - 4e_\ell \sin^2\theta_W$ and $a_\ell = 2I_{3\ell}$, and $P_2(x)$ is the 2nd degree Legendre polynomial:

$$P_2(x) = \frac{1}{2}(3x^2 - 1) \qquad (\text{with } x \in \{\cos\theta_1, \cos\theta_2\}). \tag{1.12}$$

We have chosen to express the the differential decay rate in terms of Legendre polynomials for $\cos\theta_1$ and $\cos\theta_2$ and Fourier series for ϕ. This ensures that each term in Eq. (1.7) is orthogonal to any other term in the distribution. The Legendre polynomials $P_m(\cos\theta_1)$ and $P_m(\cos\theta_2)$ satisfy the orthogonality condition since the range of $\cos\theta_1$ and $\cos\theta_2$ is -1 to 1, whereas that of ϕ is 0 to 2π. Our approach of using Legendre polynomials and the choice of helicity amplitudes in transversity basis classified by parity form the corner-stone of our analysis. The same technique will be used in Sec. 1.2.2 to analyze the Spin-2 case.

An interesting observation in the scalar case is that the coefficients of $P_2(\cos\theta_1)$ and $P_2(\cos\theta_2)$ are identically equal to $\frac{1}{2}(1 - 3|F_L|^2)$ in both magnitude and sign. It is worth noting that the coefficients of $\cos 2\phi\ P_2(\cos\theta_1)$ and $\cos 2\phi\ P_2(\cos\theta_2)$ are also identically equal to $\frac{1}{4}(|F_\||^2 - |F_\perp|^2)$ in both magnitude and sign.

Integrating Eq. (1.7) with respect to $\cos\theta_1$ or $\cos\theta_2$ or ϕ, the following uniangular distributions are obtained:

$$\frac{1}{\Gamma_f}\frac{d^2\Gamma}{dq_2^2\, d\cos\theta_1} = \frac{1}{2} + T_2^{(0)}\, P_2(\cos\theta_1) - T_1^{(0)}\cos\theta_1, \tag{1.13}$$

$$\frac{1}{\Gamma_f}\frac{d^2\Gamma}{dq_2^2\, d\cos\theta_2} = \frac{1}{2} + T_2^{(0)}\, P_2(\cos\theta_2) + T_1^{(0)}\cos\theta_2, \tag{1.14}$$

$$\frac{2\pi}{\Gamma_f}\frac{d^2\Gamma}{dq_2^2\, d\phi} = 1 + U_2^{(0)}\cos 2\phi + V_2^{(0)}\sin 2\phi + U_1^{(0)}\cos\phi + V_1^{(0)}\sin\phi, \tag{1.15}$$

where

$$
\begin{aligned}
T_2^{(0)} &= \frac{1}{4}(1 - 3\,|F_L|^2), && (1.16)\\
U_2^{(0)} &= \frac{1}{4}(|F_\parallel|^2 - |F_\perp|^2), && (1.17)\\
V_2^{(0)} &= \frac{1}{2}\,\mathrm{Im}(F_\parallel F_\perp^*), && (1.18)\\
T_1^{(0)} &= \frac{3}{2}\,\eta \mathrm{Re}(F_\parallel F_\perp^*), && (1.19)\\
U_1^{(0)} &= -\frac{9\pi^2}{32\sqrt{2}}\eta^2\,\mathrm{Re}(F_L F_\parallel^*), && (1.20)\\
V_1^{(0)} &= -\frac{9\pi^2}{32\sqrt{2}}\eta^2\,\mathrm{Im}(F_L F_\perp^*), && (1.21)
\end{aligned}
$$

are explicitly functions of q_2^2. The superscript (0) indicates the spin of H. As $P_0(\cos\theta_{1,2}) = 1$, $P_1(\cos\theta_{1,2}) = \cos\theta_{1,2}$, $P_2(\cos\theta_1)$, $\cos\phi$, $\sin\phi$, $\cos 2\phi$ and $\sin 2\phi$ are orthogonal functions, the coefficients of each of the terms can be extracted individually. We can also extract all the above coefficients in terms of asymmetries defined as below:

$$
\begin{aligned}
T_1^{(0)} &= \left(\int_{-1}^{0} - \int_{0}^{+1}\right) d\cos\theta_1 \,\left(\frac{1}{\Gamma_f}\frac{d^2\Gamma}{dq_2^2\; d\cos\theta_1}\right)\\
&= \left(-\int_{-1}^{0} + \int_{0}^{+1}\right) d\cos\theta_2 \,\left(\frac{1}{\Gamma_f}\frac{d^2\Gamma}{dq_2^2\; d\cos\theta_2}\right), && (1.22)\\
T_2^{(0)} &= \frac{4}{3}\left(\int_{-1}^{-\frac{1}{2}} - \int_{-\frac{1}{2}}^{+\frac{1}{2}} + \int_{+\frac{1}{2}}^{+1}\right) d\cos\theta_{1,2} \,\left(\frac{1}{\Gamma_f}\frac{d^2\Gamma}{dq_2^2\; d\cos\theta_{1,2}}\right), && (1.23)\\
U_1^{(0)} &= \frac{1}{4}\left(-\int_{-\pi}^{-\frac{\pi}{2}} + \int_{-\frac{\pi}{2}}^{+\frac{\pi}{2}} - \int_{+\frac{\pi}{2}}^{+\pi}\right) d\phi \,\left(\frac{2\pi}{\Gamma_f}\frac{d^2\Gamma}{dq_2^2\; d\phi}\right), && (1.24)\\
U_2^{(0)} &= \frac{1}{4}\left(\int_{-\pi}^{-\frac{3\pi}{4}} - \int_{-\frac{3\pi}{4}}^{-\frac{\pi}{4}} + \int_{-\frac{\pi}{4}}^{\frac{\pi}{4}} - \int_{\frac{\pi}{4}}^{\frac{3\pi}{4}} + \int_{\frac{3\pi}{4}}^{\pi}\right) d\phi \,\left(\frac{2\pi}{\Gamma_f}\frac{d^2\Gamma}{dq_2^2\; d\phi}\right), && (1.25)\\
V_1^{(0)} &= \frac{1}{4}\left(-\int_{-\pi}^{0} + \int_{0}^{+\pi}\right) d\phi \,\left(\frac{2\pi}{\Gamma_f}\frac{d^2\Gamma}{dq_2^2\; d\phi}\right), && (1.26)\\
V_2^{(0)} &= \frac{1}{4}\left(\int_{-\pi}^{-\frac{\pi}{2}} - \int_{-\frac{\pi}{2}}^{0} + \int_{0}^{+\frac{\pi}{2}} - \int_{+\frac{\pi}{2}}^{+\pi}\right) d\phi \,\left(\frac{2\pi}{\Gamma_f}\frac{d^2\Gamma}{dq_2^2\; d\phi}\right). && (1.27)
\end{aligned}
$$

As had already been realized from Eq. (1.7), the coefficients of $P_2(\cos\theta_1)$ and $P_2(\cos\theta_2)$ as well as the coefficients of $\cos\theta_1$ and $\cos\theta_2$ in Eqs. (1.13) and (1.14) are identical. This results in a maximum of 6 possible independent measurements $T_1^{(0)}$, $U_1^{(0)}$, $V_1^{(0)}$, $T_2^{(0)}$, $U_2^{(0)}$ and $V_2^{(0)}$ using uniangular analysis. For the decay under consideration, $v_\ell = -1+4\sin^2\theta_W$ and $a_\ell = -1$. Substituting the experimental value for the weak mixing angle: $\sin^2\theta_W = 0.231$, we get $\eta = 0.151$ and $\eta^2 = 0.0228$. Owing to such small values of η and η^2 it is unlikely that $T_1^{(0)}$, $U_1^{(0)}$ and $V_1^{(0)}$ can be measured using the small data sample current available at LHC, reducing the number of independent measurable to three.

Using Eqs. (1.16) and (1.17) and the identity $|F_L|^2 + \left|F_{||}\right|^2 + |F_\perp|^2 = 1$, the following solutions for $|F_L|^2$, $\left|F_{||}\right|^2$ and $|F_\perp|^2$ are obtained:

$$|F_L|^2 = \frac{1}{3}\left(1 - 4\,T_2^{(0)}\right), \tag{1.28}$$

$$\left|F_{||}\right|^2 = \frac{1}{3}\left(1 + 2\,T_2^{(0)}\right) + 2\,U_2^{(0)}, \tag{1.29}$$

$$|F_\perp|^2 = \frac{1}{3}\left(1 + 2\,T_2^{(0)}\right) - 2\,U_2^{(0)}. \tag{1.30}$$

We have shown that one can easily measure all the three helicity fractions using uniangular distributions. We can also measure $\mathrm{Im}(F_{||}F_\perp^*)$, which is proportional to sine of the phase difference between the two helicity amplitudes $A_{||}$ and $A_\perp$. In other words, we can also measure the relative phase between the parity-odd and parity-even amplitudes. Such a phase can arise if CP-symmetry is violated in HZZ interactions or could indicate pseudo-time reversal violation arising from loop level contributions or rescattering effects akin to the strong phase in strong interactions. Since such a term requires contributions from both parity-even and parity-odd partial waves, $V_2^{(0)} = 0$ in SM. In the case of SM we have $a = 1$ and $b = c = 0$. Assuming narrow width approximation for the on-shell Z_1 we get

$$F_\perp = 0, \tag{1.31}$$

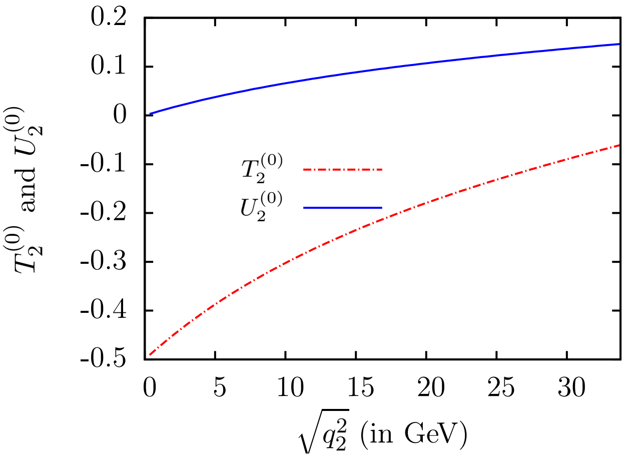

(a) Plot of $T_2^{(0)}$ and $U_2^{(0)}$ vs $\sqrt{q_2^2}$.

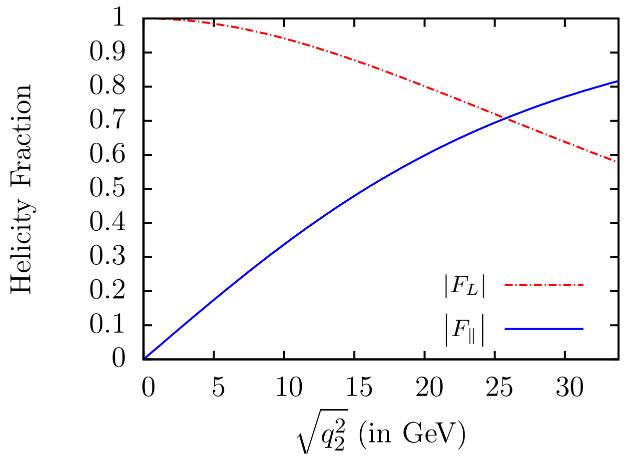

(b) Plot of F_L and $F_{\parallel}$ vs. $\sqrt{q_2^2}$.

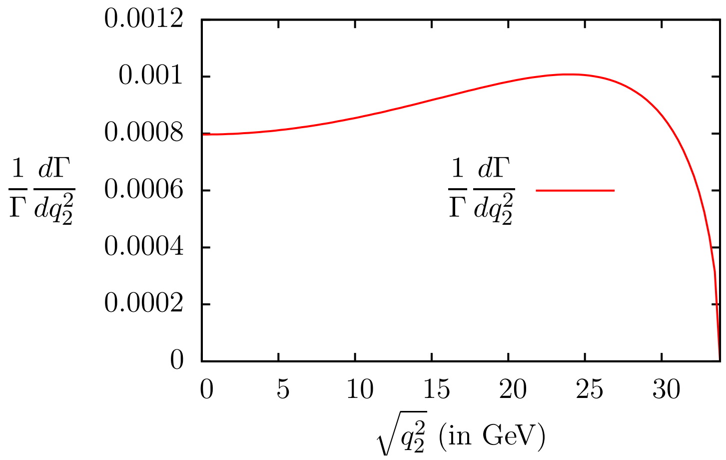

(c) Plot of $\frac{1}{\Gamma}\frac{d\Gamma}{dq_2^2}$ vs $\sqrt{q_2^2}$.

Figure 1.2: Plots of various observables in SM only. We have used $M_H = 125$ GeV, $\sqrt{q_1^2} = 91.18$ GeV for the above plots. The integrated values for the observables $T_2^{(0)}$ and $U_2^{(0)}$ are uniquely predicted in SM at tree level to be -0.148 and 0.117 respectively.

$$\frac{F_L}{F_{\|}} \equiv \mathsf{T} = \frac{M_H^2 - M_Z^2 - q_2^2}{2\sqrt{2}M_Z\sqrt{q_2^2}}. \tag{1.32}$$

Clearly, for the case of SM the term T has a characteristic dependence on $\sqrt{q_2^2}$. Demanding $F_\perp = 0$, we get

$$U_2^{(0)} = \frac{1}{6}\left(1 + 2\,T_2^{(0)}\right), \tag{1.33}$$

and

$$|\mathsf{T}| = \frac{1 - 4\,T_2^{(0)}}{2 + 4\,T_2^{(0)}}. \tag{1.34}$$

Thus for SM we can predict the experimental values for the coefficients $T_2^{(0)}$ and $U_2^{(0)}$ as:

$$T_2^{(0)} = \frac{1}{4}\left(\frac{1 - 2\,|\mathsf{T}|}{1 + |\mathsf{T}|}\right), \qquad U_2^{(0)} = \frac{1}{4\,(1 + |\mathsf{T}|)}. \tag{1.35}$$

It is evident that $T_2^{(0)}$ and $U_2^{(0)}$ are functions of $\sqrt{q_2^2}$ alone and are uniquely predicted in the SM. $T_2^{(0)}$ and $U_2^{(0)}$ are pure numbers for a given value of $\sqrt{q_2^2}$. Their variation with respect to $\sqrt{q_2^2}$ is shown in Fig. 1.2a. It is clear from the plot that $T_2^{(0)}$ is always negative while $U_2^{(0)}$ is always positive in the SM. The variation of the helicity fractions with respect to $\sqrt{q_2^2}$ is shown in Fig. 1.2b. Fig. 1.2c also shows the variation of the normalized differential decay width of the SM Higgs decaying to four charged leptons via two Z bosons, with respect to $\sqrt{q_2^2}$. Fig. 1.2 contains all the vital experimental signatures of the SM Higgs and must be verified in order for the new boson to be consistent with the SM Higgs boson. We emphasize that a nonzero measurement of $F_\perp$ will be a litmus test indicating a non-SM behavior for the Higgs. Furthermore, a non-zero $V_2^{(0)}$ would imply that the observed resonance is not of definite parity.

If we find the new boson to be of $J^{PC} = 0^{++}$, but still not exactly like the SM Higgs, then we need to know the values of a and b in the vertex factor of Eq. (1.1). It is easy to find that for a general 0^{++} boson, the values of both a and b are given by

$$a = \frac{F_{\parallel}\sqrt{\Gamma_f/\mathcal{N}}}{\sqrt{2}M_Z\sqrt{q_2^2}}, \tag{1.36}$$

$$b = \frac{\sqrt{\Gamma_f/\mathcal{N}}}{M_H^2 X^2}\left(F_L - \frac{M_H^2 - M_Z^2 - q_2^2}{2\sqrt{2}M_Z\sqrt{q_2^2}}F_{\parallel}\right). \tag{1.37}$$

For SM $a = 1$ and $b = 0$ at tree level only. At loop level even within SM these values would differ. It may be hoped that a and b determined in this way may enable testing SM even at one loop level once sufficient data is acquired. This is significant as triple-Higgs vertex contributes at one loop level and *measurement of b may provide the first verification of the Higgs-self coupling*. Even if the scalar boson is not a parity eigenstate but an admixture of even and odd parity states, Eqs. (1.36) and (1.37) can be used to determine a and b. We can determine c by measuring $F_\perp$:

$$c = \frac{F_{\perp}\sqrt{\Gamma_f/\mathcal{N}}}{\sqrt{2}M_Z\sqrt{q_2^2}M_H X}, \tag{1.38}$$

Therefore, it is possible to get exact solutions for a, b, c in terms of the experimentally observable quantities like F_L, $F_{\parallel}$, $F_\perp$ and Γ_f.

We want to stress that it is impossible to extract out both a and b by measuring only one uniangular distribution (corresponding to either $\cos\theta_1$ or $\cos\theta_2$), since the helicity amplitude A_L contains both a and b. Hence, it is not possible to conclude that the 0^{++} boson is a Standard Model Higgs by studying $\cos\theta_1$ or $\cos\theta_2$ distributions alone.

The current data set is limited and may allow binning only in one variable. We therefore examine what conclusions can be made if q_2^2 is also integrated out and only the three uniangular distributions are studied individually. As can be seen from Eqs. (1.36), (1.37) and (1.38) we can obtain some weighted averages of a and c. These equations will only allow us to verify whether $a = 1$ and $c = 0$. In addition the presence of any phase between the parity-even and parity-odd amplitudes can still be inferred from Eq. (1.18). The integrated values for the observables $T_2^{(0)}$ and $U_2^{(0)}$ are uniquely predicted in SM at tree level to be -0.148 and 0.117 respectively.

1.2.2 If the 125 GeV resonance were Spin-2

As stated in the Introduction we shall use the same symbol H to denote the boson even if it is of Spin-2. The most general HZZ vertex factor $V_{HZZ}^{\mu\nu;\alpha\beta}$ for Spin-2 boson, with polarization $\epsilon_{(T)}^{\mu\nu}$ has the following tensor structure

$$\begin{aligned}
V_{HZZ}^{\mu\nu;\alpha\beta} \;=\;& A\left(g^{\alpha\nu}\, g^{\beta\mu} + g^{\alpha\mu}\, g^{\beta\nu}\right) + B\left(Q^{\mu}\left(Q^{\alpha}\, g^{\beta\nu} + Q^{\beta}\, g^{\alpha\nu}\right) + Q^{\nu}\left(Q^{\alpha}\, g^{\beta\mu} + Q^{\beta}\, g^{\alpha\mu}\right)\right) \\
&+C\left(Q^{\mu}\, Q^{\nu}\, g^{\alpha\beta}\right) - D\left(Q^{\alpha}\, Q^{\beta}\, Q^{\mu}\, Q^{\nu}\right) + 2i\, E(g^{\beta\nu}\, \epsilon^{\alpha\mu\rho\sigma} - g^{\alpha\nu}\, \epsilon^{\beta\mu\rho\sigma} \\
&+g^{\beta\mu}\, \epsilon^{\alpha\nu\rho\sigma} - g^{\alpha\mu}\, \epsilon^{\beta\nu\rho\sigma})q_{1\rho}q_{2\sigma} + i\, F(Q^{\beta}\, (Q^{\nu}\, \epsilon^{\alpha\mu\rho\sigma} + Q^{\mu}\, \epsilon^{\alpha\nu\rho\sigma}) \\
&-Q^{\alpha}\left(Q^{\nu}\, \epsilon^{\beta\mu\rho\sigma} + Q^{\mu}\, \epsilon^{\beta\nu\rho\sigma}\right))q_{1\rho}q_{2\sigma},
\end{aligned} \tag{1.39}$$

where ϵ_α and ϵ_β are the polarizations of the two Z bosons; A, B, C, D, E and F are arbitrary coefficients and Q is the difference of the four momenta of the two Z's, i.e. $Q = q_1 - q_2$. Only the term that is associated with the coefficient A is dimensionless. The form of the vertex factor ensures that $P_\mu\epsilon_{(T)}^{\mu\nu} = P_\nu\epsilon_{(T)}^{\mu\nu} = 0$ and $g_{\mu\nu}\epsilon_{(T)}^{\mu\nu} = 0$, which stem from the fact that the field of a Spin-2 particle is described by a symmetric, traceless tensor with null four-divergence. Here like the Spin-0 case P is the sum of the four-momenta of the two Z's, i.e. $P = q_1 + q_2$. Since we are considering the decay of Higgs to two Z bosons, the vertex factor must be symmetric under exchange of the two identical bosons. This is taken care of by making the vertex factor symmetric under simultaneous exchange of α, β and corresponding momenta of Z_1 and Z_2. The Lagrangian that gives rise to the vertex factor $V_{HZZ}^{\mu\nu;\alpha\beta}$ contains higher dimensional operators, which are responsible for the momentum dependence of the form factors.

In $V_{HZZ}^{\mu\nu;\alpha\beta}$ the terms that are proportional to E and F are parity-odd and the rest of the terms in $V_{HZZ}^{\mu\nu;\alpha\beta}$ are parity-even. From helicity analysis it is known that the decay of a massive Spin-2 particle to two identical, massive, Spin-1 particles is described by six helicity amplitudes. Bose symmetry between the pair of Z bosons [38, 39] imposes constraints on the vertex $V_{HZZ}^{\mu\nu;\alpha\beta}$ such that it gets contributions from two parity-odd terms that are admixture of one $\mathcal{P}$-wave and one $\mathcal{F}$-wave, and four parity-even terms that are some combinations of one $\mathcal{S}$-wave, two $\mathcal{D}$-waves and one $\mathcal{G}$-wave contributions. Even for the case of Spin-2 boson we choose to work with helicity amplitudes as they are orthogonal but choose a basis such that amplitudes have definite parity associated with them. We find the following six helicity amplitudes in transversity basis:

$$A_L = \frac{4X}{3\mathsf{u}_1}\Big(E\left(\mathsf{u}_2^4 - M_H^2\mathsf{u}_1^2\right) + F\left(4\mathsf{u}_1^2 M_H^2 X^2\right)\Big), \tag{1.40}$$

$$A_M = \frac{8\sqrt{q_1^2\,q_2^2}\,\mathsf{v}X}{3\sqrt{3}\mathsf{u}_1}\,E, \tag{1.41}$$

$$\begin{aligned} A_1 = \frac{2\sqrt{2}}{3\sqrt{3}M_H^2}\Big(&A\left(M_H^4 - \mathsf{u}_2^4\right) - B\left(8M_H^4X^2\right) \\ &+ C\left(4M_H^2X^2\right)\left(\mathsf{u}_1^2 - M_H^2\right) \\ &- D\left(8M_H^4X^4\right)\Big), \end{aligned} \tag{1.42}$$

$$A_2 = \frac{8\sqrt{q_1^2\,q_2^2}}{3\sqrt{3}}\left(A + 4X^2C\right), \tag{1.43}$$

$$A_3 = \frac{4}{3M_H\mathsf{u}_1}\Big(A\left(\mathsf{u}_2^4 - M_H^2\mathsf{u}_1^2\right) + B\left(4\mathsf{u}_1^2M_H^2X^2\right)\Big), \tag{1.44}$$

$$A_4 = \frac{8\sqrt{q_1^2\,q_2^2}\,\mathsf{w}}{3M_H\mathsf{u}_1}\,A, \tag{1.45}$$

where u_1, u_2, v and w are defined as

$$\mathsf{u}_1^2 = q_1^2 + q_2^2, \tag{1.46}$$

$$\mathsf{u}_2^2 = q_1^2 - q_2^2, \tag{1.47}$$

$$\mathsf{v}^2 = 4M_H^2\mathsf{u}_1^2 + 3\mathsf{u}_2^4, \tag{1.48}$$

$$\mathsf{w}^2 = 2M_H^2\mathsf{u}_1^2 + \mathsf{u}_2^4. \tag{1.49}$$

The quantity Z' is as defined in Eq. (1.5).

We wish to clarify that our vertex factor $V_{HZZ}^{\mu\nu;\alpha\beta}$ is the most general one. An astute reader can easily write down terms that are not included in our vertex and wonder how such a conclusion of generality can be made. For example, one can add a new possible term such as $i\,G\,\left(\epsilon^{\alpha\beta\nu\rho}P_\rho Q^\mu + \epsilon^{\alpha\beta\mu\rho}P_\rho Q^\nu\right)$. It is easy to verify that this new form factor G enters our helicity amplitudes A_L and A_M in the combination $(E-2G)$:

$$A_L = \frac{4X}{3\mathsf{u}_1}\Big((E-2G)\left(\mathsf{u}_2^4 - M_H^2\mathsf{u}_1^2\right) + F\left(4\mathsf{u}_1^2M_H^2X^2\right)\Big), \tag{1.50}$$

$$A_M = \frac{8\sqrt{q_1^2\,q_2^2}\,\mathsf{v}X}{3\sqrt{3}\mathsf{u}_1}\;(E-2G)\,. \tag{1.51}$$

Note that only this combination of E and G is accessible to experiments and all other helicity amplitudes remain unchanged. Since, there exist only six independent helicity amplitudes corresponding to six partial waves for the Spin-2 case, the number of helicity amplitudes in the transversity basis must also be six. Adding any new terms to the vertex factor will simply modify the expressions for the helicity amplitudes. The generality of our vertex $V_{HZZ}^{\mu\nu;\alpha\beta}$ is therefore very robust. Having established the generality of $V_{HZZ}^{\mu\nu;\alpha\beta}$ we will henceforth not consider any term absent in the vertex of Eq. (1.39). Our helicity amplitudes are different from those given in Ref. [86]. In Ref. [86], they provide eight independent helicity amplitudes. If we consider the Bose symmetry of the two identical vector bosons to which H is decaying, then these should reduce to six independent helicity amplitudes. Again as stated in the scalar case, our helicity amplitudes are classified by their parity and thus differ from those in Ref. [86]. Our amplitudes A_L and A_M have parity-odd behavior, and the rest of the helicity amplitudes have parity-even behavior. In contrast not all the amplitudes enunciated in Ref. [86] have clear parity characteristics.

Once again just as in the scalar case we will start by assuming that Z_1 is on-shell while Z_2 is off-shell. The integration over q_1^2 is done using the narrow width approximation of the Z. In tensor case, however, off-shell Z_1 will also have to be considered in a special case. We hence consider that q_1^2 is explicitly integrated out whether Z_1 is off-shell or fully on-shell. In case Z_1 is off-shell the resulting helicities are some weighted averaged value and should not be confused with well defined values at $q_1^2 \equiv M_Z^2$. The differential decay rate for the process $H \to Z_1 + Z_2^* \to (\ell_1^- + \ell_1^+) + (\ell_2^- + \ell_2^+)$, after integrating over q_1^2 (assuming Z_1 is on-shell or even otherwise) can now be written in terms of the angular distribution using the vertex given in Eq. (1.39) as:

$$
\begin{aligned}
&\frac{8\pi}{\Gamma_f}\frac{d^4\Gamma}{dq_2^2\, d\cos\theta_1\, d\cos\theta_2\, d\phi} \\
&= 1 + \left(\frac{1}{4}|F_2|^2 - \left(M_H^2\frac{\mathsf{u}_1^2}{\mathsf{v}^2}\right)|F_M|^2\right)\cos 2\phi\,(1-P_2(\cos\theta_1))\,(1-P_2(\cos\theta_2)) \\
&\quad + \left(M_H\frac{\mathsf{u}_1}{\mathsf{v}}\right)\mathrm{Im}(F_2F_M^*)\,\sin 2\phi\,(1-P_2(\cos\theta_1))\,(1-P_2(\cos\theta_2)) \\
&\quad + \frac{P_2(\cos\theta_1)}{2}\Bigg(\left(-2|F_1|^2+|F_2|^2\right)+\left(|F_3|^2+|F_L|^2\right)\left(\frac{q_1^2-2q_2^2}{\mathsf{u}_1^2}\right) \\
&\quad + |F_M|^2\left(4M_H^2\frac{\mathsf{u}_1^2}{\mathsf{v}^2}+3\frac{\mathsf{u}_2^4}{\mathsf{u}_1^2\mathsf{v}^2}\left(q_2^2-2q_1^2\right)\right)+|F_4|^2\left(2M_H^2\frac{\mathsf{u}_1^2}{\mathsf{w}^2}+\frac{\mathsf{u}_2^4}{\mathsf{u}_1^2\mathsf{w}^2}\left(q_2^2-2q_1^2\right)\right) \\
&\quad + \left(6\sqrt{q_1^2\,q_2^2}\frac{\mathsf{u}_2^2}{\mathsf{u}_1^2\mathsf{w}}\right)\mathrm{Re}(F_3F_4^*)+\left(6\sqrt{3}\sqrt{q_1^2\,q_2^2}\frac{\mathsf{u}_2^2}{\mathsf{u}_1^2\mathsf{v}}\right)\mathrm{Re}(F_LF_M^*)\Bigg) \\
&\quad + \frac{P_2(\cos\theta_2)}{2}\Bigg(\left(-2|F_1|^2+|F_2|^2\right)+\left(|F_3|^2+|F_L|^2\right)\left(\frac{q_2^2-2q_1^2}{\mathsf{u}_1^2}\right) \\
&\quad + |F_M|^2\left(4M_H^2\frac{\mathsf{u}_1^2}{\mathsf{v}^2}+3\frac{\mathsf{u}_2^4}{\mathsf{u}_1^2\mathsf{v}^2}\left(q_1^2-2q_2^2\right)\right)+|F_4|^2\left(2M_H^2\frac{\mathsf{u}_1^2}{\mathsf{w}^2}+\frac{\mathsf{u}_2^4}{\mathsf{u}_1^2\mathsf{w}^2}\left(q_1^2-2q_2^2\right)\right)
\end{aligned}
$$

$$
\begin{aligned}
&- \left(6\sqrt{q_1^2\, q_2^2}\frac{\mathsf{u}_2^2}{\mathsf{u}_1^2\mathsf{w}}\right)\ \mathrm{Re}(F_3F_4^*) - \left(6\sqrt{3}\sqrt{q_1^2\, q_2^2}\frac{\mathsf{u}_2^2}{\mathsf{u}_1^2\mathsf{v}}\right)\ \mathrm{Re}(F_LF_M^*)\Bigg) \\
&+ \frac{P_2(\cos\theta_1)P_2(\cos\theta_2)}{2}\Bigg(2\,|F_1|^2 + \frac{1}{2}\,|F_2|^2 - |F_3|^2 - |F_L|^2 - \left(\frac{\mathsf{u}_2^4 - M_H^2\mathsf{u}_1^2}{\mathsf{w}^2}\right)|F_4|^2 \\
&+ \left(\frac{2M_H^2\mathsf{u}_1^2 - 3\mathsf{u}_2^4}{\mathsf{v}^2}\right)|F_M|^2\Bigg) + \frac{9\sin 2\theta_1\sin 2\theta_2\cos\phi}{16}\Bigg(\left(|F_3|^2 - |F_L|^2\right)\left(\frac{\sqrt{q_1^2\, q_2^2}}{\mathsf{u}_1^2}\right) \\
&+ 3\,|F_M|^2\left(\sqrt{q_1^2\, q_2^2}\frac{\mathsf{u}_2^4}{\mathsf{u}_1^2\mathsf{v}^2}\right) - |F_4|^2\left(\sqrt{q_1^2\, q_2^2}\frac{\mathsf{u}_2^4}{\mathsf{u}_1^2\mathsf{w}^2}\right) \\
&- \left(\frac{\mathsf{u}_2^4}{\mathsf{u}_1^2\mathsf{w}}\right)\mathrm{Re}(F_3F_4^*) + \left(\sqrt{3}\frac{\mathsf{u}_2^4}{\mathsf{u}_1^2\mathsf{v}}\right)\mathrm{Re}(F_LF_M^*) - \sqrt{2}\,\mathrm{Re}(F_1F_2^*)\Bigg) \\
&+ \frac{9\sin 2\theta_1\sin 2\theta_2\sin\phi}{16}\Bigg(\left(2\frac{\sqrt{q_1^2\, q_2^2}}{\mathsf{u}_1^2}\right)\mathrm{Im}(F_3F_L^*) - \left(\sqrt{3}\frac{\mathsf{u}_2^4}{\mathsf{u}_1^2\mathsf{v}}\right)\mathrm{Im}(F_3F_M^*) \\
&- \left(\frac{\mathsf{u}_2^4}{\mathsf{u}_1^2\mathsf{w}}\right)\mathrm{Im}(F_4F_L^*) - \left(2\sqrt{3}\sqrt{q_1^2\, q_2^2}\frac{\mathsf{u}_2^4}{\mathsf{u}_1^2\mathsf{v}\mathsf{w}}\right)\mathrm{Im}(F_4F_M^*) - \left(2\sqrt{2}M_H\frac{\mathsf{u}_1}{\mathsf{v}}\right)\mathrm{Im}(F_1F_M^*)\Bigg) \\
&+ \mathscr{M},
\end{aligned}
\tag{1.52}
$$

where $\mathscr{M}$ includes all the terms that are proportional to η and η^2 written explicitly in the AppendixA.2, Eq. (A.25). The helicity fractions are defined as

$$
F_i = \frac{A_i}{\sqrt{\sum_j \left|A_j\right|^2}}, \tag{1.53}
$$

and $\Gamma_f$is given by

$$
\Gamma_f \equiv \frac{d\Gamma}{dq_2^2} = \frac{1}{5}\ \frac{9}{2^{10}}\ \frac{1}{\pi^3}\ X\ \frac{\mathrm{Br}_{\ell\ell}^2}{M_H^2}\ \frac{\Gamma_Z}{M_Z^3}\ \frac{\sum_j \left|A_j\right|^2}{\left(\left(q_2^2 - M_Z^2\right)^2 + M_Z^2\Gamma_Z^2\right)}, \tag{1.54}
$$

where $i, j \in \{L, M, 1, 2, 3, 4\}$ and we have averaged over the 5 initial polarization states of the Spin-2 boson.

The uniangular distributions are given by

$$\frac{1}{\Gamma_f}\frac{d^2\Gamma}{dq_2^2\, d\cos\theta_1} = \frac{1}{2} + T_2^{(2)}\, P_2(\cos\theta_1) - T_1^{(2)}\, \cos\theta_1, \tag{1.55}$$

$$\frac{1}{\Gamma_f}\frac{d^2\Gamma}{dq_2^2\, d\cos\theta_2} = \frac{1}{2} + T_2'^{(2)}\, P_2(\cos\theta_2) + T_1'^{(2)}\, \cos\theta_2, \tag{1.56}$$

$$\frac{2\pi}{\Gamma_f}\frac{d^2\Gamma}{dq_2^2\, d\phi} = 1 + U_2^{(2)}\, \cos 2\phi + V_2^{(2)}\, \sin 2\phi + U_1^{(2)}\, \cos\phi + V_1^{(2)}\, \sin\phi, \tag{1.57}$$

where the superscript (2) is used to denote the fact that the concerned coefficients are for Spin-2 resonance, and

$$\begin{aligned} T_2^{(2)} = \frac{1}{4}\Big(&- 2\,|F_1|^2 + |F_2|^2 + \big(|F_3|^2 + |F_L|^2\big)\left(\frac{q_1^2 - 2q_2^2}{\mathsf{u}_1^2}\right) \\ &+ |F_4|^2 \left(2M_H^2\frac{\mathsf{u}_1^2}{\mathsf{w}^2} + \frac{\mathsf{u}_2^4}{\mathsf{u}_1^2\mathsf{w}^2}\left(q_2^2 - 2q_1^2\right)\right) + |F_M|^2 \left(4M_H^2\frac{\mathsf{u}_1^2}{\mathsf{v}^2} + 3\frac{\mathsf{u}_2^4}{\mathsf{u}_1^2\mathsf{v}^2}\left(q_2^2 - 2q_1^2\right)\right) \\ &+ 6\sqrt{q_1^2\, q_2^2}\frac{\mathsf{u}_2^2}{\mathsf{u}_1^2\mathsf{v}\mathsf{w}}\left(\mathsf{v}\,\mathrm{Re}(F_3F_4^*) + \sqrt{3}\mathsf{w}\,\mathrm{Re}(F_LF_M^*)\right)\Big), \end{aligned} \tag{1.58}$$

$$\begin{aligned} T_2'^{(2)} = \frac{1}{4}\Big(&- 2\,|F_1|^2 + |F_2|^2 + \big(|F_3|^2 + |F_L|^2\big)\left(\frac{q_2^2 - 2q_1^2}{\mathsf{u}_1^2}\right) \\ &+ |F_4|^2 \left(2M_H^2\frac{\mathsf{u}_1^2}{\mathsf{w}^2} + \frac{\mathsf{u}_2^4}{\mathsf{u}_1^2\mathsf{w}^2}\left(q_1^2 - 2q_2^2\right)\right) + |F_M|^2 \left(4M_H^2\frac{\mathsf{u}_1^2}{\mathsf{v}^2} + 3\frac{\mathsf{u}_2^4}{\mathsf{u}_1^2\mathsf{v}^2}\left(q_1^2 - 2q_2^2\right)\right) \\ &- 6\sqrt{q_1^2\, q_2^2}\frac{\mathsf{u}_2^2}{\mathsf{u}_1^2\mathsf{v}\mathsf{w}}\left(\mathsf{v}\,\mathrm{Re}(F_3F_4^*) + \sqrt{3}\mathsf{w}\,\mathrm{Re}(F_LF_M^*)\right)\Big), \end{aligned} \tag{1.59}$$

$$U_2^{(2)} = \frac{1}{4}\,|F_2|^2 - \frac{M_H^2\mathsf{u}_1^2}{\mathsf{v}^2}\,|F_M|^2\,, \tag{1.60}$$

$$V_2^{(2)} = M_H\frac{\mathsf{u}_1}{\mathsf{v}}\,\mathrm{Im}(F_2F_M^*), \tag{1.61}$$

$$\begin{aligned} T_1^{(2)} = \frac{3\eta}{2\mathsf{u}_1^2\mathsf{v}\mathsf{w}}\Big(&2M_H\mathsf{u}_1^3\mathsf{w}\,\mathrm{Re}(F_2F_M^*) + q_1^2\mathsf{v}\mathsf{w}\,\mathrm{Re}(F_3F_L^*) \\ &+ \sqrt{q_2^2}\mathsf{u}_2^2\left(\sqrt{3}\sqrt{q_1^2}\mathsf{w}\,\mathrm{Re}(F_3F_M^*) + \sqrt{q_1^2}\mathsf{v}\,\mathrm{Re}(F_4F_L^*) + \sqrt{3}\sqrt{q_2^2}\mathsf{u}_2^2\,\mathrm{Re}(F_4F_M^*)\right)\Big), \end{aligned} \tag{1.62}$$

$$T_1'^{(2)} = \frac{3\eta}{2\mathsf{u}_1^2\mathsf{v}\mathsf{w}}\Big(2M_H\mathsf{u}_1^3\mathsf{w}\,\mathrm{Re}(F_2F_M^*) + q_2^2\mathsf{v}\mathsf{w}\,\mathrm{Re}(F_3F_L^*)$$

$$+ \sqrt{q_1^2}\mathsf{u}_2^2 \left(-\sqrt{3}\sqrt{q_2^2}\mathsf{w}\,\mathrm{Re}(F_3 F_M^*) - \sqrt{q_2^2}\mathsf{v}\,\mathrm{Re}(F_4 F_L^*) + \sqrt{3}\sqrt{q_1^2}\mathsf{u}_2^2\,\mathrm{Re}(F_4 F_M^*) \right) \Big), \tag{1.63}$$

$$U_1^{(2)} = \frac{9\pi^2\eta^2}{64\mathsf{u}_1^2\mathsf{v}^2\mathsf{w}^2} \Big(\sqrt{2}\mathsf{u}_1^2\mathsf{v}^2\mathsf{w}^2\,\mathrm{Re}(F_1 F_2^*) - \mathsf{u}_2^4\mathsf{v}^2\mathsf{w}\,\mathrm{Re}(F_3 F_4^*) + |F_3|^2\sqrt{q_1^2\,q_2^2}\mathsf{v}^2\mathsf{w}^2$$
$$- |F_4|^2\sqrt{q_1^2\,q_2^2}\mathsf{u}_2^4\mathsf{v}^2 + \sqrt{3}\mathsf{u}_2^4\mathsf{v}\mathsf{w}^2\,\mathrm{Re}(F_L F_M^*) - |F_L|^2\sqrt{q_1^2\,q_2^2}\mathsf{v}^2\mathsf{w}^2$$
$$+ 3\,|F_M|^2\sqrt{q_1^2\,q_2^2}\mathsf{u}_2^4\mathsf{w}^2 \Big), \tag{1.64}$$

$$V_1^{(2)} = \frac{9\pi^2\eta^2}{64\mathsf{u}_1^2\mathsf{v}\mathsf{w}} \Big(2\sqrt{2}M_H\mathsf{u}_1^3\mathsf{w}\,\mathrm{Im}(F_1 F_M^*) + 2\sqrt{q_1^2\,q_2^2}\mathsf{v}\mathsf{w}\,\mathrm{Im}(F_3 F_L^*)$$
$$- \sqrt{3}\mathsf{u}_2^4\mathsf{w}\,\mathrm{Im}(F_3 F_M^*) - \mathsf{u}_2^4\mathsf{v}\,\mathrm{Im}(F_4 F_L^*) - 2\sqrt{3}\mathsf{u}_2^4\sqrt{q_1^2\,q_2^2}\,\mathrm{Im}(F_4 F_M^*) \Big). \tag{1.65}$$

These coefficients can again be extracted from asymmetries similar to those defined in Eqs. (1.22), (1.23), (1.24), (1.25), (1.26) and (1.27) for the Spin-0 case. We find that the angular distributions corresponding to $P_2(\cos\theta_1)$ and $P_2(\cos\theta_2)$ are different in the Spin-2 case in contrast to the Spin-0 case. This feature can enable us to distinguish between the two spins, unless the difference happens to be zero for certain choice of parameters, even in the Spin-2 case. Considering only the η independent terms in Eqs. (1.55) and (1.56), the difference Δ between the coefficients of $P_2(\cos\theta_1)$ and $P_2(\cos\theta_2)$ in $\dfrac{1}{\Gamma_f}\dfrac{d^2\Gamma}{dq_2^2\;d\cos\theta_1}$ and $\dfrac{1}{\Gamma_f}\dfrac{d^2\Gamma}{dq_2^2\;d\cos\theta_2}$ respectively, is

$$\Delta = \frac{3\mathsf{u}_2^2}{4\mathsf{u}_1^2\mathsf{v}^2\mathsf{w}^2} \Big(\mathsf{v}^2\mathsf{w}^2 \left(|F_3|^2 + |F_L|^2 \right)$$
$$- \mathsf{u}_2^4 \left(\mathsf{v}^2\,|F_4|^2 + 3\,\mathsf{w}^2\,|F_M|^2 \right) \Big)$$
$$+ \frac{3\sqrt{q_1^2\,q_2^2}\mathsf{u}_2^2}{\mathsf{u}_1^2\mathsf{v}\mathsf{w}} \Big(\mathsf{v}\,\mathrm{Re}(F_3 F_4^*) + \sqrt{3}\,\mathsf{w}\,\mathrm{Re}(F_L F_M^*) \Big). \tag{1.66}$$

If we find that $\Delta = 0$ for all $\sqrt{q_2^2}$, then the tensor case would have similar characteristics in the uniangular distributions as discussed in the scalar case. However, this can only happen if helicity amplitudes (or equivalently the corresponding coefficients A, B, C, D, E and F) have the explicit momentum dependence so as to absorb $\sqrt{q_2^2}$ completely in Δ. The reader can examine the expression for Δ to conclude that this is impossible and the only way Δ can be equated to zero for all $\sqrt{q_2^2}$, is when

$$F_3 = F_4 = F_L = F_M = 0. \tag{1.67}$$

In such a special case all the form-factors in vertex $V_{HZZ}^{\mu\nu;\alpha\beta}$ vanish, except C and D. This special case explicitly implies that the parity of the Spin-2 boson is even. We will refer to this case as the special $J^P = 2^+$ case, since the uniangular distribution mimics the $J^P = 0^+$ case. Working under this special case

$$\frac{1}{\Gamma_f}\frac{d^2\Gamma}{dq_2^2\, d\cos\theta_1} = \frac{1}{2} + T_2^{(2)} P_2(\cos\theta_1), \tag{1.68}$$

$$\frac{1}{\Gamma_f}\frac{d^2\Gamma}{dq_2^2\, d\cos\theta_2} = \frac{1}{2} + T_2^{(2)} P_2(\cos\theta_2), \tag{1.69}$$

$$\frac{2\pi}{\Gamma_f}\frac{d^2\Gamma}{dq_2^2\, d\phi} = 1 + U_2^{(2)}\cos 2\phi + U_1^{(2)}\cos\phi, \tag{1.70}$$

where the $T_2^{(2)}$, $U_2^{(2)}$ and $U_1^{(2)}$ are now given by

$$T_2^{(2)} = \frac{1}{4}\left(|F_2|^2 - 2\,|F_1|^2\right), \tag{1.71}$$

$$U_2^{(2)} = \frac{1}{4}\,|F_2|^2\,, \tag{1.72}$$

$$U_1^{(2)} = \frac{9\pi^2}{32\sqrt{2}}\,\eta^2\,\mathrm{Re}(F_1 F_2^*) \tag{1.73}$$

Now using the identity $|F_1|^2 + |F_2|^2 = 1$, we get

$$U_2^{(2)} = \frac{1}{6}\left(1 + 2T_2^{(2)}\right). \tag{1.74}$$

Note the similarity between Eqs. (1.33) and (1.74). The conclusions that $J^P = 2^\pm$ when $\Delta \neq 0$ can also be drawn if Δ integrated over q_1^2 and q_2^2 is found to be non zero. However, it clear from Eq. (1.66) that the domain of integration for q_1^2 and q_2^2 cannot be symmetric.

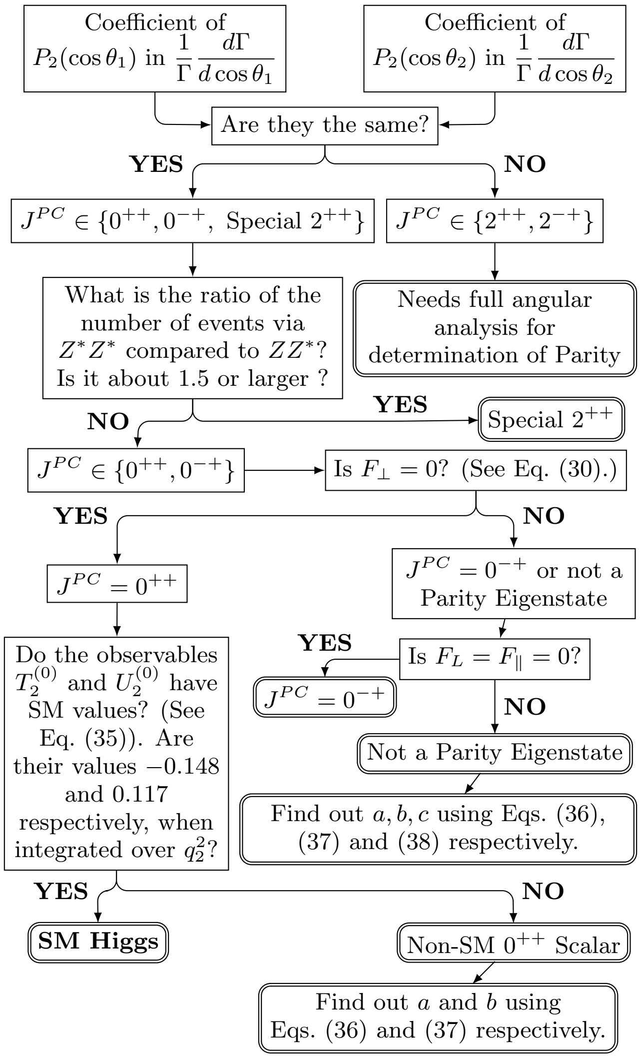

Figure 1.3: Flow chart for determination of spin and parity of the new boson. See text for details.

1.2.3 Comparison Between Spin-0 and Spin-2

Having discussed both the scalar and tensor case, we summarize the procedure to distinguish the spin and parity states of the new boson in a flowchart in Fig. 3.2. The procedure entailed, ensures that we convincingly determine the spin and parity of the boson. The first step should be to compare the uniangular distributions in $\cos\theta_1$ and $\cos\theta_2$. If the distribution is found to be different the boson cannot be the SM Higgs and indeed must have Spin-2. However, if the distributions are found to be identical the resonance can have Spin-0 or be a very special case of Spin-2 arising only from C and D terms in the vertex in Eq. (1.39). The similarity between Eqs. (1.33) and (1.74) makes it impossible to distinguish these two cases by looking at angular distributions alone.

The special $J^P = 2^+$ case can nevertheless still be identified by examining the surviving helicity amplitudes A_1 and A_2. The helicity amplitudes given in Eqs. (1.42) and (1.43) reduce in this special case to,

$$A_1 = -\frac{16\sqrt{2}}{3\sqrt{3}}\, X^2 \left(q_1.q_2\, C + M_H^2 X^2\, D\right), \tag{1.75}$$

$$A_2 = \frac{32}{3\sqrt{3}}\, \sqrt{q_1^2\, q_2^2}\, X^2\, C. \tag{1.76}$$

These may be compared with Eqs. (1.2) and (1.3) to notice that they have identical form, except for an additional X^2 dependence in A_1 and A_2 expressions above. The additional X^2 dependence increases the contribution from both off-shell Z's (called Z^*Z^*) significantly in comparison to the dominant one on-shell and one off-shell Z (called ZZ^*) contribution expected in SM. In the SM one would expect the ratio of the number of events in Z^*Z^* to ZZ^* channel to be about 0.2. However, in the special $J^P = 2^+$ case we would expect this ratio to be about 1.5. Thef reader is cautioned not to confuse this explicit X^2 dependence with any assumption on the momentum dependence of the form-factors. Throughout the analysis we have assumed the most general form-factors a, b, c, A, B, C, D, E and F, nevertheless A_1 and A_2 turn out to have additional X^2 dependence in comparison to A_L and $A_\parallel$ respectively. This explicit X^2 dependence arises due to contributions only from higher dimensional operators in the special $J^P = 2^+$ case.

Having excluded the Spin-2 possibility, the resonance would be a parity-odd state (0^{-+}) if $F_L = F_{\|} = 0$ and a parity-even state (0^{++}) if $F_\perp = 0$. If the resonance is found to be in 0^{++} state, we need to check whether $T_2^{(0)}$ and $U_2^{(0)}$ terms are as predicted in SM. The values of $T_2^{(0)}$ and $U_2^{(0)}$ as a function of $\sqrt{q_2^2}$ are plotted in Fig. 1.2. The q_2^2 integrated values for the observables $T_2^{(0)}$ and $U_2^{(0)}$ are uniquely predicted in SM at tree level to be -0.148 and 0.117 respectively. These tests would ascertain whether the 0^{++} state is the SM Higgs or some non-SM boson. If it turns out to be a non-SM boson, we can also measure the coefficients a, b, c by using Eqs. (1.36), (1.37) and (1.38).

Finally we emphasize that our approach is unique in using helicity amplitudes in the transversity basis so that the amplitudes are classified by parity. We also use orthogonality of Legendre polynomials in $\cos\theta_1$ and $\cos\theta_2$ as well as a Fourier series in ϕ to unambiguously determine the spin and parity of the new resonance. Another significant achievement is the use of the most general HZZ vertex factors for both Spin-0 and Spin-2 cases allowing us to determine the nature of H be it in any extension of the SM. We wish to stress that we consider neither any specific mode of production of the new resonance (like gluon-gluon fusion or vector boson fusion), nor any specific model for its couplings. The production channel for the new resonance has no role in our analysis. We consider its decay only to four leptons via two Z bosons. Most discussions in current literature deal either with specific production channels or with specific models of new physics which restrict the couplings to specific cases both for Spin-0 and Spin-2. Refs. [68, 71, 72, 79, 80] deal with graviton-like Spin-2 particles, while Ref. [81] deals with Spin-2 states that are singlet or triplet under $SU(2)$. Ref. [68] considers polar angle distribution of $\gamma\gamma$ and angular correlations between the charged leptons coming from WW^* decays to differentiate the Spin-0 and Spin-2 possibilities. While Ref. [71] looks at 'Higgs'-strahlung process to distinguish the various spin and parity possibilities, Ref. [72] compares branching ratios of the new boson decaying to $\gamma\gamma$, WW^* and ZZ^* channels as a method to measure the spin and parity of the new boson. In Ref. [79] the authors propose a new observable that can distinguish SM Higgs from a Spin-2 possibility. They consider the three-body decay of the new resonance to a SM vector boson and a fermion-antifermion pair. Ref. [80] shows that the current data disfavors a particular type of graviton-like Spin-2 particle that appears in scenarios with a warped extra dimension of the AdS type. Refs. [81, 82] deal with Spin-0 or Spin-2 particles produced via vector boson fusion process alone. Our discussion subsumes all of the above special cases. Moreover, unlike other discussions in the literature we provide clearly laid out steps to measure the couplings, spin and parity of the new resonance H without any ambiguity. We want to reiterate that it is important to measure not only the spin and parity of the new resonance but also its couplings before any conclusive statements can be made that it is the SM Higgs.

1.2.4 Numerical study of the uniangular distributions

In this sub-section we study the possibility of using the uniangular distributions, given in previous sub-section to differentiate the different possible spin CP states. For simplicity throughout this sub-section we will neglect the q^2 dependence of a, b and c. The signal and background events were generated using the MadEvent5 [98] event generator interfaced with PYTHIA 6.4 [99] and PGS 4 [100]. The vertex of Eq. (1.1) was implemented into the UFO format of Madgraph5 using Feynrules 1.6.18 [101]. Unlike the earlier sub-sections we also include the $2e^+2e^-$ and $2\mu^+2\mu^-$ final states because the identification of Z_1 being the mother particle of the pair of same flavor opposite sign leptons with an invariant mass closest to the M_Z breaks the exchange symmetry of these final states in most regions of phase space. As the analysis of this thesis has to do purely with the shape of the partial widths in the $Z^{(*)}Z^{(*)}$ channel, the production mechanism is not crucial to understanding the spin and CP properties of the resonance at 125 GeV. However to be concrete, these samples were generated for pp collisions at $\sqrt{s} = 8$ TeV using the

CTEQ6L1 parton distribution functions (PDFs) [102]. We choose to follow the ATLAS cut based analysis of Ref. [103] instead of the CMS analysis [104] because the CMS analysis has used a more sophisticated multi-variate analysis (MVA) technique. We set the Higgs boson mass $m_H = 125$ GeV, which is close to what has been measured in Ref. [103]. The branching ratios and decay widths are set appropriately using the values from the Higgs working group webpage [105].

Following the analysis of Ref. [103] we impose the following lepton selection cuts and triggers. In particular, the single lepton trigger thresholds are $p_T^l > 24(25)$ GeV for a muon(electron). The di-muon trigger thresholds used are $p_T > 13$ GeV for the symmetric case and $p_T^1 > 18$ GeV and $p_T^2 > 8$ GeV for the asymmetric case. For di-electrons the thresholds are $p_T > 12$ GeV. The lepton identification cuts require that each electron(muon) must have $E_T > 7$ GeV ($p_T > 6$ GeV) with $|\eta| < 2.4(2.7)$. Sorting leptons in decreasing order of p_T, we also impose the selection criteria $p_T^{\ell_1} > 20$ GeV, $p_T^{\ell 2} > 15$ GeV and $p_T^{\ell_3} > 10$ GeV. For same flavor leptons we also require that $\Delta R > 0.1$ while for opposite flavor $\Delta R > 0.2$. Furthermore we also impose the invariant mass cuts on the m_{Z_1}, m_{Z_2} and $m_{4\ell}$ described in Table 3.2 to reduce the Standard Model background. m_{Z_1} is the invariant mass of the pair of opposite sign same flavor leptons closest to m_Z while m_{Z_2} is the other combination. The number of signal events in our simulation is in good agreement with the SM predicted value quoted in Ref. [103], while the background rate is slightly lower than total background rate because we have not included the sub-dominant processes like Z+jets and $t\bar{t}$.

In order to quantify the effect of using the uniangular distributions to extract the nature of the 125 GeV resonance we construct the test statistic q based on the ratio of the likelihoods

$$q = \ln \frac{\mathcal{L}_{0^+}}{\mathcal{L}_{0^-}} , \tag{1.77}$$

Cuts	$m_H = 125$ GeV	SM ZZ^*
Selection	22	1542
50 GeV $< m_{Z_1} <$ 106 GeV	20	1432
12 GeV $< m_{Z_2} <$ 115 GeV	19	1294
115 GeV $< m_{4\ell} <$ 130 GeV	19	14

Table 1.1: Effect of the sequential cuts on the simulated Signal and the dominant continuum ZZ background, where the k-factors are 1.3 for signal and 2.2 for background using MCFM 6.6 [106] for 20.7 fb^{-1}.

where the $\mathcal{L}$ is the unbinned likelihood function

$$\mathcal{L} = \sum_{\mu_s} \left(\prod_i^{N_{\rm obs}} \frac{\mu_s P_s(\mathbf{x}_i) + \mu_b P_b(\mathbf{x}_i)}{\mu_s + \mu_b} \right)_{\rm ave} . \tag{1.78}$$

As our acceptances are in good agreement with the ATLAS predictions for the rest of our analysis we will assume a background rate $\mu_b = 16$ events for luminosity $L = 20.7$ fb^{-1} due to the continuum ZZ background. However as the total observed number of events are slightly above the expected rate we need to marginalize over the expected signal rate. In particular we assume a bayesian prior flat distribution for $\mu_s \in [0.5, 2.0] \times \mu_s^{\rm SM}(=$ 18 at a luminosity of 20.7fb^{-1}). For a particular value of μ_s we generate ensembles of $N_{\rm obs}$ events to find the average of the product within the brackets in Eq. (1.78). The probability density function (PDF) for signal is the product of the distributions

$$\frac{1}{\Gamma}\frac{d\Gamma}{d\cos\theta_1} = \frac{1}{2} - \mathcal{T}_1^{(0)}(a,B,C)\,\cos\theta_1 + \mathcal{T}_2^{(0)}(a,B,C)\,P_2(\cos\theta_1), \tag{1.79}$$

$$\frac{1}{\Gamma}\frac{d\Gamma}{d\cos\theta_2} = \frac{1}{2} + \mathcal{T}_1^{(0)}(a,B,C)\,\cos\theta_2 + \mathcal{T}_2^{(0)}(a,B,C)\,P_2(\cos\theta_2), \tag{1.80}$$

$$\frac{1}{\Gamma}\frac{d\Gamma}{d\phi} = \frac{1}{2\pi} + \mathcal{U}_1^{(0)}(a,B,C)\,\cos\phi + \mathcal{U}_2^{(0)}(a,B,C)\,\cos 2\phi, \tag{1.81}$$

where $B = b \times (100 \text{ GeV})^2$, $C = c \times (100 \text{ GeV})^2$ and

$$\Gamma \equiv \Gamma(a,B,C) \simeq 2.24\times 10^{-8}\, x_H^{14}\,(a^2 + 0.19\,a\,B + 2.22\times 10^{-2}\,B^2\,x_H^2 + 2.14\times 10^{-2}\,C^2\,x_H^6), \quad (1.82)$$

$$\mathcal{T}_1^{(0)}(a,B,C) \simeq \frac{2.14\times 10^{-2}\,a\,C\,x_H^3}{a^2 + 0.19\,a\,B + 2.22\times 10^{-2}\,B^2\,x_H^2 + 2.14\times 10^{-2}\,C^2\,x_H^6}, \quad (1.83)$$

$$\mathcal{T}_2^{(0)}(a,B,C) \simeq \frac{-0.15\,a^2 - 9.65\times 10^{-2}\,a\,B\,x_H^3 + 5.35\times 10^{-3}\,C^2\,x_H^9}{x_H^3\left(a^2 + 0.19\,a\,B + 2.22\times 10^{-2}\,B^2\,x_H^2 + 2.14\times 10^{-2}\,C^2\,x_H^6\right)}, \quad (1.84)$$

$$\mathcal{U}_1^{(0)}(a,B,C) \simeq \frac{-3.44\times 10^{-3}\,a^2 - 5.50\times 10^{-4}\,a\,B\,x_H^2}{a^2 + 0.19\,a\,B + 2.22\times 10^{-2}\,B^2\,x_H^2 + 2.14\times 10^{-2}\,C^2\,x_H^6}, \quad (1.85)$$

$$\mathcal{U}_2^{(0)}(a,B,C) \simeq \frac{1.88\times 10^{-2}\,a^2\,x_H - 8.51\times 10^{-4}\,C^2\,x_H^6}{a^2 + 0.19\,a\,B + 2.22\times 10^{-2}\,B^2\,x_H^2 + 2.14\times 10^{-2}\,C^2\,x_H^6}, \quad (1.86)$$

while for the background $P_b = 1/(8\pi)$. In the above approximations for we have neglected the q^2 dependences of a, b and c and integrated Eq (1.9), Eq. (1.13), Eq. (1.14) and Eq. (1.15) over q_2^2. Furthermore we have performed a power law fit in term of $x_H = m_H/(120 \text{ GeV})$ for each of the coefficients. As b and c have dimensions of mass squared, in the above approximations for the different coefficients we have used the dimensionless coefficients B and C instead. By definition, the 0^+ hypothesis corresponds to $(a, B, C) = (1, 0, 0)$ and the 0^- hypothesis corresponds to $(a, B, C) = (0, 0, 1)$. When $a = 0$ the magnitude of C is not crucial as we normalize the 0^+ and 0^- cross-sections so as to produce the same number of signal events.

To quantify power of the uniangular distributions in hypothesis testing, we present the q test-statisic for the 0^+ and 0^- hypotheses in Fig. 1.4. In particular, we have applied the q-statistic in Eq. (1.77) to samples of Monte Carlo events that have passed the above cuts in Tab. 3.2, where we assumed the above bayesian prior for the mean signal rate. The red (dark grey) curve corresponds to 0^- events while the green (light grey) curve corresponds to 0^+ events. The solid curves correspond to a gaussian fit to these distributions and using

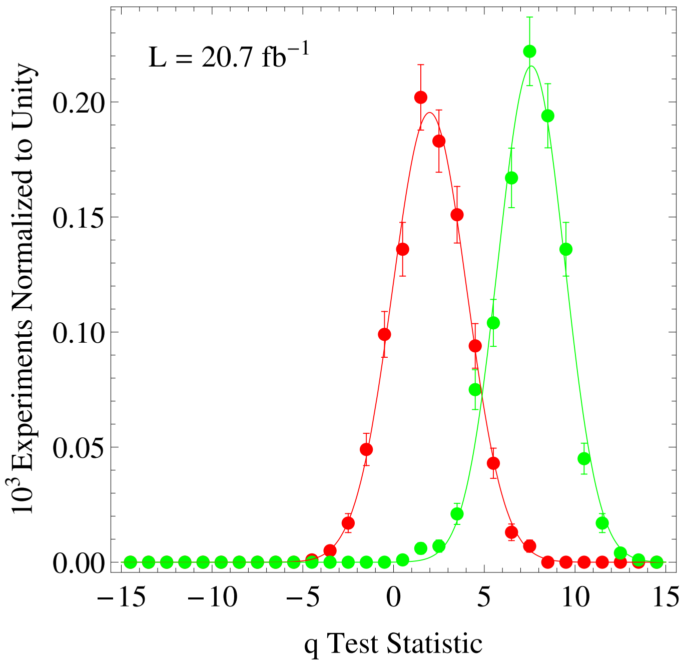

Figure 1.4: Comparison of the q test-statistic using the uniangular distribution approach in the 4ℓ channel for the 0^+ events in red (gray) vs. 0^- events in green (light gray).

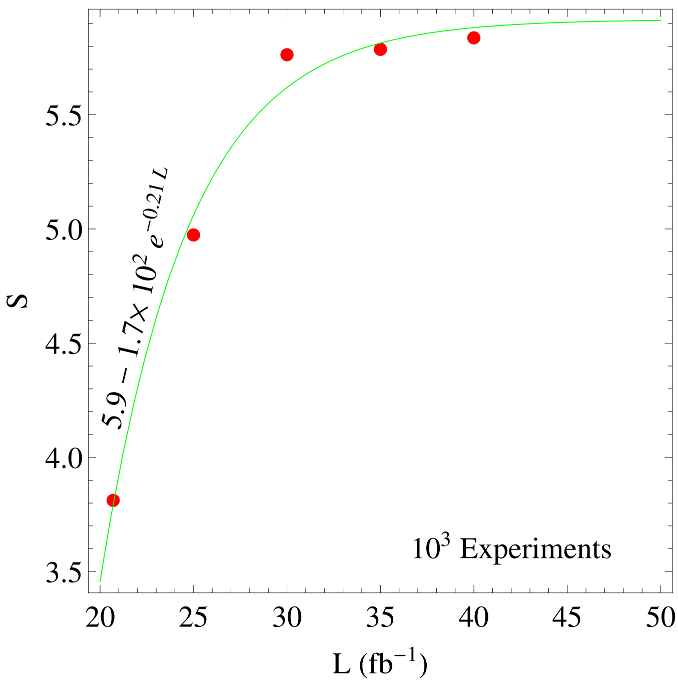

Figure 1.5: Separation power for q-test statistic using the uniangular distributions as a function of Luminosity. The red (dark grey) points are the simulated separation power and the green (light grey) curve is the fit to the data

them we define the separation power as

$$S = \frac{2A}{\sigma}, \tag{1.87}$$

where A is the area under the curve calculated from the point on the q-axis which satisfies the condition that the area under the right tail of the left distribution is equal to the left tail of the right distribution and σ is the maximum of the two standard deviations.

The separation power using the q test statistic works well for low luminosity, but this approach loses sensitivity at larger luminosity. To illustrate this point we present Fig. 1.5 at a function of luminosity. The red (dark grey) points correspond calculated separation power for a particular luminosity while the green (light grey) curve is a fit to the data. The lowest data point corresponds to a luminosity of 20.7 fb^{-1} with an observation of 43 events while for at higher luminosities we have assumed that the number of observed events agrees with the expected rates. Furthermore this extrapolation assumes the same cuts and efficiencies for higher luminosities. For luminosities greater that 40 fb^{-1}, a χ^2 fit of the uniangular distributions would probably provide a stronger hypothesis test.

It would seem that the values of all the form factors a, b and c can be extracted using the there uniangular distributions Eq. (1.79)-(1.81) along with Eq. (1.82)-(1.86). However, the difference between the uniangular distributions in Eq. (1.79) and Eq. (1.80) is small because it is proportional to η. Given the small sample of 43 events this would essentially imply that only two parameters can be obtained. Our numerical work confirms this fact. Since $P_0(\cos\theta_{1,2}) = 1$, $P_1(\cos\theta_{1,2})$, $P_2(\cos\theta_{1,2})$, $\cos\phi$ and $\cos 2\phi$ are orthogonal functions the coefficients of each of the terms can be extracted individually. As discussed in Sec. 1.2.1 this would result in four observables. We emphasize that as the data sample increases the additional information can be used to measure relative phases between a, b and c. For 43 events, as expected from the discussions in Sec. 1.2.1 based on the small value of η in SM, we find we could only extract stable values of b/a and c/a

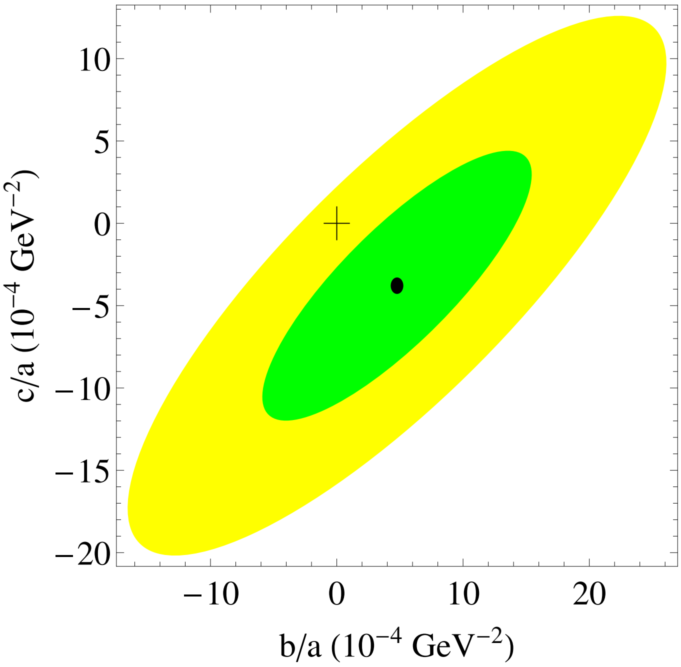

Figure 1.6: c/a vs b/a 1σ (green) and 2σ (yellow) contours assuming the Standard Model value of the partial decay width to 4ℓ. The central values $(b/a, c/a) = (4.77 \pm 21.23, -3.79 \pm 16.4) \times 10^{-4}$ GeV^{-2} is shown by the block dot. The cross-hair corresponds to $b = c = 0$.

by maximizing the likelihood function $\mathcal{L}_{0^+}$. One can also estimate the errors in b/a and c/a from the inverse of the covariance matrix $V_{ij} = cov[\theta_i, \theta_j]$ defined as

$$\hat{V}^{-1} = -\left(\frac{\partial^2 \ln \mathcal{L}}{\partial\theta_i \partial\theta_j}\right)_{\hat{\theta}} \tag{1.88}$$

where $\theta_i, \theta_j = b/a, c/a$. Here $\hat{\theta}$ denotes those values of the parameters that maximizes the likelihood function. In Fig. 1.6 we present the extract values of b/a and c/a for a sample of 43 events. Using these values of b/a and c/a, the value of a can also be found by fitting the decay width in Eq. (1.82) to the Standard Model partial width. Using this approach, the values of a, b and c with their respective errors are

$$a = 2.11 \pm 3.55, \tag{1.89}$$

$$b = (10.09 \pm 47.99) \times 10^{-4}\ \text{GeV}^{-2}, \tag{1.90}$$

$$c = -(8.01 \pm 37.20) \times 10^{-4}\ \text{GeV}^{-2}. \tag{1.91}$$

1.3 Summary

We conclude that by looking at the three uniangular distributions and examining the numbers of Z^*Z^* to ZZ^* events one can unambiguously confirm whether the new boson is indeed the Higgs with $J^{PC} = 0^{++}$ and with couplings to Z bosons exactly as predicted in the Standard Model. We show that the terms in the angular distribution corresponding to $P_2(\cos\theta_1)$ and $P_2(\cos\theta_2)$ play a critical role in distinguishing the $J = 2$ and $J = 0$ states. The distributions are identical for Spin-0 case, but must be different for Spin-2 state except in a special $J^P = 2^+$ case where $F_3 = F_4 = F_L = F_M = 0$. The ratio of the number of Z^*Z^* events to the number of ZZ^* events provides a unique identification for this special $J^P = 2^+$ case. In this special case the number of Z^*Z^* events dominates significantly over the number of ZZ^* events. The Spin-2 resonance can thus be unambiguously confirmed or ruled out. With Spin-2 possibility ruled out, Spin-0 can be studied in detail.

The resonance would then be a parity-odd state (0^{-+}) if $F_L = F_\parallel = 0$ and a parity-even state (0^{++}) if $F_\perp = 0$. If the resonance is found to be in 0^{++} state, we need to check whether $T_2^{(0)}$ and $U_2^{(0)}$ terms are as predicted in SM. The q_2^2 integrated values for the observables $T_2^{(0)}$ and $U_2^{(0)}$ are uniquely predicted in SM at tree level to be -0.148 and 0.117 respectively. These tests would ascertain whether the 0^{++} state is the SM Higgs or some non-SM boson. If it turns out to be a non-SM boson, we can also measure the coefficients a, b, c by using Eqs. (1.36), (1.37) and (1.38). If the boson is a mixed parity state, the relative phase between the parity-even and parity-odd amplitudes can also be measured by studying the $\sin 2\phi$ term in the uniangular distribution. We present a step by step methodology in Fig. 3.2 for a quick and sure-footed determination of spin and parity of the newly discovered boson. Our approach of using Legendre polynomials and the choice of helicity amplitudes classified by parity enable us to construct angular asymmetries that unambiguously determine if the new resonance is indeed the Standard Model Higgs.

Numerically we have have simulated the dominant continuum ZZ background and Standard Model signal shown that our acceptances are in good agreement with the ATLAS predictions. Using the uniangular distributions derived in this thesis we compute the q-statistic $q = \ln(\mathcal{L}_{0^+}/\mathcal{L}_{0^-})$. We observe the separation power of this approach is most powerful at low luminosity assuming that the cuts and the acceptances remain the same at each luminosity. For easy experimental adaption we have included power law parametrization of the various angular coefficients in terms of the fundamental Higgs vertex parameters. We also obtain fits for b/a and c/a for a 43-event sample, demonstrating that both b and c can be constrained by a rather small sample of data.

2

Measurement of HZZ couplings

2.1 Introduction

The study of the coupling of the 125 GeV resonance following its discovery is the priority for future LHC runs. A hint of anomalous nature will be exhibited via its couplings to the Standard Model (SM) particles and open up new domains of phenomenological study of physics beyond the SM. In this chapter we call this 125 GeV resonance as Higgs and also denote it by H like previous chapter. The 14 TeV LHC run, with enhanced statistics, will lay the foundation stone for the precision era of the Higgs coupling measurements. In this regard lot of studies [27, 107–125] have been made after the discovery of H. Indications from the first LHC run are that, the discovered Higgs is indeed a spin 0^+ particle, however, CP admixture is still possible in its couplings. In this thesis [28] we study how angular asymmetries can probe CP-odd admixture in the HZZ couplings via $H \to ZZ^* \to 4\ell$ channel, at the 14 TeV LHC for 300 fb^{-1} and 3000 fb^{-1}. We benchmark the angular asymmetries for SM Higgs, CP-odd admixture. We demonstrate how the ratios of couplings and their relative phases can be extracted at the 14 TeV LHC for 300

fb^{-1} and 3000 fb^{-1} luminosities.

2.2 Required Tools

In this section we first write down the HZZ vertex finally derive the expression for angular distribution of $H \to ZZ^* \to 4\ell$ process assuming H to be a spin 0 particle. In SM the process $H \to ZZ$ is characterised by the Lagrangian

$$\mathcal{L}_{HZZ} = \frac{gM_Z}{2\cos\theta_W} Z_\mu Z^\mu H \tag{2.1}$$

where θ_W is the Weinberg angle and g is the electroweak coupling constant. However there may exist anomalous couplings of H to Z boson. These couplings can in general be CP-even or CP-odd and can be generated from the effective Lagrangians

$$\mathcal{L}_e \sim -\frac{1}{4} Z^{\mu\nu} Z_{\mu\nu} H \tag{2.2}$$

and

$$\mathcal{L}_o \sim -\frac{1}{4} Z^{\mu\nu} \tilde{Z}_{\mu\nu} H \tag{2.3}$$

respectively, where $Z_{\mu\nu}$ and $\tilde{Z}_{\mu\nu}$ are defined as $Z_{\mu\nu} = \partial_\mu Z_\nu - \partial_\nu Z_\mu$ and $\tilde{Z}_{\mu\nu} = \frac{1}{2}\epsilon_{\mu\nu\rho\sigma} Z^{\rho\sigma}$ respectively. Following these Lagrangians one can write down the most general HZZ vertex as follows

$$V^{\mu\nu} = \frac{igM_Z}{\cos\theta_W}\Big(a\, g^{\mu\nu} + b\, \left(q_1 \cdot q_2\, g^{\mu\nu} - q_2^\mu q_1^\nu\right) + ic\, \epsilon^{\mu\nu\rho\sigma}\, q_{2\rho}\, q_{1\sigma}\Big). \tag{2.4}$$

It should be noted that Eq.(2.4) differs from that of Eq.(1.1)). Eq.(1.1) will be reproduced once we make substitutions $(a + b\, q_1 \cdot q_2)\, g^{\mu\nu} \to a\, g^{\mu\nu}$ and $-b\, q_2^\mu q_1^\nu \to b\, q_2^\mu q_1^\nu$

in Eq.(2.4). Correspondingly the expressions for the Helicity amplitudes in Eq. (1.2), Eq. (1.3) and Eq. (1.4) are also changed. This modifications are made to implement Eq. (2.1), Eq. (2.2) and Eq. (2.3) in the Feynrules framework for numerical simulation.

The CP-odd term c can not exist in lowest order in renormalizable gauge theories and it can arise via Eq (2.3). The CP-odd admixture is characterised by the non zero value of c. If H is a mixed CP state, c can be complex of the form $c\ e^{i\delta}$, where δ is the phase associated with c. This complex phase can arise if real particles run in the loop contributing to the effective HZZ vertex. These terms may also arise in several BSM weakly interacting and strongly interacting models. In the case of weakly interacting models the the parity of the coupling of H to gauge boson is via loop (predominantly fermion loops) effects. In these type of models c term is dependent on mass and couplings of the fermions of the underlying theory. However this loop induced effects can be very suppressed in several models. In the context of MSSM, Refs. [126,127] discuss about the strength of c term, which could be very suppressed in those models. Other models such as pseudo-axion states in Little Higgs models [128–130] can also have heavily suppressed c term. The spontaneous CP violation was first proposed by T. D. Lee [131], where he introduced two Higgs doublet without any extra symmetry in the Higgs potential and may have large CP violation. In a general type-II (2HDM) [127], for small value of $\tan\beta$ ($\tan\beta < 1$) the value of c term can be larger than the previously discussed cases. Such a small values of $\tan\beta$ are excluded in MSSM [132] by the direct searches of the MSSM Higgs however it is still allowed for type-II 2HDM. . The strongly interacting technicolor models [133, 134] the parity odd c term can also arise, where the pseudo-Nambu-Goldstone bosons (PNGB) couples to axial vector currents [135–137] as well as to the chiral anomalies.

2.3 Probing CP-odd admixture

We have selected the leptons in two sequential p_T ordered way.

i) Case-I : p_T of at least two leptons in a quadruplet must satisfy $p_T > 20$ GeV,

ii) Case-II : p_T of at least three leptons in a quadruplet must satisfy $p_T > 20$ GeV.

The leptons are required to be separated from each other by $\Delta R > 0.1$ if they are of the same flavour and $\Delta R > 0.2$ otherwise. Each event is required to have the triggering lepton(s) correctly matched to one or two of the selected leptons.

Furthermore we also impose the invariant mass cuts on the $m_{Z_1}(\sqrt{q_1^2})$, $m_{Z_2}(\sqrt{q_2^2})$ and $m_{4\ell}$ described in Table 3.2. m_{Z_1} is the invariant mass of the pair of opposite sign same flavor leptons closest to m_Z while m_{Z_2} is the other combination. The two columns of Table 3.2 demonstrate the effect of p_T ordering in event selection.

Cuts	Case-I	Case-II
Selection cuts	494	2253
50 GeV $< m_{12} <$ 106 GeV	487	2204
12 GeV $< m_{34} <$ 115 GeV	447	2071
115 GeV $< m_{4\ell} <$ 130 GeV	443	2050

Table 2.1: Effects of the sequential cuts on the simulated Signal for two different p_T ordering of Case-I(first column) and Case-II(second column). The sequential p_T ordering of Case-I is for 300 fb^{-1}, however we have used sequential p_T ordering of Case-II for 3000 fb^{-1}. The K-factor for signal is 2.5.

The three uniangular distributions and asymmetries will remain same as written in Chapter 1. Integrating Eq. (1.13),Eq. (1.14), and Eq. (1.15) over q_2^2 we get three integrated distributions as follows

$$\frac{1}{\Gamma}\frac{d\Gamma}{d\cos\theta_1} = \frac{1}{2} - \mathcal{T}_1 \cos\theta_1 + \mathcal{T}_2\, P_2(\cos\theta_1), \tag{2.5}$$

$$\frac{1}{\Gamma}\frac{d\Gamma}{d\cos\theta_2} = \frac{1}{2} + \mathcal{T}_1\, \cos\theta_2 + \mathcal{T}_2\, P_2(\cos\theta_2), \tag{2.6}$$

$$\frac{1}{\Gamma}\frac{d\Gamma}{d\phi} = \frac{1}{2\pi} + \mathcal{U}_1\, \cos\phi + \mathcal{U}_2\, \cos 2\phi + \mathcal{V}_1\, \sin\phi + \mathcal{V}_2\, \sin 2\phi, \tag{2.7}$$

where $\mathcal{T}_1$, $\mathcal{T}_2$, $\mathcal{U}_1$, $\mathcal{U}_2$, $\mathcal{V}_1$ and $\mathcal{V}_2$ are observables integrated over $m_{34}(q_2^2)$ and m_{12}.

The normalized distributions, $\frac{1}{\Gamma}\frac{d\Gamma}{d\cos\theta_1}$ vs $\cos\theta_1$, $\frac{1}{\Gamma}\frac{d\Gamma}{d\cos\theta_2}$ vs $\cos\theta_2$ and $\frac{1}{\Gamma}\frac{d\Gamma}{d\phi}$ vs ϕ for SM are shown in Fig. 3.5, Fig. 3.6 and Fig. 3.7 respectively for simulated data. It should be noted that the angular coverage for $\cos\theta_1$ or $\cos\theta_2$ covers the full range from -1 to $+1$ and coverage for ϕ from 0 to 2π are still retained even after using actual detector scenarios. The cut flow analysis of Case-I is followed for the analysis of SM Higgs and Higgs with CP-odd admixture at 300 fb^{-1}. At 3000 fb^{-1} since the statistics is higher, we will use stronger cut based analysis i.e. sequential cut flow analysis of Case-II for benchmarking SM Higgs and Higgs with different CP configuration. Moreover it should be noted that we have used the same cut based analysis for CP-odd admixture, CP-even higher derivative contribution and CP-even-odd scenario. The cross section for each benchmark scenarios are within the current experimental allowed region.

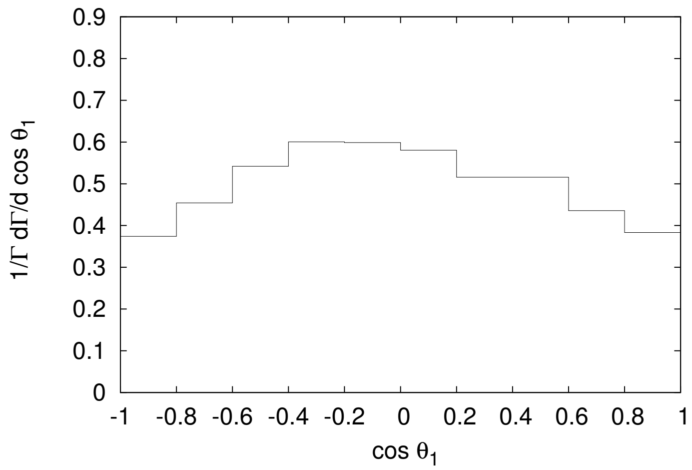

Figure 2.1: The normalized distribution $\frac{1}{\Gamma}\frac{d\Gamma}{d\cos\theta_1}$ vs $\cos\theta_1$ for SM Higgs events.

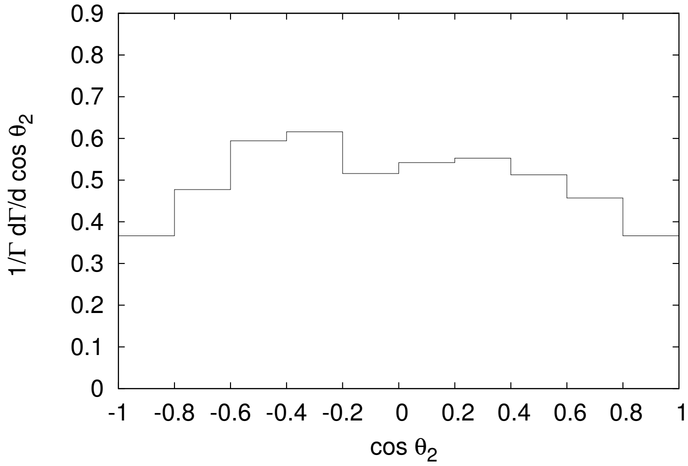

Figure 2.2: The normalized distribution $\frac{1}{\Gamma}\frac{d\Gamma}{d\cos\theta_2}$ vs $\cos\theta_2$ for SM Higgs events.

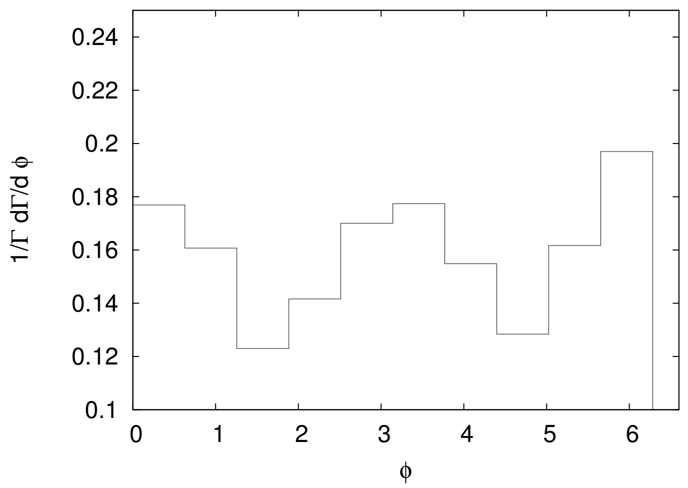

Figure 2.3: The normalized distribution $\frac{1}{\Gamma}\frac{d\Gamma}{d\phi}$ vs ϕ for SM Higgs events.

The simulated data are binned in $\cos\theta_1$, $\cos\theta_2$ and ϕ and fitted using Eq.(2.5), Eq.(2.6) and Eq.(2.7) to obtain the angular asymmetries t_1, t_2, u_1, u_2, v_1, v_2 and their errors which correspond to the angular asymmetries $\mathcal{T}_1$, $\mathcal{T}_2$, $\mathcal{U}_1$, $\mathcal{U}_2$, $\mathcal{V}_1$ and $\mathcal{V}_2$ respectively. The expressions for $\mathcal{T}_1$, $\mathcal{T}_2$, $\mathcal{U}_1$, $\mathcal{U}_2$, $\mathcal{V}_1$ and $\mathcal{V}_2$ are given in Appendix A.3. Once the values of the integrated observables t_1, t_2, u_1, u_2, v_1, v_2 and their respective errors are found, the χ^2 formula:

$$\chi^2 = \frac{(\mathcal{T}_2 - t_2)^2}{(\Delta t_2)^2} + \frac{(\cos\delta\ \mathcal{T}_1 - t_1)^2}{(\Delta t_1)^2} + \frac{(\mathcal{U}_1 - u_1)^2}{(\Delta u_1)^2} + \frac{(\mathcal{U}_2 - u_2)^2}{(\Delta u_2)^2} + \frac{(\sin\delta\ \mathcal{V}_2 - v_2)^2}{(\Delta v_2)^2} + \frac{(\sin\delta\ \mathcal{V}_1 - v_1)^2}{(\Delta v_1)^2} \tag{2.8}$$

will find the b/a, c/a and the phase δ. The errors in b/a, c/a and phase δ can also be calculated using the error matrix

$$\left(\frac{\partial^2\chi^2}{\partial\alpha_i\partial\alpha_i}\right)_{\hat{\alpha}} \tag{2.9}$$

where $\alpha_i, \alpha_j = b/a, c/a, \delta$. To find the best fit values we have used Mathematica 9.

2.3.1 Backgrounds

The backgrounds analyzed for this thesis along with their respective K- factors are tabulated in Table. 2.2 and Table. 2.3. In the Table. 2.2 have calculated the backgrounds for 14 TeV and 300 fb^{-1} LHC with sequential p_T cut of Case-I. The background analysis for 14 TeV and 3000 fb^{-1} LHC with the sequential p_T cut of Case-II is listed in Table. 2.3. The backgrounds we have looked at for our analysis are $Z\ell^+\ell^- \to 4\ell$, $Zb\bar{b} \to 2\ell 2b$. The K-factors for the backgrounds are taken from Ref. [140] for our analysis. Moreover we have also looked at $t\bar{t}$ and WZ backgrounds which are negligible compared to the dominant backgrounds $Z\ell^+\ell^- \to 4\ell$, $Zb\bar{b} \to 2\ell 2b$.

The sequential p_T cut of Case-II is specifically used to reduce the background significantly which is essential for precision measurement. This strong p_T cut of Case-II,

Cuts	$Z\ell^+\ell^-$	$Zb\bar{b}$
Selection cuts	11439	967
50GeV < m_{12} < 106 GeV	11401	948
12GeV < m_{34} < 115 GeV	10324	176
115GeV < $m_{4\ell}$ < 130 GeV	155	35

Table 2.2: The background analysis for benchmark scenarios at 14 TeV and 300 fb^{-1} luminosity with sequential p_T cut of Case-I. The second and third columns show the effect of different selection cuts on $Z\ell^+\ell^-$ and $Zb\bar{b}$ backgrounds respectively. The K-factor for $Z\ell^+\ell^-$ background is 1.2 and $Zb\bar{b}$ background is 1.42.

not only reduce the dominant $Z\ell^+\ell^-$ background but also makes the subdominant background $Zb\bar{b}$ negligible for our analysis.

Cuts	$Z\ell^+\ell^-$
Selection cuts	104202
50GeV < m_{12} < 106 GeV	103905
12GeV < m_{34} < 115 GeV	96988
115GeV < $m_{4\ell}$ < 130 GeV	270

Table 2.3: Background analysis for 14 TeV 3000 fb^{-1} benchmark scenarios with sequential p_T cut of Case-II

2.3.2 Study of angular asymmetries of the Higgs at 14 TeV and 300 fb^{-1}

The values of the observables will be different for the SM than that of CP-odd admixture as we have already discussed and we by benchmark the angular observables for SM Higgs and Higgs with CP-odd admixture this section. The measurement of the angular observables will be the stepping stone for our analysis and we will use them to estimate the values of the ratios of couplings for different benchmark scenarios. We also obtain 1σ and 2σ contours for the ratios of couplings b/a vs c/a in each cases. Furthermore, for the CP-odd benchmark scenario we also find the the phase δ vs c/a contour which is essential for the study of CP-odd admixture in HZZ couplings. This study will provide the precision at which one can rule out the anomalous contributions in HZZ couplings, establishing the SM nature of H at 14 TeV 300 fb^{-1} LHC run. The benchmark scenarios we have considered in this subsection are motivated by the results of Ref. [27]. In its first 8 TeV run with 20.7 fb^{-1} luminosity, the values of b/a and c/a that angular analysis could have probed at the LHC are $\sim 10^{-3}$ GeV^{-2}. As the total number of events will be increased at the 14 TeV LHC run, we chose our benchmark values for the couplings b/a and c/a below the values that were probed at 8 TeV LHC run.

The SM Higgs

The SM Higgs is characterised by the values of the vertex factors $a = 1$, $b = 0$, $c = 0$ in Eq.(2.4). Thus the SM Higgs events are generated with the parametrization $a = 1$, $b = 0$, $c = 0$. The fit values of the observables for the SM Higgs are tabulated in Table 2.4. The

Table 2.4: The values of the observables for the SM Higgs with respective errors at 14 TeV 300 fb^{-1} LHC.

Observables	Values with errors
t_2	-0.18 ± 0.08
t_1	$(0.7 \pm 6.16) \times 10^{-2}$
u_2	0.28 ± 0.33
u_1	$(0.76 \pm 3.64) \times 10^{-1}$
v_2	$(-0.45 \pm 3.42) \times 10^{-1}$
v_1	$(-0.48 \pm 3.14) \times 10^{-1}$

values of the observables t_2 and u_2 are large compared to other observables as discussed in the previous section, playing important role in the χ^2 expression in Eq.(2.8). The observables t_1, v_2 and v_1 provide information about phase for anomalous couplings b and c. The best fit values of b/a and c/a with their respective errors for the SM Higgs are given as follows:

$$b/a = (0.04 \pm 0.70) \times 10^{-4}\,\text{GeV}^{-2} \tag{2.10}$$

$$c/a = (0.34 \pm 1.89) \times 10^{-4}\,\text{GeV}^{-2} \tag{2.11}$$

and are consistent with the parametrization $a = 1$, $b = 0\,\text{GeV}^{-2}$, $c = 0\,\text{GeV}^{-2}$ by which the events are generated. The best fit values with 1σ and 2σ contours for b/a vs c/a are shown in Fig .2.4.

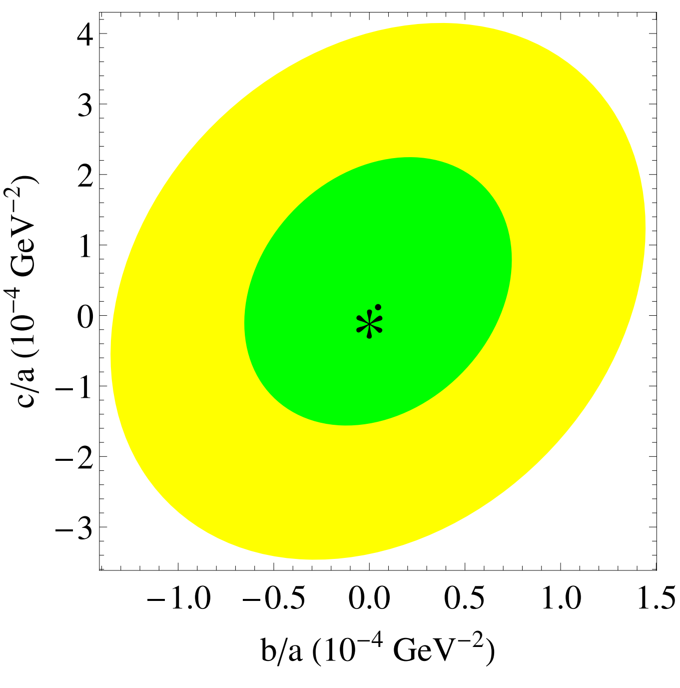

Figure 2.4: c/a vs b/a 1σ (green) and 2σ (yellow) contours for the SM Higgs at 300 fb^{-1}. The best fit values $(b/a, c/a)$ is shown by the block dot. The '$*$' corresponds to $b = c = 0\,\text{GeV}^{-2}$.

The Higgs with CP-odd admixture

The CP-odd admixture is charaterised by a non zero value of the vertex factors a and c in Eq.(2.4). For the CP-odd admixture case, Higgs events are generated using $a = 0.7$, $b = 0$ GeV^{-2} and $c = (2.2 + 2.2i) \times 10^{-4}$ GeV^{-2}. The values of the observables are given in Table 2.5. It should be noted that the benchmark parametrization of c/a for CP-odd admixture case lies beyond the error of c/a for the SM Higgs discussed in subsection 2.3.2.

Table 2.5: The values of the observables for CP-odd admixture Higgs with respective errors at 14 TeV 300 fb^{-1} LHC.

Observables	**Values with errors**
t_2	-0.07 ± 0.08
t_1	-0.06 ± 0.06
u_2	0.01 ± 0.34
u_1	$(-0.60 \pm 3.49) \times 10^{-1}$
v_2	$(0.8 \pm 3.53) \times 10^{-1}$
v_1	$(-0.37 \pm 3.45) \times 10^{-1}$

The value of t_2 has now become smaller compared to the SM case as shown in Table 2.4. Most importantly the non zero value of t_1 arises due to the complex CP-odd anomalous coupling c and play a significant role along with t_2 and u_2 in probing anomalous CP-odd admixture of HZZ couplings. The best fit values for b/a, c/a and the phase δ for CP-odd admixture are:

$$b/a = (0.30 \pm 1.22) \times 10^{-4}\,\text{GeV}^{-2} \tag{2.12}$$

$$c/a = (4.91 \pm 1.18) \times 10^{-4}\,\text{GeV}^{-2} \tag{2.13}$$

$$\delta = (0.52 \pm 2.18) \text{ in radian.} \tag{2.14}$$

and consistent with the parametrization $a = 0.7$, $b = 0$ GeV^{-2} and $c = (2.2 + 2.2i) \times 10^{-4}$ GeV^{-2}. Note that the error in δ is still very large at this luminosity.

The best fit values with 1σ and 2σ contours for c/a vs b/a and δ vs c/a are shown in Fig. 2.5 and Fig. 2.6 respectively.

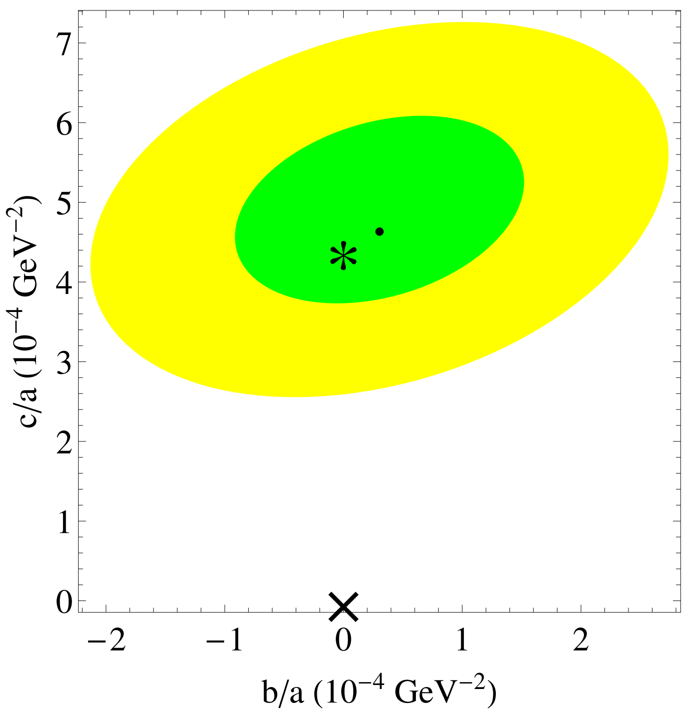

Figure 2.5: c/a vs b/a 1σ (green) and 2σ (yellow) contours for CP-odd admixture Higgs at 300 fb^{-1}. The best fit value of $(b/a, c/a)$ is shown by the block dot. The values with which data are generated ($b/a = 0$ GeV^{-2}, $c/a = 4.44 \times 10^{-4}$ GeV^{-2}) is shown by the '$*$'. The cross-hair corresponds to $b = c = 0$ GeV^{-2}.

2.3.3 Study of angular asymmetries of the Higgs at 14 TeV 3000 fb^{-1}

High Luminosity LHC (HL-LHC) i.e 14 TeV 3000 fb^{-1} run before the energy upgrade will allow us to test the CP structure of HZZ couplings even more precisely. At 3000 fb^{-1} we revisit the benchmark cases of SM and CP-odd admixture along with two new analysis of CP-even higher derivative contribution and CP-even-odd scenario. For 3000 fb^{-1} also, we have followed the same cut based analysis that we have discussed earlier

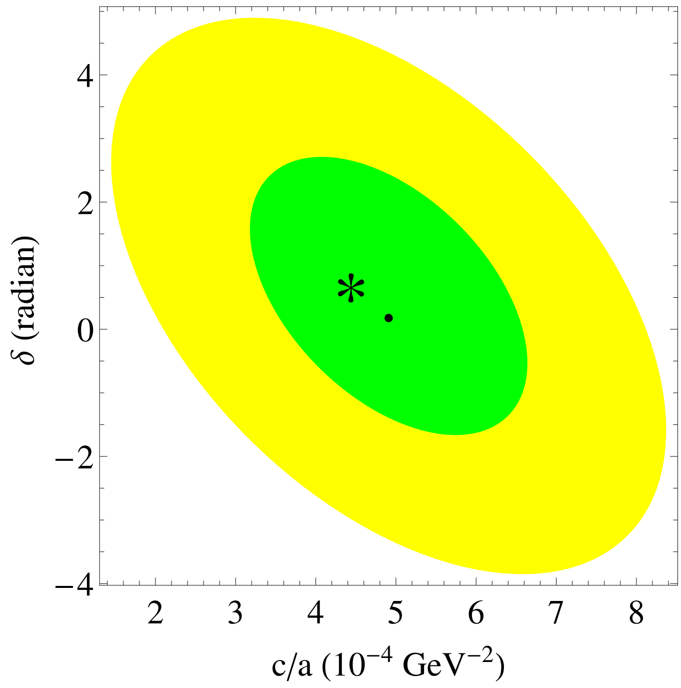

Figure 2.6: δ vs c/a 1σ (green) and 2σ (yellow) contours for CP-odd admixture Higgs at 300 fb^{-1}. The best fit values $(c/a, \delta)$ is shown by the block dot. The values with which data are generated is shown by the '$*$'.

apart from a strong sequential p_T ordering i.e. p_T of at least three leptons in a quadruplet must satisfy $p_T > 20$ GeV.

The SM Higgs and CP-odd admixture Higgs

First we investigate CP-odd Higgs and SM Higgs and find out the values of angular observables along with their respective errors. For CP-odd admixture we have again taken $a = 0.7$, $b = 0$ GeV^{-2}, $c = (2.2 + 2.2i) \times 10^{-4}$ GeV^{-2} and SM Higgs $a = 1$, $b = 0$ GeV^{-2}, $c = 0$ GeV^{-2}. The fit values of the observables t_2, t_1, u_2, u_1, v_2, v_1 for the SM and CP-odd admixture Higgs are tabulated in Table 2.6 and Table 2.7 respectively. The errors have significantly reduced for all the observables and the fit values for ratios of couplings for the SM Higgs b/a, c/a (as expected due to enhanced statistics) are given

$$b/a = (0.34 \pm 0.44) \times 10^{-4}\,\text{GeV}^{-2} \tag{2.15}$$

Table 2.6: The values of the observables for the SM Higgs with respective errors at 14 TeV 3000 fb^{-1}.

Observables	**Values with errors**
t_2	-0.20 ± 0.04
t_1	$(0.20 \pm 0.32) \times 10^{-1}$
u_2	0.21 ± 0.18
u_1	$(0.35 \pm 1.93) \times 10^{-1}$
v_2	$(0.16 \pm 1.84) \times 10^{-1}$
v_1	$(-0.37 \pm 1.73) \times 10^{-1}$

$$c/a = (0.63 \pm 0.76) \times 10^{-4}\,\text{GeV}^{-2} \tag{2.16}$$

and are consistent with the values $a = 1$, $b = 0$ GeV^{-2}, $c = 0$ GeV^{-2}. The 1σ and 2σ contours for b/a vs c/a are shown in Fig. 2.7

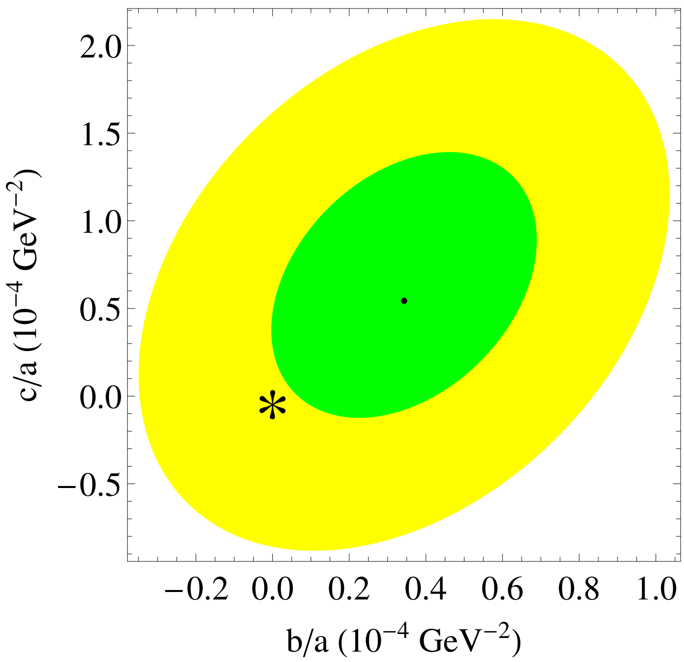

Figure 2.7: c/a vs b/a 1σ (green) and 2σ (yellow) contours for the SM Higgs at 3000 fb^{-1}. The best fit values $(b/a, c/a)$ is shown by the block dot. The '$*$' corresponds to $b = c = 0$ GeV^{-2}.

Table 2.7: The values of the observables for CP-odd admixture Higgs with respective errors at 14 TeV 3000 fb^{-1}

Observables	**Values with errors**
t_2	-0.10 ± 0.04
t_1	-0.05 ± 0.03
u_2	0.02 ± 0.17
u_1	$(-0.18 \pm 1.77) \times 10^{-1}$
v_2	$(0.66 \pm 1.73) \times 10^{-1}$
v_1	$(0.67 \pm 1.73) \times 10^{-1}$

At 3000 fb^{-1} from Table 2.7 one can see that the errors in t_1 and t_2 are much reduced, making them very good observables for probing CP-odd admixture. The best fit values for b/a, c/a and phase δ for CP-odd admixture are given as

$$b/a = (0.15 \pm 0.56) \times 10^{-4}\,\mathrm{GeV}^{-2} \tag{2.17}$$

$$c/a = (4.09 \pm 0.64) \times 10^{-4}\,\mathrm{GeV}^{-2} \tag{2.18}$$

$$\delta = 0.56 \pm 1.90 \text{ in radian.} \tag{2.19}$$

It should be noted that the error in δ has become lower due to the fact that the error in t_1, which constraints the phase δ, is much reduced.

The 1σ and 2σ contours for b/a vs c/a and δ vs c/a are shown in Fig. 2.8 and Fig. 2.9 respectively.

2.4 Summary

We demonstrated how angular asymmetries will provide a strong and efficient tool to probe Higgs couplings in high luminosity future LHC runs. With the increased statistics

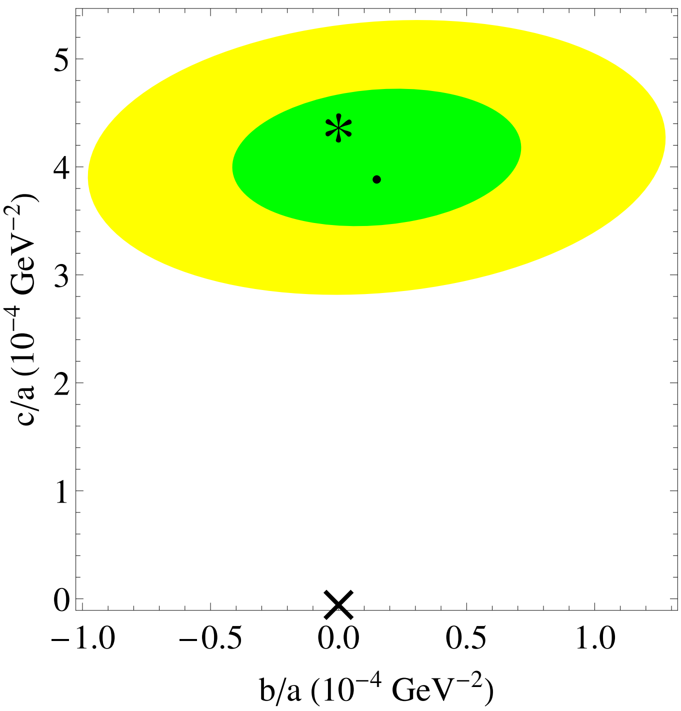

Figure 2.8: c/a vs b/a 1σ (green) and 2σ (yellow) contours for CP-odd admixture Higgs at 3000 fb^{-1}. The best fit value of $(b/a, c/a)$ is shown by the block dot. The values with which data are generated ($b/a = 0$ GeV^{-2}, $c/a = 4.44 \times 10^{-4}$ GeV^{-2}) is shown by the '$*$'. The cross-hair corresponds to $b = c = 0$ GeV^{-2}.

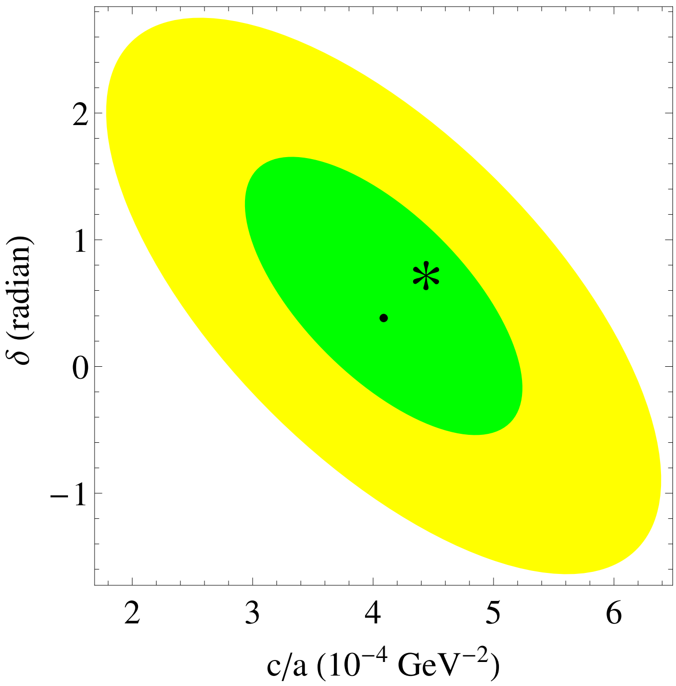

Figure 2.9: δ vs c/a 1σ (green) and 2σ (yellow) contours for CP-odd admixture Higgs at 3000 fb^{-1}. The best fit values $(c/a, \delta)$ is shown by the block dot. The value with which data are generated is shown by the '$*$'.

at 14 TeV run, LHC will enter into precision era and angular analysis will offer a step by step methodology to study the Higgs couplings. We have shown, using angular asymmetries one can probe HZZ couplings for the SM Higgs as well as Higgs with mixed CP scenarios at 14 TeV LHC, for two different luminosity 300 fb^{-1} and 3000 fb^{-1}. The values of the observables vary depending on the values of a, b and c. The observables T_1, V_1 and V_2 are sensitive to CP-odd admixture and can be a good candidate to probe CP-odd admixture. Finally the best fit values for the ratios of the couplings, b/a and c/a are calculated using Eq.(2.8). However several models still can have smaller c/a that can even survive the precision reach of 14 TeV 3000 fb^{-1} LHC. It will require higher statistics to probe CP-odd admixture of HZZ couplings in those models.

Part III

A spin 1 particle: Z'

3

Z' boson

3.1 Introduction

With the recent discovery of the 'Higgs' boson, all the ingredients of the standard model of particle physics (SM) have been found. However, we do know that the SM does not fully explain the whole of nature at its most fundamental level. For example, the problem of naturalness, the existence of extremely small masses for the neutrinos required to explain the observed neutrino oscillations, the abundance of matter over anti-matter in our observable universe and the constituents of dark matter (which is about five times more abundant than the ordinary matter) are a few of many issues which cannot be handled in the SM. So the SM encompasses an incomplete description of nature and hence it must be supplemented or extended with some other hitherto unknown new physics. Any model of new physics invariably includes new interactions and thus many new particles. In order to have a comprehensive view of new physics it is therefore essential to look for new fundamental particles in experiments such as the Large Hadron Collider (LHC) or in the proposed future experiments such as the International Linear Collider (ILC), Circular Electron Positron Collider (CEPC) and Super Proton-Proton Collider (SppC)

. It is however important to have model independent methods in place to characterize resonances that could be observed in these high luminosity and high energy experiments.

We start by considering [37] the most general vertex for Spin-1 possibility of $\mathcal{X}$ ($\equiv Z'$) decaying to two Z bosons and then write down the corresponding decay vertices. We evaluate the partial decay rate of Z' in terms of the invariant mass squared of the dileptons produced from the two Z decays and the angular distributions of the four lepton final state. We demonstrate that by studying three uniangular distributions (i.e. *distributions involving only one angle*) one can determine the spin and parity of Z' and also explore anomalous couplings in the most general fashion. For this we again express our uniangular distributions in terms of helicity amplitudes, in the transversity basis, which are very effective in their sensitivity to the parity of the parent particle.

We show numerically that the uniangular distributions can indeed be used to study the spin and parity of the resonance Z'. We first construct a effective model for a heavy Z' and find out the discovery potential of such a resonance in future LHC runs. We then extract angular asymmetries for the 14 TeV and 33 TeV LHC runs of both Spin-1^+ and Spin-1^- Z'.

3.2 The Formalism

The most general Lorentz invariant and gauge invariant vertex factor for Spin-1 resonance can be written as

$$V^{\mu\alpha\beta} = O_1 \ \left(g^{\alpha\mu} q_1^{\beta} + g^{\beta\mu} q_2^{\alpha}\right) + i \ E_1 \ \epsilon^{\alpha\beta\mu\nu} \ Q_\nu, \tag{3.1}$$

where O_1 and E_1 are parity odd and even vertex factors respectively

One can have two helicity amplitude and they can be written in transversity basis as:

$$A_{o1} = \frac{\sqrt{2}}{3} D_1\, O_1, \tag{3.2}$$
$$A_{e1} = \frac{1}{3} D_2\, E_1, \tag{3.3}$$

with "o" and "e" stands for parity odd and even helicity amplitudes respectively and 1 in the subscript denotes the Spin-1 nature of the resonance. The expressions D_1 and D_2 are used to make the helicity amplitude expressions look simple and they are defined as

$$D_1^2 = 2M_{Z'}^6 \mathsf{u}_1^2 - \frac{1}{2}M_{Z'}^4 \left(5\mathsf{u}_1^4 + \mathsf{u}_2^4\right) + 6M_{Z'}^2 \left(\mathsf{u}_1^6 - \mathsf{u}_1^2\mathsf{u}_2^4\right) + \frac{3}{2}\mathsf{u}_1^4\mathsf{u}_2^4 - \frac{1}{2}\mathsf{u}_2^8, \tag{3.4}$$
$$D_2^2 = 16M_{Z'}^6\mathsf{u}_1^2 + 56M_{Z'}^4\mathsf{u}_1^4 - 86M_{Z'}^2\mathsf{u}_1^6 + \mathsf{u}_2^4\left(-85M_{Z'}^4 + 96M_{Z'}^2\mathsf{u}_1^2 - 35\mathsf{u}_1^4\right) + 38\mathsf{u}_2^8, \tag{3.5}$$

Finally one can similarly find three uniangular distributions for a Spin-1 resonance as:

$$\frac{1}{\Gamma_f^{(1)}}\frac{d^3\Gamma^{(1)}}{dq_1^2\, dq_2^2\, d\cos\theta_1} = \frac{1}{2} + T_1^{(1)}\ \cos\theta_1 + T_2^{(1)}\ P_2(\cos\theta_1), \tag{3.6}$$
$$\frac{1}{\Gamma_f^{(1)}}\frac{d^3\Gamma^{(1)}}{dq_1^2\, dq_2^2\, d\cos\theta_2} = \frac{1}{2} + T_1^{'(1)}\cos\theta_2 + T_2^{'(1)}P_2(\cos\theta_2), \tag{3.7}$$
$$\frac{2\pi}{\Gamma_f^{(1)}}\frac{d^3\Gamma^{(1)}}{dq_1^2\, dq_2^2\, d\phi} = 1 + U_1^{(1)}\ \cos\phi + U_2^{(1)}\ \cos 2\phi + V_1^{(1)}\ \sin\phi + V_2^{(1)}\ \sin 2\phi. \tag{3.8}$$

The expressions for $T_1^{(1)}, T_1^{'(1)}, T_2^{(1)}, T_2^{'(1)}$ $U_1^{(1)}, U_2^{(1)}, V_1^{(1)}$ and $V_2^{(1)}$ can be found out in the Appendix A.4.

We can extract the observables in a similar fashion like we did for H and they are

$$T_1^{(1)} = \left(-\int_{-1}^{0} + \int_{0}^{+1}\right) d\cos\theta_1\ \left(\frac{1}{\Gamma_f^{(1)}}\frac{d^3\Gamma^{(1)}}{dq_1^2\ dq_2^2\ d\cos\theta_1}\right), \tag{3.9}$$

$$T_2^{(1)} = \frac{4}{3}\left(\int_{-1}^{-\frac{1}{2}} - \int_{-\frac{1}{2}}^{0} - \int_{0}^{+\frac{1}{2}} + \int_{+\frac{1}{2}}^{+1}\right) d\cos\theta_1 \left(\frac{1}{\Gamma_f^{(1)}} \frac{d^3\Gamma^{(1)}}{dq_1^2\, dq_2^2\, d\cos\theta_1}\right), \tag{3.10}$$

$$T_1^{'(1)} = \left(-\int_{-1}^{0} + \int_{0}^{+1}\right) d\cos\theta_2 \left(\frac{1}{\Gamma_f^{(1)}} \frac{d^3\Gamma^{(1)}}{dq_1^2\, dq_2^2\, d\cos\theta_2}\right), \tag{3.11}$$

$$T_2^{'(1)} = \frac{4}{3}\left(\int_{-1}^{-\frac{1}{2}} - \int_{-\frac{1}{2}}^{0} - \int_{0}^{+\frac{1}{2}} + \int_{+\frac{1}{2}}^{+1}\right) d\cos\theta_2 \left(\frac{1}{\Gamma_f^{(1)}} \frac{d^3\Gamma^{(1)}}{dq_1^2\, dq_2^2\, d\cos\theta_2}\right), \tag{3.12}$$

$$U_1^{(1)} = \frac{1}{4}\left(-\int_{-\pi}^{-\frac{\pi}{2}} + \int_{-\frac{\pi}{2}}^{+\frac{\pi}{2}} - \int_{+\frac{\pi}{2}}^{+\pi}\right) d\phi \left(\frac{2\pi}{\Gamma_f^{(1)}} \frac{d^3\Gamma^{(1)}}{dq_1^2\, dq_2^2\, d\phi}\right), \tag{3.13}$$

$$U_2^{(1)} = \frac{1}{4}\left(\int_{-\pi}^{-\frac{3\pi}{4}} - \int_{-\frac{3\pi}{4}}^{-\frac{\pi}{4}} + \int_{-\frac{\pi}{4}}^{+\frac{\pi}{4}} - \int_{+\frac{\pi}{4}}^{+\frac{3\pi}{4}} + \int_{+\frac{3\pi}{4}}^{+\pi}\right) d\phi \left(\frac{2\pi}{\Gamma_f^{(1)}} \frac{d^3\Gamma^{(1)}}{dq_1^2\, dq_2^2\, d\phi}\right), \tag{3.14}$$

$$V_1^{(1)} = \frac{1}{4}\left(-\int_{-\pi}^{0} + \int_{0}^{+\pi}\right) d\phi \left(\frac{2\pi}{\Gamma_f^{(1)}} \frac{d^3\Gamma^{(1)}}{dq_1^2\, dq_2^2\, d\phi}\right), \tag{3.15}$$

$$V_2^{(1)} = \frac{1}{4}\left(\int_{-\pi}^{-\frac{\pi}{2}} - \int_{-\frac{\pi}{2}}^{0} + \int_{0}^{+\frac{\pi}{2}} - \int_{+\frac{\pi}{2}}^{+\pi}\right) d\phi \left(\frac{2\pi}{\Gamma_f^{(1)}} \frac{d^3\Gamma^{(1)}}{dq_1^2\, dq_2^2\, d\phi}\right). \tag{3.16}$$

It is easy to find that the observables $T_2^{(1)}$ and $T_2^{'(1)}$ are not identical for a Spin-1 particle and hence we can define $\Delta^{(1)}$ as

$$\Delta^{(1)} = 6M_{Z'}^2 \mathsf{u}_2^2 Y^2 \left(\frac{|F_{o1}|^2 \left(M_{Z'}^2 + \mathsf{u}_1^2\right)}{D_1^2} + \frac{2\,|F_{e1}|^2 \left(5M_{Z'}^2 + \mathsf{u}_1^2\right)}{D_2^2}\right), \tag{3.17}$$

where F_{o1} and F_{e1} parity odd and parity even helicity fractions for a Spin-1 particle and $Y^2 = \frac{\sqrt{\lambda(M_Z'^2, M_1^2, M_2^2)}}{2M_Z'}$. Unlike the case of the 125 GeV H, Z' could be heavy such that for $M_{Z'} > 2M_Z$ both the Z bosons can be on-shell i.e. $\sqrt{q_1^2} \equiv M_1$ and $\sqrt{q_2^2} \equiv M_2$.

Now if we combine this result with the results from Chapter.1 we get a combined methodology shown in Fig. (3.2), to disentangle the spin and parity of a bosonic resonance (say $\mathcal{X}$) with arbitrary mass via gold-plated decay mode. It should be noted that this methodology is applied for non-identical leptons in the final state as one has to anti-symmetrize for identical leptons in the final state. Although for a resonance $M_{\mathcal{X}} < 2M_{Z'}$

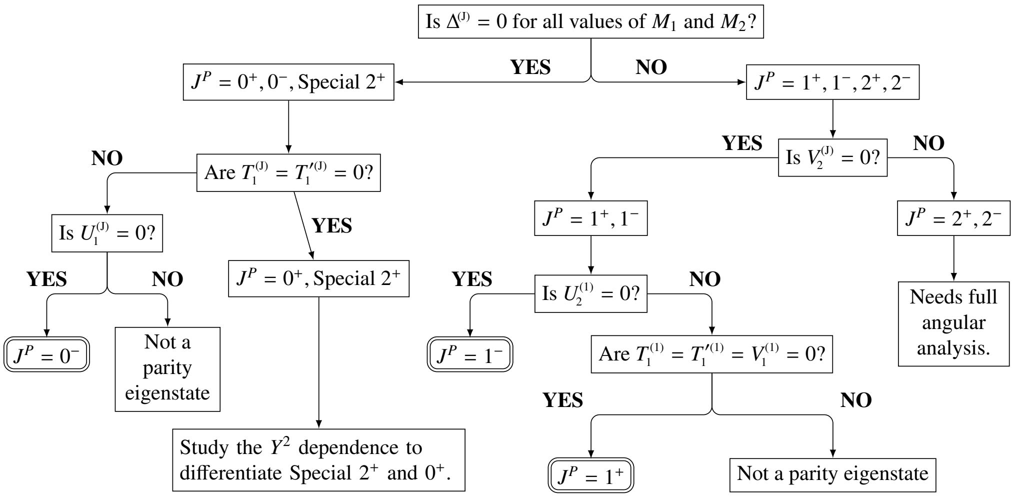

Figure 3.1: Flowchart to determine the spin and parity of a resonance $\mathcal{X}$ decaying as $\mathcal{X} \to Z^{(*)}Z^{(*)} \to \ell_1^-\ell_1^+\ell_2^-\ell_2^+$. $Z^{(*)}$ includes both on-shell and off-shell contributions. This mt

this is automatically taken care of as discussed in the case of 125 GeV H.

3.3 Numerical Study

In this section we will show how the uniangular distributions given in Eqs. (3.6), (3.7) and (3.8) can be used to find out the values of the angular observables defined in Eqs. (3.9), (3.10), (3.11), (3.12), (3.13), (3.14), (3.15) and (3.16). We shall elucidate the methodology by concentrating on heavy Z' ($\mathcal{X}$ = Spin-1) resonance and study the observables for them. We start by investigating how the mass and decay width of such resonances affect their production cross section in the future LHC runs. We then benchmark the angular observables for Spin-1^+ and Spin-1^- resonances for two different Center-of-Momentum (CM) energies: 14 TeV and 33 TeV with 3000 fb^{-1} luminosity.

Let us consider a heavy Spin-1 resonance Z' of mass $M_{Z'}$ and decay width $\Gamma_{Z'}$, decaying into four charged leptons via two Z bosons. We shall assume that the resonance Z' is produced via annihilation of quark (q) and antiquark ($\bar{q}$) pairs. The production process is characterized by the effective Lagrangian,

$$\mathscr{L}_{eff} = \sum_q \left(\tilde{c}_q \; \bar{q}\gamma^\mu q \; Z'_\mu + c_q \; \bar{q}\gamma^\mu \gamma^5 q \; Z'_\mu \right), \tag{3.18}$$

where $q = u, d, c, s, b$ quarks and $\tilde{c}_q$, c_q are the coupling strengths of Z' to vector, axial vector currents respectively; i.e. for a Spin-1^+ resonance $\tilde{c}_q = 0$ and for a Spin-1^- resonance $c_q = 0$. Just for simplicity of the analysis we have further assumed that all the quarks couple to the resonance Z' with the same strength. The production cross section for the resonance Z' can be easily obtained from Eq. (3.18) by considering appropriate parton distribution functions in the process $pp \to Z'$. The production cross section does depend on the mass of the resonance Z': the larger the mass, the lower the production cross section at a given CM energy.

The partial decay width for $Z' \to ZZ$ for Spin-1 resonance is given by

$$\Gamma_{ZZ} = O_1^2 \frac{M_{Z'}^3}{32 M_Z^2 \pi} \left(1 - \frac{4M_Z^2}{M_{Z'}^2} \right)^{\frac{3}{2}} + E_1^2 \frac{M_{Z'}^3}{32 M_Z^2 \pi} \left(1 - \frac{4M_Z^2}{M_{Z'}^2} \right)^{\frac{5}{2}}. \tag{3.19}$$

For a Spin-1^+ resonance $O_1 = 0$ and for a Spin-1^- resonance $E_1 = 0$.

The partial decay width for $Z' \to q\bar{q}$ for a Spin-1 resonance is given by

$$\Gamma_{q\bar{q}} = c_q^2 \frac{M_{Z'}}{4\pi} \left(1 - \frac{4m_q^2}{M_{Z'}^2} \right)^{\frac{3}{2}} + \tilde{c}_q^2 \frac{(M_{Z'}^2 + 2m_q^2)}{4 M_{Z'} \pi} \left(1 - \frac{4m_q^2}{M_{Z'}^2} \right)^{\frac{1}{2}}, \tag{3.20}$$

where m_q is the mass of the quark q (or of antiquark $\bar{q}$), and $c_q = 0$ for a Spin-1^- resonance and $\tilde{c}_q = 0$ for a Spin-1^+ resonance. Let us further assume that Z' decays to all quark-antiquark pairs and to a pair of Z bosons only, i.e. the total decay width is given by

$$\Gamma_{Z'} = \Gamma_{ZZ} + \sum_q \Gamma_{q\bar{q}}. \tag{3.21}$$

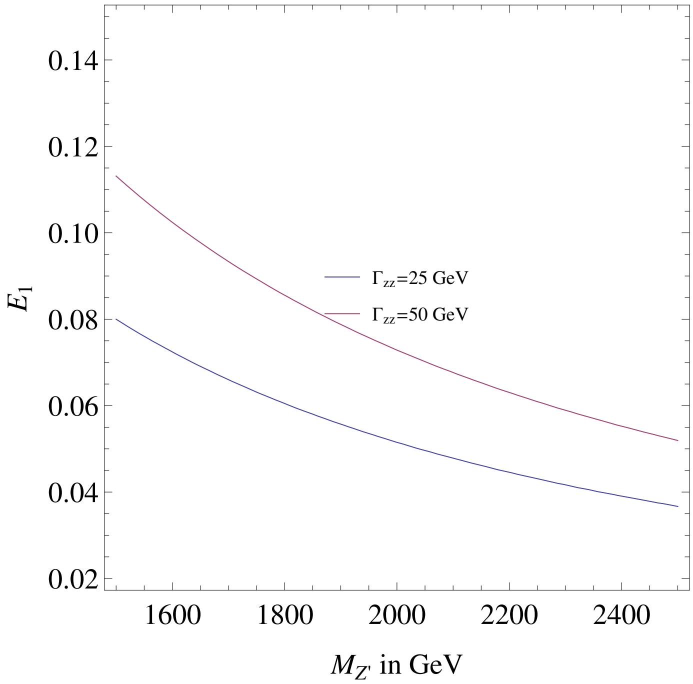

Figure 3.2: Mass ($M_{Z'}$) vs. E_1 plot of a Spin-1^+ resonance for different Γ_{ZZ}. The blue curve for $\Gamma_{ZZ} = 25$ and the purple curve for $\Gamma_{ZZ} = 50$.

One can relax these simple assumptions and do a detailed analysis where other decay channels also exist. This will lead to modifications to Eq. (3.21). In Fig. 3.2 we show how the partial decay width Γ_{ZZ} varies with the mass $M_{Z'}$ of the Spin-1^+ resonance, with $M_Z \ll M_{Z'}$. The Spin-1^- resonances also exhibit a similar plot for $M_Z \ll M_{Z'}$.

The current limit on the mass of a heavy Z' resonance is 1.7 TeV [138]. The current limit of $\tilde{c}_q$ and c_q for a particular mass $M_{Z'}$ of the resonance Z', can be extracted out from the $\sigma \times Br \times \mathcal{A}$ vs. resonance mass ($M_{Z'}$) plot of Ref. [138], where σ is the cross section for the process $pp \to Z'$, Br is the branching fraction of the decay $Z' \to q\bar{q}$ and $\mathcal{A}$ is the acceptance. Since the analysis of Ref. [138] deals with the search for a heavy resonance Z' decaying to di-jet, which is an isotropic decay (two body final state), the acceptance $\mathcal{A}$ is approximately 0.6 and is independent of the mass of Z'.

Following the analysis of Ref. [138] we find the allowed region for the couplings c_q and E_1 for two different masses, $M_{Z'} = 1.8$ TeV and 2 TeV, shown in Figs. 3.3 and

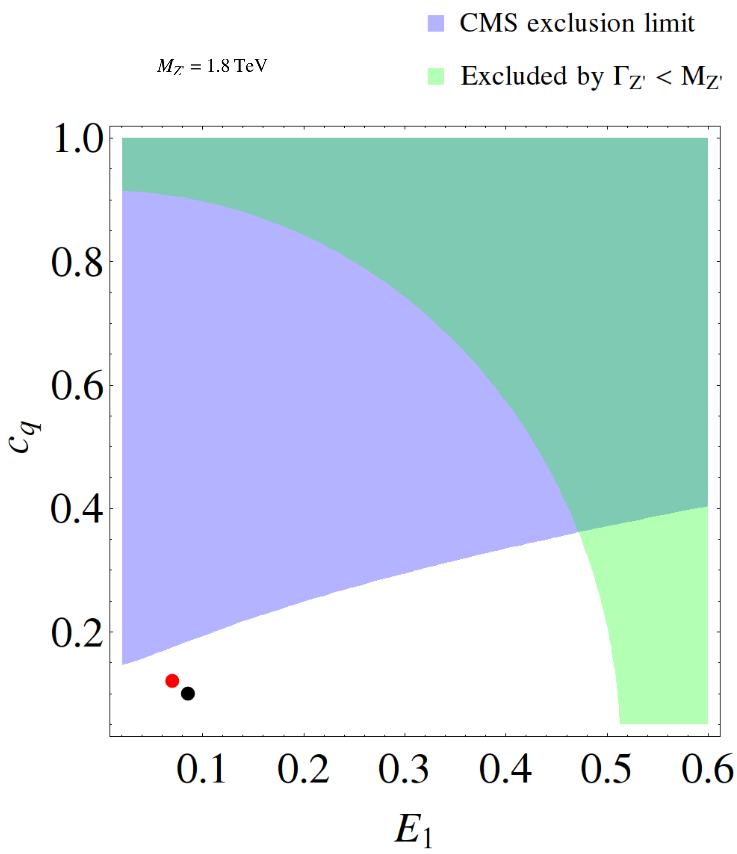

Figure 3.3: The allowed region for the couplings c_q and E_1 for a Spin-1^+ resonance of mass $M_{Z'} = 1.8$ TeV. The green and the blue regions are excluded by $\Gamma_{Z'} < M_{Z'}$ limit and CMS limit from Ref. [138] respectively. The red ($E_1 = 7.00 \times 10^{-2}, c_q = 0.12$) and the black ($E_1 = 8.56 \times 10^{-2}, c_q = 0.10$) dots are the two benchmark points for our analysis.

3.4 respectively. From the allowed regions shown in Figs. 3.3 and 3.4, we choose three benchmark scenarios for masses $M_{Z'} = 1.8$ TeV and $M_{Z'} = 2.0$ TeV for our numerical study. The benchmark values of c_q and E_1 corresponding to both the masses are tabulated in Table 3.1.

Once the values of $M_{Z'}$, c_q(or $\tilde{c_q}$) and E_1(or O_1) for a Spin-1^+ (or Spin-1^-) resonance are chosen, the total decay width $\Gamma_{Z'}$ as well as the cross section for the process $pp \to Z' \to ZZ \to e^+e^-\mu^+\mu^-$ get fixed. The reader should note that the process under consideration is within the narrow width approximation where $\Gamma_{Z'} \ll M_{Z'}$.

For event generation we used the MADEVENT5 [98] event generator interfaced with

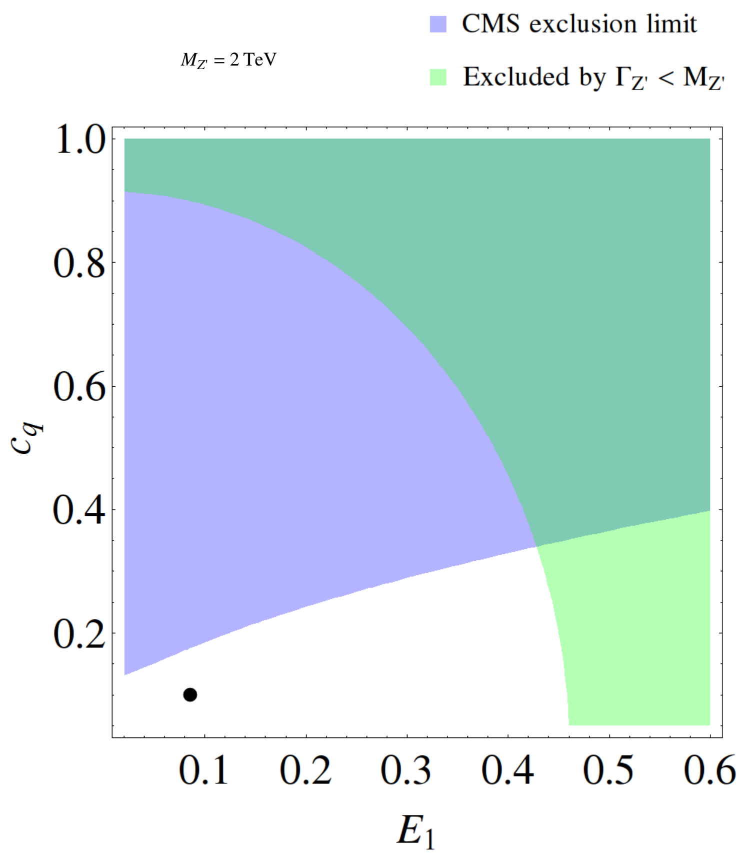

Figure 3.4: The allowed region for the couplings c_q and E_1 for a Spin-1^+ resonance of mass $M_{Z'} = 2$ TeV. The green and the blue regions are excluded by $\Gamma_{Z'} < M_{Z'}$ limit and CMS limit respectively. The black dot ($E_1 = 8.56 \times 10^{-2}$, $c_q = 0.10$) is the benchmark point for our analysis.

Mass	Coupling c_q	Coupling E_1	$\Gamma_{Z'}$ in GeV
1.8 TeV	0.12	7.00×10^{-2}	64.40
1.8 TeV	0.10	8.56×10^{-2}	71.52
2.0 TeV	0.10	8.56×10^{-2}	92.84

Table 3.1: The benchmark values of the couplings c_q and E_1 are listed for Spin-1^+ resonances of masses 1.8 TeV and 2 TeV respectively for our analysis. The values of the corresponding decay widths $\Gamma_{Z'}$ are also tabulated in the last column for both the masses.

PYTHIA6.4 [99] and Delphes 3 [139]. The events are generated by pp collisions via $q\bar{q} \to Z'$, for the CM energies $\sqrt{s}$ = 14 TeV and 33 TeV, using the parton distribution functions CTEQ6L1 [102]. Triggers as well as electron and muon identification cuts are set following the analysis presented in Refs. [103, 140]. We have only selected events with final states $e^+e^-\mu^+\mu^-$, as our analysis is applicable only to four non-identical final state leptons. We have kept the trigger values the same as those for 14 TeV, for the 33 TeV LHC analysis. However, it should be noted that in the future 33 TeV LHC run, the trigger values may change, which could further improve the statistics. The electron (muon) must satisfy $E_T > 7$ GeV ($p_T > 6$ GeV) and the pseudo-rapidity cut for electron (muon) is $|\eta| < 2.47$ ($|\eta| < 2.7$). The leptons are required to be separated from each other by $\Delta R > 0.1$ if they are of the same flavour and $\Delta R > 0.2$ otherwise. The invariant mass cuts that are applied in our analysis are 60 GeV $< m_{ee} <$ 120 GeV, 60 GeV $< m_{\mu\mu} <$ 120 GeV and 1000 GeV $< m_{4\ell}$.

The effects of mass $M_{Z'}$ and width $\Gamma_{Z'}$ on $\sigma \times Br$ are shown in Table 3.2 for a Spin-1^+ resonance. The statistics decrease as the resonance gets heavier. However, the statistics improve for a resonance with the same mass but narrower decay width. This dependence is easily discernible in Table 3.2 for a Spin-1^+ resonance. This mass and width dependence on the cross sections for the $pp \to Z' \to ZZ \to e^+e^-\mu^+\mu^-$ process also shows the same behavior for a Spin-1^- resonance in the limit $m_q \ll M_{Z'}$ and $M_Z \ll M_{Z'}$.

So far we have not discussed the background for the $pp \to Z' \to e^+e^-\mu^+\mu^-$ process. This is discussed in the following subsection.

3.3.1 Study of the angular asymmetries for a Spin-1^+ resonance:

In this subsection we discuss the uniangular distributions and show how to extract the angular observables from them for a Spin-1^+ resonance of mass $M_{Z'}$ = 1.8 TeV and

Cuts in GeV	$M_{Z'}$ = 1.8 TeV, $\Gamma_{Z'}$ = 64.40 GeV	$M_{Z'}$ = 1.8 TeV, $\Gamma_{Z'}$ = 71.52 GeV	$M_{Z'}$ = 2 TeV, $\Gamma_{Z'}$ = 92.84 GeV
Selection cuts	231	216	111
$60 < m_{ee} < 120$	231	216	111
$60 < m_{\mu\mu} < 120$	222	208	106
$1000 < m_{4\ell}$	221	207	106

Table 3.2: Effects of the sequential cuts on the simulated events at 14 TeV 3000 fb^{-1} LHC for different values of $M_{Z'}$ and $\Gamma_{Z'}$ of a Spin-1$^+$ resonance. It is easy to observe from the benchmark scenarios considered in this table that at a given CM energy the production cross section decreases with increase in $M_{Z'}$ and for a fixed value of $M_{Z'}$ the production cross section decreases as the value of the decay width $\Gamma_{Z'}$ increases.

decay width $\Gamma_{Z'} = 64.40$ GeV. We choose this benchmark scenario as the statistics are higher for this than the other cases. We analyse the angular observables for this benchmark scenario for two different CM energies 14 TeV and 33 TeV at an integrated luminosity 3000 fb^{-1} in future LHC runs. The values of the couplings for this benchmark scenarios are $c_q = 0.12$ and $E_1 = 7.00 \times 10^{-2}$. The effects of the sequential cuts for the benchmark scenarios are tabulated in Table 3.3. The three uniangular distributions for a Spin-1$^+$ resonance, $\frac{1}{\Gamma}\frac{d\Gamma}{d\cos\theta_1}$ vs. $\cos\theta_1$, $\frac{1}{\Gamma}\frac{d\Gamma}{d\cos\theta_2}$ vs. $\cos\theta_2$ and $\frac{1}{\Gamma}\frac{d\Gamma}{d\phi}$ vs. ϕ are shown in Figs. 3.5, 3.6 and 3.7 respectively. It should be noted that the uniangular distributions cover the full kinematic ranges for the three variables $\cos\theta_1$, $\cos\theta_2$ and ϕ.

However, while extracting observables one has to take the background processes into account. The $pp \to e^+e^-\mu^+\mu^-$ process is a continuum background to the process $pp \to ZZ \to e^+e^-\mu^+\mu^-$. The effects of the sequential cuts on the background processes for the 14 TeV and 33 TeV 3000 fb^{-1} LHC runs, are shown in Table 3.4.

In our simplistic model, we have considered the decays of Z' to quarks and Z bosons only. Thus we have not considered the effect of the process $Z' \to \gamma^*\gamma^* \to \ell_1^+\ell_1^-\ell_2^+\ell_2^-$ in our analysis. In general, models might have such irreducible backgrounds to the process

Cuts in GeV	14 TeV, 3000 fb^{-1}	33 TeV, 3000 fb^{-1}
Selection cuts	231	1212
$60 < m_{ee} < 120$	231	1212
$60 < m_{\mu\mu} < 120$	222	1159
$1000 < m_{4\ell}$	221	1154

Table 3.3: The effects of the sequential cuts on the simulated signal events at 14 TeV and 33 TeV LHC with 3000 fb^{-1} luminosity for a Spin-1^+resonance with $M_{Z'} = 1.8$ TeV and width $\Gamma_{Z'} = 64.40$ GeV.

Cuts in GeV	14 TeV, 3000 fb^{-1}	33 TeV, 3000 fb^{-1}
Selection cuts	24530	48588
$60 < m_{ee} < 120$	23320	46949
$60 < m_{\mu\mu} < 120$	18468	40082
$1000 < m_{4\ell}$	41	238

Table 3.4: The effects of the sequential cuts on the simulated background events at 14 TeV and 33 TeV LHC with 3000 fb^{-1} luminosity.

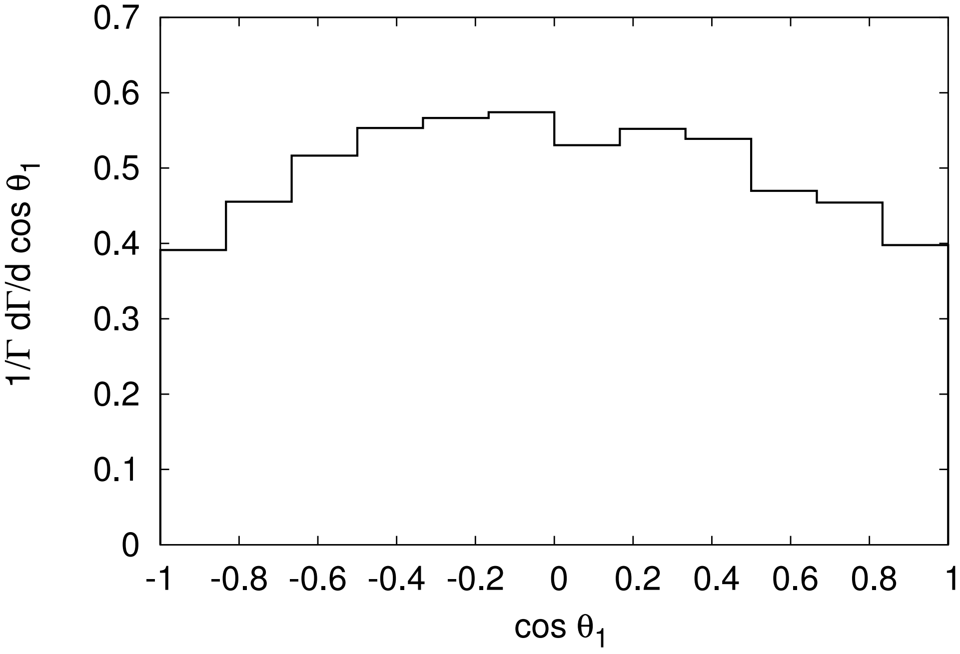

Figure 3.5: The normalized distribution $\frac{1}{\Gamma}\frac{d\Gamma}{d\cos\theta_1}$ vs. $\cos\theta_1$ for a Spin-1^+ resonance of mass $M_{Z'} = 1.8$ TeV and width $\Gamma_{Z'} = 64.04$ GeV.

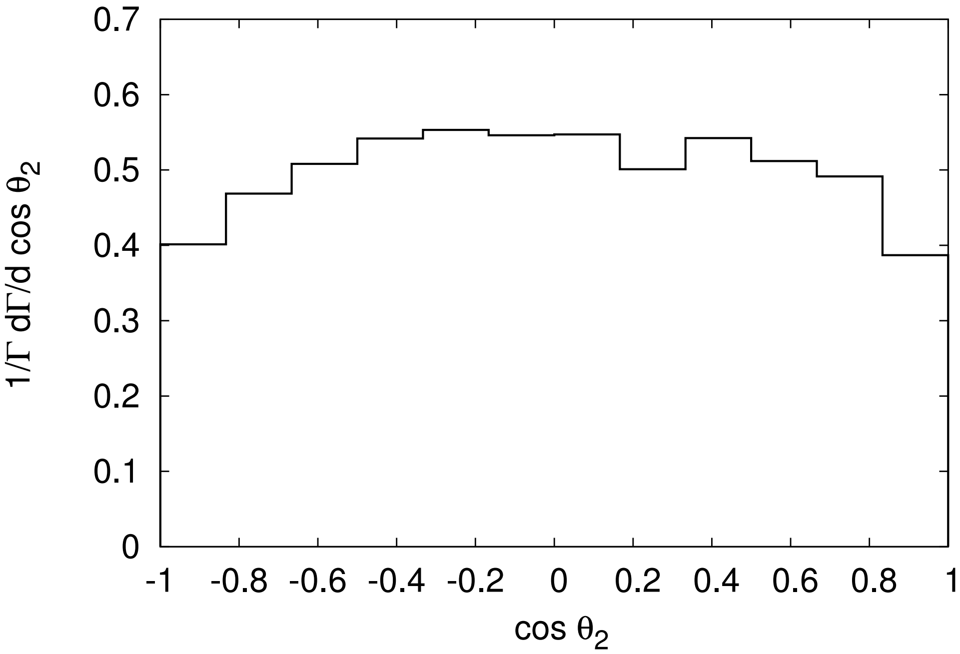

Figure 3.6: The normalized distribution $\frac{1}{\Gamma}\frac{d\Gamma}{d\cos\theta_2}$ vs. $\cos\theta_2$ for a Spin-1^+ resonance of mass $M_{Z'} = 1.8$ TeV and width $\Gamma_{Z'} = 64.04$ GeV.

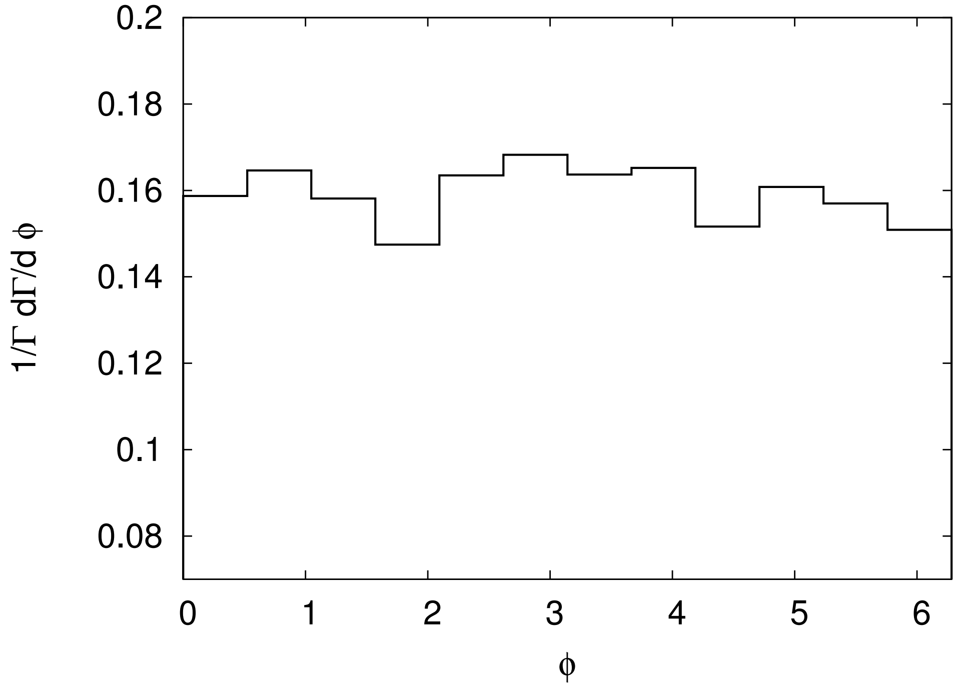

Figure 3.7: The normalized distribution $\frac{1}{\Gamma}\frac{d\Gamma}{d\phi}$ vs. ϕ for a Spin-1^+ resonance of mass $M_{Z'} = 1.8$ TeV and width $\Gamma_{Z'} = 64.04$ GeV.

$Z' \to ZZ \to \ell_1^+\ell_1^-\ell_2^+\ell_2^-$. However, the cross section to $Z' \to ZZ \to \ell_1^+\ell_1^-\ell_2^+\ell_2^-$ will be huge compared to the process $Z' \to \gamma^*\gamma^* \to \ell_1^+\ell_1^-\ell_2^+\ell_2^-$. This is because Z being a massive narrow resonance, production of two on-shell Z bosons rather than two off-shell photons is highly favored by the propagator effect. The selection cuts such as $60 < m_{\ell\ell} < 120$ etc., will further reduce the cross section of the process $Z' \to \gamma^*\gamma^* \to \ell_1^+\ell_1^-\ell_2^+\ell_2^-$. Hence the effect of this process via two off-sell photons will be the further suppressed even as a background.

The simulated signal and background events are finally binned in $\cos\theta_1$, $\cos\theta_2$ and ϕ and fitted using Eqs. (3.6), (3.7) and (3.8) integrated over $m_{ee}^2 \left(\equiv q_1^2\right)$ and $m_{\mu\mu}^2 \left(\equiv q_2^2\right)$ to obtain the fit values *integrated* angular observables $\mathcal{T}_1^{(1)}$, $\mathcal{T}_1^{\prime(1)}$, $\mathcal{T}_2^{(1)}$, $\mathcal{T}_2^{\prime(1)}$, $\mathcal{U}_1^{(1)}$, $\mathcal{U}_2^{(1)}$, $\mathcal{V}_1^{(1)}$ and $\mathcal{V}_2^{(1)}$ with their respective errors. The fit values of the observables are tabulated in Table 3.5 for the two different CM energies. It is clear from Table 3.5 that the fit values

Observables	14 TeV, 3000 fb^{-1}	33 TeV, 3000 fb^{-1}
$\mathcal{T}_2^{(1)}$	-0.19 ± 0.11	-0.18 ± 0.06
$\mathcal{T}_1^{(1)}$	0.07 ± 0.09	0.01 ± 0.04
$\mathcal{T}_2^{\prime(1)}$	-0.09 ± 0.12	-0.10 ± 0.06
$\mathcal{T}_1^{\prime(1)}$	-0.04 ± 0.10	-0.03 ± 0.05
$\mathcal{U}_2^{(1)}$	0.08 ± 0.51	0.04 ± 0.24
$\mathcal{U}_1^{(1)}$	$(-0.87 \pm 5.33) \times 10^{-1}$	$(-0.17 \pm 2.40) \times 10^{-1}$
$\mathcal{V}_2^{(1)}$	$(-0.41 \pm 5.32) \times 10^{-1}$	$(0.21 \pm 2.36) \times 10^{-1}$
$\mathcal{V}_1^{(1)}$	$(-0.32 \pm 5.11) \times 10^{-1}$	$(0.30 \pm 2.34) \times 10^{-1}$

Table 3.5: The fit values and the respective errors of the observables $\mathcal{T}_1^{(1)}$, $\mathcal{T}_1^{\prime(1)}$, $\mathcal{T}_2^{(1)}$, $\mathcal{T}_2^{\prime(1)}$, $\mathcal{U}_1^{(1)}$, $\mathcal{U}_2^{(1)}$, $\mathcal{V}_1^{(1)}$ and $\mathcal{V}_2^{(1)}$ for a Spin-1^+ resonance of mass $M_{Z'} = 1.8$ TeV and width $\Gamma_{Z'} = 64.04$ GeV at 14 TeV and 33 TeV LHC run (with 3000 fb^{-1} luminosity).

observables $\mathcal{T}_2^{(1)}$ and $\mathcal{T}_2^{\prime(1)}$, extracted from the $\cos\theta_1$ and $\cos\theta_2$ distributions respectively, match within 2σ error for both 14 and 33 TeV LHC runs. This is expected since both q_1^2 and q_2^2 are integrated over the same range and hence $\Delta^{(1)}$ should also be equal to 0. A full implementation of the flow chart (shown in Fig. 3.2) will require a fit with at least two regions $q_1^2 < q_2^2$ and $q_1^2 > q_2^2$. However, given the heavy mass for Z' the production cross section is low, hence, the errors are still large and more statistics are needed to undertake such a study.

3.3.2 Study of the angular asymmetries for a Spin-1^- resonance

We have so far discussed the possibility of finding a heavy Spin-1^+ resonance. However, the resonance may well be a Spin-1^-. The limits on the couplings $\tilde{c}_q$ and O_1 can also be found from $\sigma \times Br \times \mathcal{A}$ limit from Ref. [138]. In the limit $M_Z \ll M_{Z'}$ and $m_q \ll M_{Z'}$, the coupling $\tilde{c}_q \approx c_q$ and $O_1 \approx E_1$. Hence, we choose the values $\tilde{c}_q = 0.12$ and $O_1 = 7.00 \times 10^{-2}$ for the couplings as a benchmark scenario for our analysis of a Spin-

1^- resonance of mass 1.8 TeV and decay width $\Gamma_{Z'} = 64.40$ GeV. We perform the same analysis as given in Sec. 3.3.1 and extract out the values of the angular observables at two different CM energies, 14 TeV and 33 TeV, at an integrated luminosity of 3000 fb^{-1}. We also find three uniangular distributions for the Spin-1^- resonance, shown in Figs. 3.8, 3.9 and 3.10 respectively. The effects of the sequential cuts are tabulated in Table 3.6 at 14 TeV and 33 TeV LHC for 3000 fb^{-1} luminosity. The background analysis for a Spin-1^- resonance would remain the same as stated in Sec 3.3.1.

Cuts in GeV	14 TeV, 3000 fb^{-1}	33 TeV, 3000 fb^{-1}
Selection cuts	220	1155
$60 < m_{ee} < 120$	200	1154
$60 < m_{\mu\mu} < 120$	211	1108
$1000 < m_{4\ell}$	210	1105

Table 3.6: The effects of the sequential cuts on the simulated signal events at 14 TeV 3000 fb^{-1} and 33 TeV 3000 fb^{-1} LHC of a Spin-1^-resonance with $M_{Z'} = 1.8$ TeV and width $\Gamma_{Z'} = 64.40$ GeV.

The observables extracted from the uniangular distributions of the Spin-1^-resonance are given in Table 3.7. Apart from T_2 the errors of the other observables are still not small and require higher statistics to fully study the flowchart in Fig. 3.2.

If a heavy Spin-1 resonance is seen at the LHC, the full angular analysis and the extraction of all the observables may not be entirely possible at a 33 TeV 3000 fb^{-1} run. Once such a resonance is observed, a future high luminosity machine could disentangle the exact spin and parity of the resonance by studying the observables extracted from uniangular distributions. Moreover, we have not discussed the Spin-1 resonance with mixed parity configuration, which would typically require higher statistics as well, to completely disentangle.

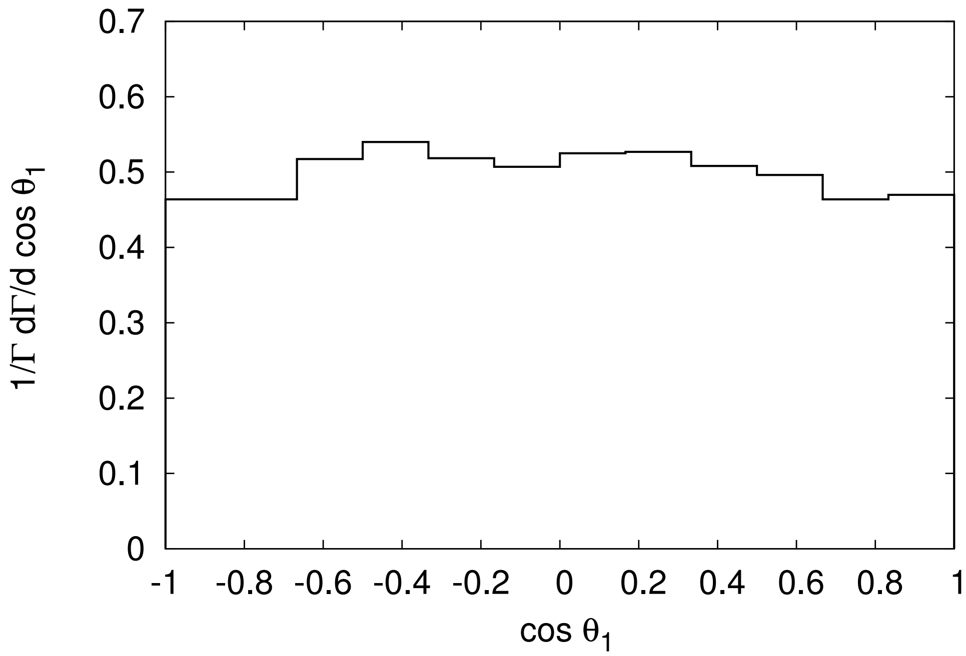

Figure 3.8: The normalized distribution $\dfrac{1}{\Gamma}\dfrac{d\Gamma}{d\cos\theta_1}$ vs. $\cos\theta_1$ for a Spin-1^- resonance of mass $M_{Z'} = 1.8$ TeV and width $\Gamma_{Z'} = 64.04$ GeV.

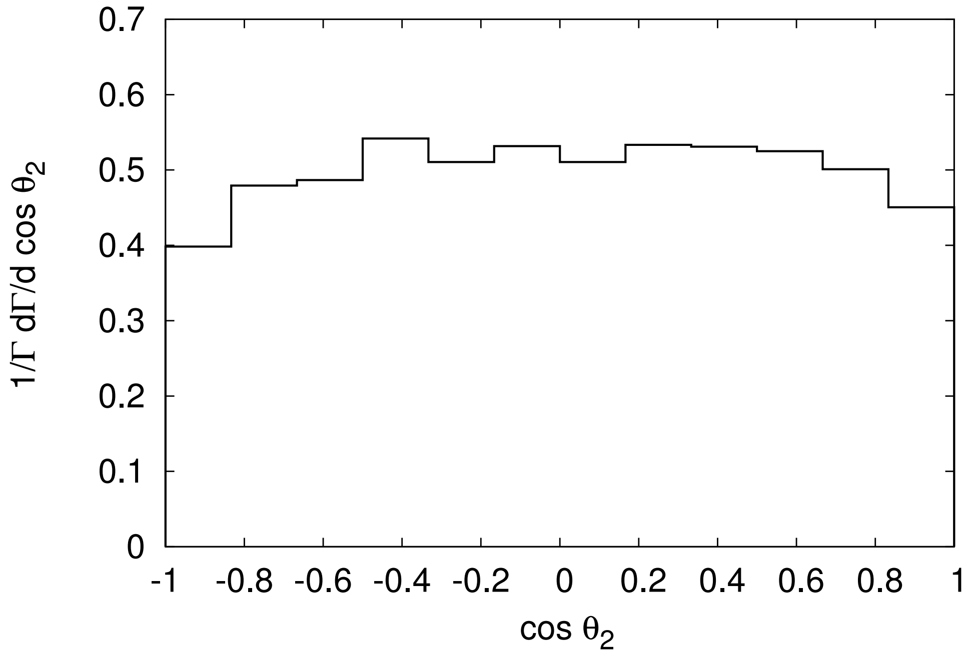

Figure 3.9: The normalized distribution $\dfrac{1}{\Gamma}\dfrac{d\Gamma}{d\cos\theta_2}$ vs. $\cos\theta_2$ for a Spin-1^- resonance of mass $M_{Z'} = 1.8$ TeV and width $\Gamma_{Z'} = 64.04$ GeV.

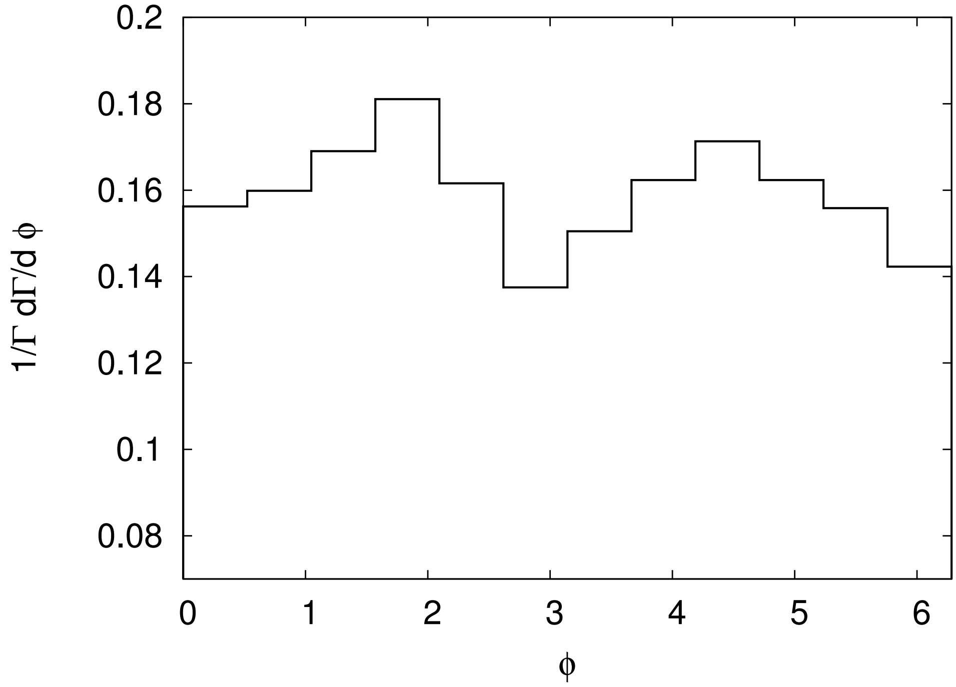

Figure 3.10: The normalized distribution $\dfrac{1}{\Gamma}\dfrac{d\Gamma}{d\phi}$ vs. ϕ for a Spin-1^- resonance of mass $M_{Z'} = 1.8$ TeV and width $\Gamma_{Z'} = 64.04$ GeV.

Observables	14 TeV, 3000 fb^{-1}	33 TeV, 3000 fb^{-1}
$\mathcal{T}_2^{(1)}$	-0.07 ± 0.13	-0.12 ± 0.06
$\mathcal{T}_1^{(1)}$	0.06 ± 0.10	0.01 ± 0.04
$\mathcal{T}_2^{'(1)}$	-0.04 ± 0.13	-0.07 ± 0.06
$\mathcal{T}_2^{'(1)}$	0.09 ± 0.10	-0.01 ± 0.04
$\mathcal{U}_2^{(1)}$	-0.08 ± 0.54	-0.05 ± 0.24
$\mathcal{U}_1^{(1)}$	$(1.99 \pm 5.16) \times 10^{-1}$	$(1.20 \pm 2.32) \times 10^{-1}$
$\mathcal{V}_2^{(1)}$	$(-0.14 \pm 5.27) \times 10^{-1}$	$(0.58 \pm 2.33) \times 10^{-1}$
$\mathcal{V}_1^{(1)}$	$(-0.27 \pm 5.46) \times 10^{-1}$	$(-0.63 \pm 2.39) \times 10^{-1}$

Table 3.7: The fit values and the errors of the observables $\mathcal{T}_1^{(1)}$, $\mathcal{T}_1^{'(1)}$, $\mathcal{T}_2^{(1)}$, $\mathcal{T}_2^{'(1)}$, $\mathcal{U}_1^{(1)}$, $\mathcal{U}_2^{(1)}$, $\mathcal{V}_1^{(1)}$ and $\mathcal{V}_2^{(1)}$ for a Spin-1^- resonance of mass $M_{Z'} = 1.8$ TeV and width $\Gamma_{Z'} = 64.04$ GeV for signal plus background. The values are extracted for two different CM energies, 14 TeV and 33 TeV LHC runs, with luminosity 3000 fb^{-1}.

3.4 Summary

We conclude that by looking at three *normalized* uniangular distributions, for the decay of a resonance to four charged final leptons via two Z bosons, one can infer to a fairly good accuracy the spin and parity of the parent particle. We show that it is possible for a *special* 2^+ resonance to give angular distributions comparable to those of a 0^+ resonance. It is in this special case that one needs to study the Y^2 dependence of the helicity amplitudes in order to distinguish the two cases. Since the Spin-1 case has only two helicity amplitudes, it needs a minimum number of observables to get confirmed or ruled out. We have also provided a step-by-step methodology that must be followed to distinguish the various spin, parity possibilities that are allowed in the case under consideration. A numerical analysis has also been performed for a heavy Spin-1 resonance to validate our formalism. It would therefore not be an overstatement to say that this method can play a crucial role at future high luminosity machines in discovering the Spin-parity nature of any new resonance, such as a heavy scalar boson or a Z' boson or a Kaluza-Klein boson or any such resonance found to decay to four final charged leptons via two Z bosons.

PART IV

Summary

4

Summary

The significance of the LHC lies in its potential to discover new particles. In the first run both ATLAS and CMS collaborations at the LHC have discovered a bosonic resonance mass around 125 GeV. A scalar particle namely Higgs boson was required to complete the particle content of the SM. Such scalar particles are also present in the particle content of several other BSM models following their theoretical constructions. After its discovery, unbiased analysis tools are required to study its spin, parity and measure its couplings to existing SM particles.

In this thesis we outline a step by step methodology to determine the spin, parity and couplings of this 125 GeV resonance (H). We choose experimentally clean "gold-plated" decay mode of H where it decays to two Z bosons followed by subsequent decays of the two Z bosons into four non-identical charged leptons. Since the resonance is found to be decaying into di-photon channel i.e. $H \to \gamma\gamma$ it can not be a Spin-1 particle, prohibited by Landau-Yang theorem. We begin with writing down the most general Lorentz and gauge invariant vertex factor of H for both the spin possibilities i.e. Spin-0 and Spin-2. We then derive three uniangular distributions in terms of several angular asymmetries. These angular asymmetries have definite parity signatures and are orthogonal to each other. Thus they can be measured independently. We find that these asymmetries have different characteristics for a Spin-0 resonance compared to a Spin-2 resonance and can be used to determine the spin of H. After identifying the spin, these asymmetries can be used to study the parity of H. We corroborate our methodology by numerical analysis.

In SM the value of the HZZ couplings are uniquely predicted. After the discovery of H, one needs to study the HZZ couplings precisely to confirm its SM nature. Although 8 TeV run indicates H to be a Spin-0 resonance with even parity, a considerable amount of CP-odd admixture is still possible. We show in this thesis, how one can precisely probe CP-odd admixtures of HZZ couplings at 14 TeV LHC run for two different luminosities. The direct measurement of the absolute values of the couplings are beyond the scope of the LHC which requires a precise measurement of the partial rate $H \to ZZ^* \to \ell_1^+\ell_1^-\ell_2^+\ell_2^-$. We show how using angular asymmetries one can obtain the ratios of couplings and the relative phases between them. This precision measurement of HZZ couplings have the potential to find New Physics beyond SM.

LHC or future colliders may discover new heavy resonances predicted by several BSM models. Almost all GUT motivated theories predict the existence of a massive Z' which is a Spin-1 boson. Finding such particle would give us the understanding of the physics beyond the Standard Model. In this thesis we show how three uniangular distributions can be used to probe the spin, parity and couplings of a Z' via gold-plated decay mode $Z' \to Z^{(*)}Z^{(*)} \to \ell_1^+\ell_1^-\ell_2^+\ell_2^-$. A numerical analysis is also performed to show the applicability of our methodology for experimental study. We have constructed an effective model for a Z' and found the discovery potential of such resonance in the future runs of LHC. We have studied the uniangular asymmetries of both Spin-1^+ and Spin-1^- resonances.

Finally we have combined the results and presented a step by step methodology to uniquely determine the spin, parity and couplings of a new resonance via gold-plated decay mode of any arbitrary mass. Although full implementation of the methodology depends on the massiveness, nature of the couplings etc., it would not be a overstatement that uniangular distributions have the potential to determine the true characteristic of bosonic a resonance.

PART V

Appendices and References

A

Appendices

A.1 Phase Space

The differential decay width for the decay

$$H(p) \to Z_1(q_1)Z_2(q_2) \to (\ell_1^-(k_1) + \ell_1^+(k_2)) + (\ell_2^-(k_3) + \ell_2^+(k_4))$$

is given by:

$$\begin{aligned} d\Gamma &= \frac{1}{2M_H} |\mathscr{M}|^2 \prod_{i=1}^{4} \left(\frac{d^3\vec{k}_i}{(2\pi)^3 2E_i} \right) \times (2\pi)^4 \delta^{(4)} (p - k_1 - k_2 - k_3 - k_4) \\ &= \frac{1}{2M_H} \frac{|\mathscr{M}|^2}{(2\pi)^8} \prod_{i=1}^{4} \left(\frac{d^3\vec{k}_i}{2E_i} \right) \times \delta^{(4)} (p - k_1 - k_2 - k_3 - k_4) \\ &= \frac{1}{2M_H} \frac{|\mathscr{M}|^2}{(2\pi)^8} d_4 (PS \quad H \to 4 \text{ leptons}) , \end{aligned} \tag{A.1}$$

where

$$d_4 (PS \quad H \to 4 \text{ leptons}) = \prod_{i=1}^{4} \left(\frac{d^3\vec{k}_i}{2E_i} \right) \times \delta^{(4)} (p - k_1 - k_2 - k_3 - k_4) \tag{A.2}$$

The invariant phase space is given by:

$$\begin{aligned} d_4\left(PS \quad H \to 4 \text{ leptons}\right) = d_2\left(PS \quad H \to Z_1 Z_2\right) \times dM_1^2\, dM_2^2 \\ \times d_2\left(PS \quad Z_1 \to \ell_1^+ + \ell_1^-\right) \\ \times d_2\left(PS \quad Z_2 \to \ell_2^+ + \ell_2^-\right). \end{aligned} \tag{A.3}$$

For a general two body decay $A \to B + C$ we know that

$$d_2\left(PS \quad A \to B + C\right) = \frac{\pi}{2}\sqrt{\lambda\left(1, \frac{M_B^2}{M_A^2}, \frac{M_C^2}{M_A^2}\right)}\, \frac{d\Omega}{4\pi}. \tag{A.4}$$

Applying this result to our decay mode under consideration, we get

$$d_2\left(PS \quad H \to Z_1 Z_2\right) = \frac{\pi}{2}\sqrt{\lambda\left(1, \frac{M_1^2}{M_H^2}, \frac{M_2^2}{M_H^2}\right)}\, \frac{d\Omega_H}{4\pi}, \tag{A.5}$$

$$d_2\left(PS \quad Z_1 \to \ell_1^+ + \ell_1^-\right) = \frac{\pi}{2}\sqrt{\lambda\left(1, 0, 0\right)}\, \frac{d\Omega_{Z_1}}{4\pi}, \tag{A.6}$$

$$d_2\left(PS \quad Z_2 \to \ell_2^+ + \ell_2^-\right) = \frac{\pi}{2}\sqrt{\lambda\left(1, 0, 0\right)}\, \frac{d\Omega_{Z_2}}{4\pi}, \tag{A.7}$$

where we have considered the final leptons to be massless. It is easy to see that

$$\lambda\left(1, 0, 0\right) = 1, \tag{A.8}$$

$$\lambda\left(1, \frac{M_1^2}{M_H^2}, \frac{M_2^2}{M_H^2}\right) = \frac{1}{M_H^4}\lambda\left(M_H^2, M_1^2, M_2^2\right). \tag{A.9}$$

We define a quantity X as

$$X = \frac{1}{2M_H}\sqrt{\lambda\left(M_H^2, M_1^2, M_2^2\right)}. \tag{A.10}$$

In terms of X we now have

$$\lambda\left(1, \frac{M_1^2}{M_H^2}, \frac{M_2^2}{M_H^2}\right) = \frac{4X^2}{M_H^2}. \tag{A.11}$$

Therefore

$$d_2\left(PS \quad H \to Z_1 Z_2\right) = \frac{\pi}{2}\frac{2X}{M_H}\,\frac{d\Omega_H}{4\pi}, \tag{A.12}$$

$$d_2\left(PS \quad Z_1 \to \ell_1^+ + \ell_1^-\right) = \frac{\pi}{2}\,\frac{d\Omega_{Z_1}}{4\pi} = \frac{1}{8}d\Omega_{Z_1}, \tag{A.13}$$

$$d_2\left(PS \quad Z_2 \to \ell_2^+ + \ell_2^-\right) = \frac{\pi}{2}\,\frac{d\Omega_{Z_2}}{4\pi} = \frac{1}{8}d\Omega_{Z_2}. \tag{A.14}$$

The solid angle Ω_H will be integrated out fully, and

$$d\Omega_{Z_1} = (2\pi)\; d\cos\theta_1, \tag{A.15}$$

$$d\Omega_{Z_2} = d\cos\theta_2\; d\phi. \tag{A.16}$$

Thus we have

$$\left(PS \quad H \to Z_1 Z_2\right) = \pi\frac{X}{M_H}, \tag{A.17}$$

$$d_2\left(PS \quad Z_1 \to \ell_1^+ + \ell_1^-\right) = \frac{1}{8}(2\pi)\; d\cos\theta_1 = \frac{\pi}{4}d\cos\theta_1, \tag{A.18}$$

$$d_2\left(PS \quad Z_2 \to \ell_2^+ + \ell_2^-\right) = \frac{1}{8}\; d\cos\theta_2\; d\phi. \tag{A.19}$$

Hence

$$\begin{aligned} d_4\left(PS \quad H \to 4 \text{ leptons}\right) &= \pi\frac{X}{M_H} \times dM_1^2\; dM_2^2 \times \frac{\pi}{4}d\cos\theta_1 \times \frac{1}{8}\; d\cos\theta_2\; d\phi \\ &= \frac{\pi^2}{32}\frac{X}{M_H} \times dM_1^2\; dM_2^2\; d\cos\theta_1\; d\cos\theta_2\; d\phi. \end{aligned} \tag{A.20}$$

The expression for differential decay width is now given by

$$
\begin{aligned}
d\Gamma &= \frac{1}{2M_H}\frac{|\mathscr{M}|^2}{(2\pi)^8} \times \frac{\pi^2}{32}\frac{X}{M_H} \times dM_1^2\, dM_2^2\, d\cos\theta_1\, d\cos\theta_2\, d\phi, \\
&= \frac{\pi^2}{2^{14}\,\pi^8}\,|\mathscr{M}|^2\,\frac{X}{M_H^2} \times dM_1^2\, dM_2^2\, d\cos\theta_1\, d\cos\theta_2\, d\phi, \\
&= \frac{1}{2^{14}\,\pi^6}\,|\mathscr{M}|^2\,\frac{X}{M_H^2} \times dM_1^2\, dM_2^2\, d\cos\theta_1\, d\cos\theta_2\, d\phi, \\
\implies \frac{d\Gamma}{dM_2^2} &= \frac{1}{2^{14}\,\pi^6}\,|\mathscr{M}|^2\,\frac{X}{M_H^2} \times dM_1^2\, d\cos\theta_1\, d\cos\theta_2\, d\phi. \qquad \text{(A.21)}
\end{aligned}
$$

Now we shall keep Z_1 on-shell, so we shall use the narrow width approximation for this:

$$
\frac{1}{\left[\left(q_1^2 - M_Z^2\right)^2 + M_Z^2\Gamma_Z^2\right]} \approx \frac{\pi}{M_Z\Gamma_Z}\delta\left(M_1^2 - M_Z^2\right), \qquad \text{(A.22)}
$$

where Γ_Z is the total decay width of the Z boson. So doing the integration over $M_1^2, \cos\theta_1, \cos\theta_2$ and ϕ we get

$$
\frac{d\Gamma}{dM_2^2} = \frac{1}{2^{14}\,\pi^6}\int |\mathscr{M}|^2\,\frac{X}{M_H^2}\, dM_1^2\, d\cos\theta_1\, d\cos\theta_2\, d\phi, \qquad \text{(A.23)}
$$

where X is now defined at $M_1^2 = M_Z^2$:

$$
X = \frac{1}{2M_H}\sqrt{\lambda\left(M_H^2, M_Z^2, M_2^2\right)}. \qquad \text{(A.24)}
$$

A.2 Other Terms in the Angular Distributions

In the main text, we have not included the η and η^2 dependent term in the angular distributions for the case of Spin-2 boson. However, for the sake of completeness, the η and

η^2 dependent term $\mathscr{M}$ in the angular distributions are given below.

$$
\begin{aligned}
\mathscr{M} = \eta\Bigg(& - 3M_H \mathrm{Re}(F_2F_M^*)\frac{\mathsf{u}_1}{\mathsf{v}}\left(\cos\theta_1(P_2(\cos\theta_2)+2) - \cos\theta_2(P_2(\cos\theta_1)+2)\right) \\
& - \frac{3}{\mathsf{u}_1^2}\mathrm{Re}(F_3F_L^*)\left(q_1^2\cos\theta_1(1-P_2(\cos\theta_2)) - q_2^2\cos\theta_2(1-P_2(\cos\theta_1))\right) \\
& - 3\sqrt{3}\sqrt{q_1^2\,q_2^2}\mathrm{Re}(F_3F_M^*)\frac{\mathsf{u}_2^2}{\mathsf{u}_1^2\mathsf{v}}\left(\cos\theta_1(1-P_2(\cos\theta_2)) + \cos\theta_2(1-P_2(\cos\theta_1))\right) \\
& - 3\sqrt{q_1^2\,q_2^2}\mathrm{Re}(F_4F_L^*)\frac{\mathsf{u}_2^2}{\mathsf{u}_1^2\mathsf{w}}\left(\cos\theta_1(1-P_2(\cos\theta_2)) + \cos\theta_2(1-P_2(\cos\theta_1))\right) \\
& + 12\sqrt{3}\mathsf{u}_2^4\mathrm{Re}(F_4F_M^*)\frac{1}{4\mathsf{u}_1^2\mathsf{v}^3\mathsf{w}^3}\Big(- q_2^2\mathsf{v}^2\mathsf{w}^2\cos\theta_1(1-P_2(\cos\theta_2)) \\
& + q_1^2\cos\theta_2\left(\mathsf{v}^2\mathsf{w}^2 - P_2(\cos\theta_1)\left(8M_H^4\mathsf{u}_1^4 + 10M_H^2\mathsf{u}_1^2\mathsf{u}_2^4 + 3\mathsf{u}_2^8\right)\right)\Big) \\
& + (\sin\theta_1\sin\theta_2\sin\phi)\Bigg(\frac{9}{2\sqrt{2}}\mathrm{Im}(F_1F_2^*)(\cos\theta_2 - \cos\theta_1) \\
& - \frac{9\mathsf{u}_2^2}{4}(\cos\theta_1 + \cos\theta_2)\left(\mathrm{Im}(F_3F_4^*)\frac{1}{\mathsf{w}} - \sqrt{3}\,\mathrm{Im}(F_LF_M^*)\frac{1}{\mathsf{v}}\right)\Bigg) \\
& + (\sin\theta_1\sin\theta_2\cos\phi)\Bigg(\mathrm{Re}(F_1F_M^*)(\cos\theta_1 - \cos\theta_2)\left(-\frac{9M_H\mathsf{u}_1}{\sqrt{2}\mathsf{v}}\right) \\
& - \frac{9\mathsf{u}_2^2}{4}(\cos\theta_1 + \cos\theta_2)\left(\sqrt{3}\,\mathrm{Re}(F_3F_M^*)\frac{1}{\mathsf{v}} - \mathrm{Re}(F_4F_L^*)\frac{1}{\mathsf{w}}\right)\Bigg) \\
+\eta^2\Bigg(& \frac{9}{4\mathsf{u}_1^2\mathsf{v}^2\mathsf{w}^2}(\sin\theta_1\sin\theta_2\cos\phi)\Big(\sqrt{2}\mathsf{u}_1^2\mathsf{v}^2\mathsf{w}^2\mathrm{Re}(F_1F_2^*) - \mathsf{u}_2^4\mathsf{v}^2\mathsf{w}\mathrm{Re}(F_3F_4^*) \\
+ \sqrt{3}\mathsf{u}_2^4 & \mathsf{v}\mathsf{w}^2\mathrm{Re}(F_LF_M^*) \\
& + \sqrt{q_1^2\,q_2^2}\left(\mathsf{v}^2\mathsf{w}^2\left(|F_3|^2 - |F_L|^2\right) - \mathsf{u}_2^4\left(|F_4|^2\,\mathsf{v}^2 - 3\,|F_M|^2\,\mathsf{w}^2\right)\right)\Big) \\
& + \frac{9}{4\mathsf{u}_1^2\mathsf{v}\mathsf{w}}(\sin\theta_1\sin\theta_2\sin\phi)\Big(2\sqrt{2}M_H\mathsf{u}_1^3\mathsf{w}\mathrm{Im}(F_1F_M^*) + 2\sqrt{q_1^2\,q_2^2}\mathsf{v}\mathsf{w}\mathrm{Im}(F_3F_L^*) \\
& + \mathsf{u}_2^4\left(-\sqrt{3}\mathsf{w}\mathrm{Im}(F_3F_M^*) - \mathsf{v}\mathrm{Im}(F_4F_L^*) - 2\sqrt{3}\sqrt{q_1^2\,q_2^2}\mathrm{Im}(F_4F_M^*)\right)\Big) \\
& + \frac{9}{4}\cos\theta_1\cos\theta_2\Big(- |F_2|^2 + |F_4|^2\,\frac{2M_H^2\mathsf{u}_1^2}{\mathsf{w}^2} \\
& - |F_M|^2\,\frac{\mathsf{u}_1^2}{\mathsf{v}^2\mathsf{w}^2X^2}\left(2M_H^6\mathsf{u}_1^2 - M_H^4\left(3q_1^2 + q_2^2\right)\left(q_1^2 + 3q_2^2\right) + \mathsf{u}_2^8\right)\Big)\Bigg).
\end{aligned}
\tag{A.25}
$$

A.3 Expressions for the observables $\mathcal{T}_1$, $\mathcal{T}_2$, $\mathcal{U}_1$, $\mathcal{U}_2$, $\mathcal{V}_1$ and $\mathcal{V}_2$

The expressions for $\mathcal{T}_1$, $\mathcal{T}_2$, $\mathcal{U}_1$, $\mathcal{U}_2$, $\mathcal{V}_1$ and $\mathcal{V}_2$ are

$$\mathcal{T}_1 = \frac{-1.32\times 10^{-9}y}{5.57\times 10^{-8}+2.61\times 10^{-8}x+3.98\times 10^{-9}x^2+1.60\times 10^{-10}y^2} \tag{A.26}$$

$$\mathcal{T}_2 = \frac{-9.65\times 10^{-9}+4.00\times 10^{-10}x^2+4.00\times 10^{-10}y^2}{5.57\times 10^{-8}+2.61\times 10^{-8}x+3.98\times 10^{-9}x^2+1.60\times 10^{-10}y^2} \tag{A.27}$$

$$\mathcal{U}_1 = \frac{-1.17\times 10^{-9}-6.22\times 10^{-10}x-6.90\times 10^{-11}x^2}{5.57\times 10^{-8}+2.61\times 10^{-8}x+3.98\times 10^{-9}x^2+1.60\times 10^{-10}y^2} \tag{A.28}$$

$$\mathcal{U}_2 = \frac{6.06\times 10^{-9}+4.35\times 10^{-9}x+7.97\times 10^{-10}x^2-4.00\times 10^{-10}y^2}{5.57\times 10^{-8}+2.61\times 10^{-8}x+3.98\times 10^{-9}x^2+1.60\times 10^{-10}y^2} \tag{A.29}$$

$$\mathcal{V}_1 = \frac{-3.11\times 10^{-10}y}{5.57\times 10^{-8}+2.61\times 10^{-8}x+3.98\times 10^{-9}x^2+1.60\times 10^{-10}y^2} \tag{A.30}$$

$$\mathcal{V}_2 = \frac{2.92\times 10^{-9}y}{5.57\times 10^{-8}+2.61\times 10^{-8}x+3.98\times 10^{-9}x^2+1.60\times 10^{-10}y^2} \tag{A.31}$$

where $x = \frac{b}{a}\times(100\text{Gev})^2$ and $y = \frac{c}{a}\times(100\text{Gev})^2$

A.4 Observables for a Spin 1 resonance

$$T_1^{(1)} = -\frac{6\sqrt{2}\eta M_{Z'}^3 M_1^2 Y}{D_1 D_2}\left(M_{Z'}^2 - M_1^2 + 3M_2^2\right)\ \mathrm{Re}\left(F_{\mathrm{E}1}^{(1)}F_{\mathrm{o}1}^{(1)*}\right), \tag{A.32}$$

$$T_1'^{(1)} = \frac{6\sqrt{2}\eta M_{Z'}^3 M_2^2 Y}{D_1 D_2}\left(M_{Z'}^2 + 3M_1^2 - M_2^2\right)\ \mathrm{Re}\left(F_{\mathrm{E}1}^{(1)}F_{\mathrm{o}1}^{(1)*}\right), \tag{A.33}$$

$$\begin{aligned} T_2^{(1)} = -2M_{Z'}^2 Y^2 \Bigg(& \frac{\left|F_{\mathrm{o}1}^{(1)}\right|^2}{D_1^2}\left(\left(M_{Z'}^2 - M_1^2\right)\left(M_1^2 + 4M_2^2\right) + 2M_2^4\right) \\ & + \frac{2\left|F_{\mathrm{E}1}^{(1)}\right|^2}{D_2^2}\left(M_{Z'}^2\left(M_1^2 + 16M_2^2\right) - M_2^2\left(20M_1^2 - 3M_2^2\right)\right)\Bigg), \end{aligned} \tag{A.34}$$

$$T_2'^{(1)} = -2M_{Z'}^2 Y^2 \Bigg(\frac{\left|F_{\mathrm{o}1}^{(1)}\right|^2}{D_1^2}\left(\left(M_{Z'}^2 - M_2^2\right)\left(4M_1^2 + M_2^2\right) + 2M_1^4\right)$$

$$+ \frac{2\left|F^{(1)}_{\mathrm{E}1}\right|^2}{D_2^2}\left(M^2_{Z'}\left(16M_1^2+M_2^2\right)-M_1^2\left(20M_2^2-3M_1^2\right)\right)\Bigg), \tag{A.35}$$

$$U^{(1)}_1 = \frac{9\pi^2\eta^2 M^2_{Z'}M_1M_2}{16D_1^2D_2^2}\Big(4\left|F^{(1)}_{\mathrm{O}1}\right|^2 M^2_{Z'}Y^2\Big(16M^6_{Z'}\mathsf{u}_1^2$$
$$+ M^4_{Z'}\left(56\mathsf{u}_1^4-85\mathsf{u}_2^4\right)+M^2_{Z'}\left(96\mathsf{u}_1^2\mathsf{u}_2^4-86\mathsf{u}_1^6\right)$$
$$-35\mathsf{u}_1^4\mathsf{u}_2^4+38\mathsf{u}_2^8\Big)$$
$$-\left|F^{(1)}_{\mathrm{E}1}\right|^2\left(\left(M^2_{Z'}-2\mathsf{u}_1^2\right)^2-\mathsf{u}_2^4\right)\Big(4M^6_{Z'}\mathsf{u}_1^2$$
$$-M^4_{Z'}\left(5\mathsf{u}_1^4+\mathsf{u}_2^4\right)$$
$$+12M^2_{Z'}\mathsf{u}_1^2\left(\mathsf{u}_1^4-\mathsf{u}_2^4\right)+3\mathsf{u}_1^4\mathsf{u}_2^4-\mathsf{u}_2^8\Big)\Big), \tag{A.36}$$

$$U^{(1)}_2 = -\frac{8M_1^2M_2^2\mathsf{u}_2^4}{D_2^2}\left|F^{(1)}_{\mathrm{E}1}\right|^2, \tag{A.37}$$

$$V^{(1)}_1 = -\frac{9\pi^2\eta^2 M_{Z'}M_1M_2Y}{2\sqrt{2}D_1D_2}\left(M^4_{Z'}-2M^2_{Z'}\mathsf{u}_1^2-\mathsf{u}_2^4\right)$$
$$\times\ \mathrm{Im}\left(F^{(1)}_{\mathrm{E}1}F^{(1)*}_{\mathrm{O}1}\right), \tag{A.38}$$

$$V^{(1)}_2 = 0, \tag{A.39}$$

$$\tag{A.40}$$

B

References

[1] 'Quarks and Leptons: An introductory course in Modern Particle Physics, F.Halzen and A.D.Martin , Ed. John Wiley: New York, 1984;

[2] S. L. Glashow, Nucl. Phys. **22**, 579 (1961). doi:10.1016/0029-5582(61)90469-2

[3] J. Goldstone, Nuovo Cim. **19**, 154 (1961). J. Goldstone, A. Salam and S. Weinberg, Phys. Rev. **127**, 965 (1962).

[4] Y. Nambu, Phys. Rev. Lett. **4**, 380 (1960). doi:10.1103/PhysRevLett.4.380

[5] P. W. Higgs, Phys. Lett. **12**, 132 (1964); F. Englert and R. Brout, Phys. Rev. Lett. **13**, 321 (1964); G. S. Guralnik, C. R. Hagen and T. W. B. Kibble, Phys. Rev. Lett. **13**, 585 (1964); P. W. Higgs, Phys. Rev. **145**, 1156 (1966); T. W. B. Kibble, Phys. Rev. **155**, 1554 (1967).

[6] S. Weinberg, Phys. Rev. Lett. **19**, 1264 (1967).

[7] G. 't Hooft, Nucl. Phys. B **33**, 173 (1971). doi:10.1016/0550-3213(71)90395-6

[8] F. J. Hasert *et al.* [Gargamelle Neutrino Collaboration], Phys. Lett. B **46**, 138 (1973).

[9] N. Cabibbo, Phys. Rev. Lett. **10**, 531 (1963). doi:10.1103/PhysRevLett.10.531

[10] S. L. Glashow, J. Iliopoulos and L. Maiani, Phys. Rev. D **2**, 1285 (1970). doi:10.1103/PhysRevD.2.1285

[11] J. J. Aubert *et al.* [E598 Collaboration], Phys. Rev. Lett. **33**, 1404 (1974); J. E. Augustin *et al.* [SLAC-SP-017 Collaboration], Phys. Rev. Lett. **33**, 1406 (1974) [Adv. Exp. Phys. **5**, 141 (1976)].

[12] M. L. Perl *et al.*, Phys. Rev. Lett. **35**, 1489 (1975). doi:10.1103/PhysRevLett.35.1489

[13] S. W. Herb *et al.*, Phys. Rev. Lett. **39**, 252 (1977).

[14] F. Abe *et al.* [CDF Collaboration], Phys. Rev. Lett. **73**, 225 (1994) [hep-ex/9405005];

[15] F. Abe *et al.* [CDF Collaboration], Phys. Rev. D **50**, 2966 (1994);

[16] F. Abe *et al.* [CDF Collaboration], Phys. Rev. Lett. **74**, 2626 (1995) [hep-ex/9503002];

[17] S. Abachi *et al.* [D0 Collaboration], Phys. Rev. Lett. **74**, 2632 (1995) [hep-ex/9503003].

[18] M. Kobayashi and T. Maskawa, Prog. Theor. Phys. **49**, 652 (1973). doi:10.1143/PTP.49.652

[19] G. Arnison *et al.* [UA1 Collaboration], Phys. Lett. B **122**, 103 (1983); M. Banner *et al.* [UA2 Collaboration], Phys. Lett. B **122**, 476 (1983).

[20] G. Aad *et al.* [ATLAS Collaboration], Phys. Lett. B **716**, 1 (2012) [arXiv:1207.7214 [hep-ex]].

[21] G. Aad *et al.* [ATLAS Collaboration], Science 21 December 2012: Vol. 338 no. 6114 pp. 1576-1582.

[22] S. Chatrchyan *et al.* [CMS Collaboration], Phys. Lett. B **716**, 30 (2012) [arXiv:1207.7235 [hep-ex]].

[23] S. Chatrchyan *et al.* [CMS Collaboration], Science 21 December 2012: Vol. 338 no. 6114 pp. 1569-1575.

[24] S. Chatrchyan *et al.* [CMS Collaboration], arXiv:1212.6639 [hep-ex].

[25] L. D. Landau, Dokl. Akad. Nauk Ser. Fiz. **60**, 207 (1948).

[26] C. -N. Yang, Phys. Rev. **77**, 242 (1950).

[27] A. Menon, T. Modak, D. Sahoo, R. Sinha and H. Y. Cheng, Phys. Rev. D **89**, no. 9, 095021 (2014) doi:10.1103/PhysRevD.89.095021 [arXiv:1301.5404 [hep-ph]].

[28] B. Bhattacherjee, T. Modak, S. K. Patra and R. Sinha, arXiv:1503.08924 [hep-ph].

[29] V. D. Barger, N. G. Deshpande and K. Whisnant, Phys. Rev. Lett. **56**, 30 (1986).

[30] V. D. Barger, N. G. Deshpande and K. Whisnant, Phys. Rev. D **35**, 1005 (1987).

[31] V. D. Barger, N. G. Deshpande, J. L. Rosner and K. Whisnant, Phys. Rev. D **35**, 2893 (1987).

[32] P. Langacker, R. W. Robinett and J. L. Rosner, Phys. Rev. D **30**, 1470 (1984). doi:10.1103/PhysRevD.30.1470

[33] J. L. Hewett and T. G. Rizzo, Phys. Rept. **183**, 193 (1989). doi:10.1016/0370-1573(89)90071-9

[34] V. D. Barger, W. Y. Keung and E. Ma, Phys. Lett. B **94**, 377 (1980). doi:10.1016/0370-2693(80)90900-4

[35] S. Chaudhuri, S.-W. Chung, G. Hockney and J. D. Lykken, Nucl. Phys. B **456**, 89 (1995) doi:10.1016/0550-3213(95)00147-7 [hep-ph/9501361].

[36] W. -Y. Keung, I. Low and J. Shu, Phys. Rev. Lett. **101**, 091802 (2008) [arXiv:0806.2864 [hep-ph]].

[37] T. Modak, D. Sahoo, R. Sinha, H. Y. Cheng and T. C. Yuan, arXiv:1408.5665 [hep-ph].

[38] M. Jacob and G. C. Wick, Annals Phys. **7**, 404 (1959) [Annals Phys. **281**, 774 (2000)].

[39] Suh-Urk Chung, "Spin formalisms, Updated Version", Brookhaven Nat. Lab., Upton, NY, 2008. This report is an updated version of CERN-71-08.

[40] C. A. Nelson, Phys. Rev. D **30**, 1937 (1984).

[41] J. R. Dell'Aquila and C. A. Nelson, Phys. Rev. D **33**, 80 (1986).

[42] C. A. Nelson, Phys. Rev. D **37**, 1220 (1988).

[43] M. Kramer, J. H. Kuhn, M. L. Stong and P. M. Zerwas, Z. Phys. C **64**, 21 (1994) [hep-ph/9404280].

[44] V. D. Barger, K. -M. Cheung, A. Djouadi, B. A. Kniehl and P. M. Zerwas, Phys. Rev. D **49**, 79 (1994) [hep-ph/9306270].

[45] J. F. Gunion and X. -G. He, Phys. Rev. Lett. **76**, 4468 (1996) [hep-ph/9602226].

[46] D. J. Miller, S. Y. Choi, B. Eberle, M. M. Muhlleitner and P. M. Zerwas, Phys. Lett. B **505**, 149 (2001) [hep-ph/0102023].

[47] G. R. Bower, T. Pierzchala, Z. Was and M. Worek, Phys. Lett. B **543**, 227 (2002) [hep-ph/0204292].

[48] S. Y. Choi, “Measuring the spin of the Higgs bosons,”in 10th International Conference on Supersymmetry, Edited by P. Nath, P. M. Zerwas, C. Grosche. Hamburg, DESY, 2002.

[49] S. Y. Choi, D. J. Miller, M. M. Muhlleitner and P. M. Zerwas, Phys. Lett. B **553**, 61 (2003) [hep-ph/0210077].

[50] R. M. Godbole, S. D. Rindani and R. K. Singh, Phys. Rev. D **67**, 095009 (2003) [Erratum-ibid. D **71**, 039902 (2005)] [hep-ph/0211136].

[51] C. P. Buszello, I. Fleck, P. Marquard and J. J. van der Bij, Eur. Phys. J. C **32**, 209 (2004) [hep-ph/0212396].

[52] K. Desch, Z. Was and M. Worek, Eur. Phys. J. C **29**, 491 (2003) [hep-ph/0302046].

[53] M. Worek, Acta Phys. Polon. B **34**, 4549 (2003) [hep-ph/0305082].

[54] A. B. Kaidalov, V. A. Khoze, A. D. Martin and M. G. Ryskin, Eur. Phys. J. C **31**, 387 (2003) [hep-ph/0307064].

[55] R. M. Godbole, S. Kraml, M. Krawczyk, D. J. Miller, P. Niezurawski and A. F. Zarnecki, hep-ph/0404024.

[56] C. P. Buszello and P. Marquard, hep-ph/0603209.

[57] H. Przysiezniak, hep-ex/0605069.

[58] M. Bluj, CMS-NOTE-2006-094.

[59] P. S. Bhupal Dev, A. Djouadi, R. M. Godbole, M. M. Muhlleitner and S. D. Rindani, Phys. Rev. Lett. **100**, 051801 (2008) [arXiv:0707.2878 [hep-ph]].

[60] R. M. Godbole, D. J. Miller, 2 and M. M. Muhlleitner, JHEP **0712**, 031 (2007) [arXiv:0708.0458 [hep-ph]].

[61] R. M. Godbole, P. S. Bhupal Dev, A. Djouadi, M. M. Muhlleitner and S. D. Rindani, eConf C **0705302**, TOP08 (2007) [arXiv:0710.2669 [hep-ph]].

[62] Y. Gao, A. V. Gritsan, Z. Guo, K. Melnikov, M. Schulze and N. V. Tran, Phys. Rev. D **81**, 075022 (2010) [arXiv:1001.3396 [hep-ph]].

[63] C. Englert, C. Hackstein and M. Spannowsky, Phys. Rev. D **82**, 114024 (2010) [arXiv:1010.0676 [hep-ph]].

[64] O. J. P. Eboli, C. S. Fong, J. Gonzalez-Fraile and M. C. Gonzalez-Garcia, Phys. Rev. D **83**, 095014 (2011) [arXiv:1102.3429 [hep-ph]].

[65] U. De Sanctis, M. Fabbrichesi and A. Tonero, Phys. Rev. D **84**, 015013 (2011) [arXiv:1103.1973 [hep-ph]].

[66] S. Berge, W. Bernreuther, B. Niepelt and H. Spiesberger, Phys. Rev. D **84**, 116003 (2011) [arXiv:1108.0670 [hep-ph]].

[67] M. C. Kumar, P. Mathews, A. A. Pankov, N. Paver, V. Ravindran and A. V. Tsytrinov, Phys. Rev. D **84**, 115008 (2011) [arXiv:1108.3764 [hep-ph]].

[68] J. Ellis and D. S. Hwang, JHEP **1209**, 071 (2012) [arXiv:1202.6660 [hep-ph]].

[69] C. Englert, M. Spannowsky and M. Takeuchi, JHEP **1206**, 108 (2012) [arXiv:1203.5788 [hep-ph]].

[70] A. Bredenstein, A. Denner, S. Dittmaier and M. M. Weber, Phys. Rev. D **74**, 013004 (2006) [hep-ph/0604011].

[71] J. Ellis, D. S. Hwang, V. Sanz and T. You, arXiv:1208.6002 [hep-ph].

[72] J. Ellis, R. Fok, D. S. Hwang, V. Sanz and T. You, arXiv:1210.5229 [hep-ph].

[73] P. P. Giardino, K. Kannike, M. Raidal and A. Strumia, arXiv:1207.1347 [hep-ph].

[74] S. Y. Choi, M. M. Muhlleitner and P. M. Zerwas, arXiv:1209.5268 [hep-ph].

[75] R. Boughezal, T. J. LeCompte and F. Petriello, arXiv:1208.4311 [hep-ph].

[76] S. Banerjee, J. Kalinowski, W. Kotlarski, T. Przedzinski and Z. Was, arXiv:1212.2873 [hep-ph].

[77] P. Avery, D. Bourilkov, M. Chen, T. Cheng, A. Drozdetskiy, J. S. Gainer, A. Korytov and K. T. Matchev *et al.*, arXiv:1210.0896 [hep-ph].

[78] B. Coleppa, K. Kumar and H. E. Logan, Phys. Rev. D **86**, 075022 (2012) [arXiv:1208.2692 [hep-ph]].

[79] C. -Q. Geng, D. Huang, Y. Tang and Y. -L. Wu, arXiv:1210.5103 [hep-ph].

[80] J. Ellis, V. Sanz and T. You, arXiv:1211.3068 [hep-ph].

[81] J. Frank, M. Rauch and D. Zeppenfeld, arXiv:1211.3658 [hep-ph].

[82] A. Djouadi, R.M. Godbole, B. Mellado and K. Mohan arXiv:1301.4965 [hep-ph].

[83] C. Englert, D. Goncalves-Netto, K. Mawatari and T. Plehn, arXiv:1212.0843 [hep-ph].

[84] D. Stolarski and R. Vega-Morales, Phys. Rev. D **86**, 117504 (2012) [arXiv:1208.4840 [hep-ph]].

[85] G. Kramer and T. F. Walsh, Z. Phys. **263**, 361 (1973).

[86] S. Bolognesi, Y. Gao, A. V. Gritsan, K. Melnikov, M. Schulze, N. V. Tran and A. Whitbeck, Phys. Rev. D **86**, 095031 (2012) [arXiv:1208.4018 [hep-ph]].

[87] K. Cheung and T. -C. Yuan, Phys. Rev. Lett. **108**, 141602 (2012) [arXiv:1112.4146 [hep-ph]].

[88] Z. Chacko, R. Franceschini and R. K. Mishra, arXiv:1209.3259 [hep-ph].

[89] H. de Sandes and R. Rosenfeld, Phys. Rev. D **85**, 053003 (2012) [arXiv:1111.2006 [hep-ph]].

[90] H. Kubota and M. Nojiri, arXiv:1207.0621 [hep-ph].

[91] B. Grzadkowski, J. F. Gunion and M. Toharia, Phys. Lett. B **712**, 70 (2012) [arXiv:1202.5017 [hep-ph]].

[92] V. Barger, M. Ishida and W. -Y. Keung, Phys. Rev. Lett. **108**, 101802 (2012) [arXiv:1111.4473 [hep-ph]].

[93] T. G. Rizzo, JHEP **0206**, 056 (2002) [hep-ph/0205242].

[94] T. Han, J. D. Lykken and R. -J. Zhang, Phys. Rev. D **59**, 105006 (1999) [hep-ph/9811350].

[95] R. Fok, C. Guimaraes, R. Lewis and V. Sanz, JHEP **1212**, 062 (2012) [arXiv:1203.2917 [hep-ph]].

[96] A. Alves, Phys. Rev. D **86**, 113010 (2012) [arXiv:1209.1037 [hep-ph]].

[97] G. Aad *et al.* [ATLAS Collaboration], Phys. Lett. B **726**, 120 (2013) [arXiv:1307.1432 [hep-ex]].

[98] J. Alwall, M. Herquet, F. Maltoni, O. Mattelaer and T. Stelzer, JHEP **1106** (2011) 128 [arXiv:1106.0522 [hep-ph]].

[99] T. Sjostrand, L. Lonnblad, S. Mrenna and P. Z. Skands, hep-ph/0308153.

[100] The PGS 4 webpage (`http://physics.ucdavis.edu/~conway/research/software/pgs/pgs4-general.htm`).

[101] A. Alloul, N. D. Christensen, C. Degrande, C. Duhr and B. Fuks, arXiv:1310.1921 [hep-ph].

[102] J. Pumplin, D. R. Stump, J. Huston, H. L. Lai, P. M. Nadolsky and W. K. Tung, JHEP **0207**, 012 (2002) [arXiv:hep-ph/0201195].

[103] ATLAS Collaboration, ATLAS-CONF-2013-013

[104] S. Chatrchyan *et al.* [CMS Collaboration], Phys. Rev. Lett. **110**, 081803 (2013) [arXiv:1212.6639 [hep-ex]].

[105] Webpage for Higgs cross sections at 7, 8 and 14 TeV
(LHC Higgs Cross Section Working Group)

[106] J. M. Campbell, R. K. Ellis and C. Williams, MCFM web page: http://mcfm.fnal.gov

[107] K. Cheung, J. S. Lee and P. Y. Tseng, JHEP **1305**, 134 (2013) [arXiv:1302.3794 [hep-ph]].

[108] K. Cheung, J. S. Lee and P. Y. Tseng, JHEP **1401**, 085 (2014) [arXiv:1310.3937 [hep-ph]].

[109] J. S. Gainer, J. Lykken, K. T. Matchev, S. Mrenna and M. Park, Phys. Rev. Lett. **111**, 041801 (2013) [arXiv:1304.4936 [hep-ph]].

[110] M. Chen, T. Cheng, J. S. Gainer, A. Korytov, K. T. Matchev, P. Milenovic, G. Mitselmakher and M. Park *et al.*, Phys. Rev. D **89**, no. 3, 034002 (2014) [arXiv:1310.1397 [hep-ph]].

[111] K. Cheung, J. S. Lee, E. Senaha and P. Y. Tseng, JHEP **1406**, 149 (2014) [arXiv:1403.4775 [hep-ph]].

[112] Y. Chen, A. Falkowski, I. Low and R. Vega-Morales, Phys. Rev. D **90**, no. 11, 113006 (2014) [arXiv:1405.6723 [hep-ph]].

[113] K. Cheung, J. S. Lee and P. Y. Tseng, Phys. Rev. D **90**, 095009 (2014) [arXiv:1407.8236 [hep-ph]].

[114] J. S. Gainer, J. Lykken, K. T. Matchev, S. Mrenna and M. Park, Phys. Rev. D **91**, no. 3, 035011 (2015) [arXiv:1403.4951 [hep-ph]].

[115] ATLAS Collaboration, Prospects for measurements of the HZZ vertex tensor structure in $H \to ZZ^* \to 4l$ decay channel with ATLAS ATLAS-PHYS-PUB-2013-013

[116] V. Khachatryan *et al.* [CMS Collaboration], arXiv:1411.3441 [hep-ex].

[117] I. Anderson, S. Bolognesi, F. Caola, Y. Gao, A. V. Gritsan, C. B. Martin, K. Melnikov and M. Schulze *et al.*, Phys. Rev. D **89**, no. 3, 035007 (2014) [arXiv:1309.4819 [hep-ph]].

[118] T. Modak and R. Srivastava, arXiv:1411.2210 [hep-ph].

[119] R. Godbole, D. J. Miller, K. Mohan and C. D. White, Phys. Lett. B **730**, 275 (2014) [arXiv:1306.2573 [hep-ph]].

[120] R. M. Godbole, D. J. Miller, K. A. Mohan and C. D. White, arXiv:1409.5449 [hep-ph].

[121] F. Boudjema, R. M. Godbole, D. Guadagnoli and K. A. Mohan, arXiv:1501.03157 [hep-ph].

[122] B. Dumont, arXiv:1411.3465 [hep-ph].

[123] W. Dekens and J. de Vries, JHEP **1305**, 149 (2013) [arXiv:1303.3156 [hep-ph]].

[124] N. Belyaev, R. Konoplich, L. E. Pedersen and K. Prokofiev, arXiv:1502.03045 [hep-ph].

[125] Y. Chen, R. Harnik and R. Vega-Morales, arXiv:1503.05855 [hep-ph].

[126] W. Bernreuther, P. Gonzalez and M. Wiebusch, Eur. Phys. J. C **69**, 31 (2010) [arXiv:1003.5585 [hep-ph]].

[127] T. Figy, S. Palmer and G. Weiglein, JHEP **1202**, 105 (2012) [arXiv:1012.4789 [hep-ph]].

[128] N. Arkani-Hamed, A. G. Cohen and H. Georgi, Phys. Lett. B **513**, 232 (2001) [hep-ph/0105239].

[129] N. Arkani-Hamed, A. G. Cohen, T. Gregoire and J. G. Wacker, JHEP **0208**, 020 (2002) [hep-ph/0202089].

[130] N. Arkani-Hamed, A. G. Cohen, E. Katz and A. E. Nelson, JHEP **0207**, 034 (2002) [hep-ph/0206021].

[131] T. D. Lee, Phys. Rev. D **8**, 1226 (1973). doi:10.1103/PhysRevD.8.1226

[132] S. Schael *et al.* [ALEPH and DELPHI and L3 and OPAL and LEP Working Group for Higgs Boson Searches Collaborations], Eur. Phys. J. C **47**, 547 (2006) [hep-ex/0602042].

[133] S. Weinberg, Phys. Rev. D **13**, 974 (1976).

[134] L. Susskind, Phys. Rev. D **20**, 2619 (1979).

[135] J. R. Ellis, M. K. Gaillard, D. V. Nanopoulos and P. Sikivie, Nucl. Phys. B **182**, 529 (1981).

[136] S. Dimopoulos, S. Raby and G. L. Kane, Nucl. Phys. B **182**, 77 (1981).

[137] R. S. Chivukula, R. Rosenfeld, E. H. Simmons and J. Terning, In *Barklow, T.L. (ed.) et al.: Electroweak symmetry breaking and new physics at the TeV scale* 352-382 [hep-ph/9503202].

[138] V. Khachatryan *et al.* [CMS Collaboration], Phys. Rev. D **91**, no. 5, 052009 (2015) [arXiv:1501.04198 [hep-ex]].

[139] J. de Favereau *et al.* [DELPHES 3 Collaboration], JHEP **1402**, 057 (2014) [arXiv:1307.6346 [hep-ex]].

[140] G. Aad *et al.* [ATLAS Collaboration], arXiv:0901.0512 [hep-ex].